In compliance with the
Canadian Privacy Legislation
some supporting forms
may have been removed from
this dissertation.

While these forms may be included
in the document page count,
their removal does not represent
any loss of content from the dissertation.

University of Alberta

EXACT ERROR RATE ANALYSIS OF MRC DIVERSITY WITH CHANNEL ESTIMATION ERROR

by

Lingzhi Cao

A thesis submitted to the Faculty of Graduate Studies and Research in partial fulfillment of the requirements for the degree of **Master of Science**.

Department of Electrical and Computer Engineering

Edmonton, Alberta

Fall 2003

National Library
of Canada

Acquisitions and
Bibliographic Services

395 Wellington Street
Ottawa ON K1A 0N4
Canada

Bibliothèque nationale
du Canada

Acquisisitons et
services bibliographiques

395, rue Wellington
Ottawa ON K1A 0N4
Canada

Your file Votre référence
ISBN: 0-612-87732-9
Our file Notre référence
ISBN: 0-612-87732-9

The author has granted a non-exclusive licence allowing the National Library of Canada to reproduce, loan, distribute or sell copies of this thesis in microform, paper or electronic formats.

The author retains ownership of the copyright in this thesis. Neither the thesis nor substantial extracts from it may be printed or otherwise reproduced without the author's permission.

L'auteur a accordé une licence non exclusive permettant à la Bibliothèque nationale du Canada de reproduire, prêter, distribuer ou vendre des copies de cette thèse sous la forme de microfiche/film, de reproduction sur papier ou sur format électronique.

L'auteur conserve la propriété du droit d'auteur qui protège cette thèse. Ni la thèse ni des extraits substantiels de celle-ci ne doivent être imprimés ou aturement reproduits sans son autorisation.

Canada

University of Alberta

Library Release Form

Name of Author: Lingzhi Cao

Title of Thesis: Exact Error Rate Analysis of MRC Diversity with Channel Estimation Error

Degree: Master of Science

Year this Degree Granted: 2003

Permission is hereby granted to the University of Alberta Library to reproduce single copies of this thesis and to lend or sell such copies for private, scholarly or scientific research purposes only.

The author reserves all other publication and other rights in association with the copyright in the thesis, and except as herein before provided, neither the thesis nor any substantial portion thereof may be printed or otherwise reproduced in any material form whatever without the author's prior written permission.

Date: Aug. 12, 2003

University of Alberta

Faculty of Graduate Studies and Research

The undersigned certify that they have read, and recommend to the Faculty of Graduate Studies and Research for acceptance, a thesis entitled **Exact Error Rate Analysis of MRC Diversity with Channel Estimation Error** submitted by Lingzhi Cao in partial fulfillment of the requirements for the degree of **Master of Science**.

Date: 03/08/25

Abstract

In practical wireless systems, the signal fading can severely degrade the receiver performance if accurate channel amplitude and phase information is not available to the receiver. We study the system performance with pilot symbol assisted modulation(PSAM), as the channel estimation method. Maximal ratio combing(MRC), known to be the optimal linear combining technique when perfect estimation is available, is adopted as the diversity combing technique . The system performance of M-ary quadrature amplitude modulation (M-QAM) is investigated in addition to binary phase shift keying (BPSK) and quadrature phase shift keying (QPSK). The BER expressions for MRC diversity with PSAM estimation error were derived. The effects of noise and estimator decorrelation on the received bit error rate are examined. A thorough discussion for the dependency of the BER performance on the symbol location is given. The high sensitivity of diversity systems to channel estimation error is investigated and quantified. The influence of the pilot symbol interpolation filter windowing is also considered.

To my dearest parents

Acknowledgements

I would like to express my sincere thanks to my supervisor Dr. Norman C. Beaulieu for his valuable guidance, suggestions and financial support. Special thanks to David J. Young and other labmates for their continuous support on simulation and other technical issues.

As my parents' only child, I would like to extend my deepest gratitude to my dearest parents thousands of miles away. I thank my parents for their selfless love, heartful advice and ever-lasting support through my growing-up. Their encouragement and love always keeps me living optimistically and happily. Their support and love give me the strength to surmount life difficulties and grow strong-willed. I have always held my dreams, my hopes and my faith with my parents' endless love. They give everything they have to me and they do everything they could for me. This thesis is dedicated to my beloved father and mother.

I would also like to thank all of my friends in China and Canada for their sharing, encouragement and support in the past two years.

This thesis was financially supported through research assistantships provided by the Natural Sciences and Engineering Research Council (NSERC) and the Alberta Informatics Circle of Research Excellence (iCORE).

Contents

1 Introduction **1**

1.1 Background and Motivation 1

1.2 Thesis Outline and Contributions 4

2 Literature Review **6**

2.1 Fading channels 6

2.1.1 First-Order Distributions 8

2.1.2 Second-Order Distributions 10

2.2 Diversity 14

2.2.1 Maximal ratio Combining 17

2.3 Channel Estimation 18

2.3.1 Pilot Symbol Assisted Modulation 19

2.3.2 Estimator Error 21

2.4 Modulation and Demodulation Scheme 21

2.4.1 Binary Phase Shift Keying 23

2.4.2 Quadrature Phase Shift Keying 25

2.4.3 M-ary Quadrature Amplitude Modulation 28

2.5 Performance Analysis of Different Modulations with Perfect Channel Estimation 32

2.5.1 BER of BPSK 33

2.5.2 BER of QPSK 35

2.5.3 BER of Quadrature Amplitude Modulation 35

3 Approximate Analysis of the BER Performance with Channel Estimation Error **39**

3.1 Review of Tang et. al's Results 40

3.2 Review of Tomiuk's Result 41

3.2.1 Problems in Tomiuk's Paper Related to Gans' Results 42

4 BER Analysis with Channel Estimation Error **44**

4.1 System and Channel Model 44

4.1.1 Derivation of the Second-Order Joint Moment of g and $\hat{g}$ 45

4.1.2 Derivation of the variance of the channel estimate, $\sigma_{\hat{x}}^2$ 46

4.1.3 Derivation of Correlation Coefficient of g and $\hat{g}$ 47

4.2 BER Analysis of BPSK with Channel Estimation Error 47

4.3 BER Analysis of QPSK with Channel Estimation Error 52

4.4 BER Analysis of 16-QAM with Channel Estimation Error 54

5 BER Analysis of Diversity with Channel Estimation Error **60**

5.1 BER Analysis of Diversity BPSK with Channel Estimation Error 61

5.2 BER Analysis of Diversity QPSK with Channel Estimation Error 64

5.3 BER Analysis of Diversity 16-QAM with Channel Estimation Error 65

6 Numerical Examples and Discussion **69**

6.1 Numerical Examples 69

6.2 Discussion of the Relationships Among the Average BER, the Correlation Coefficient and the Symbol Locations 70
6.3 Selection of Window Functions for Channel Estimation/Interpolation 93

7 Conclusions **104**

List of Tables

4.1 Coefficients in the BER Expression (4.30) and (5.26) for 16-QAM 57

6.1 BER of BPSK, QPSK and 16-QAM with single branch reception 102

6.2 BER of 16-QAM with a rectangular window applied to the sinc interpolator 103

List of Figures

2.1 The PSAM system block diagram (after [1, Fig. 1]). 19

2.2 The PSAM system frame format (after [1, Fig. 7]) 19

2.3 Basic elements of a digital communication system (after [2, Fig. 1-1-1]). . . 22

2.4 A BPSK signal constellation (after [3, Fig. 4.1]). 24

2.5 A BPSK modulator (after [3, Fig. 4.3(a)]). 24

2.6 A BPSK demodulator (after [3, Fig. 4.3(b)]). 25

2.7 A QPSK signal constellation (after [3, Fig. 4.18]). 27

2.8 A QPSK modulator (after [3, Fig. 4.20(a)]). 27

2.9 A QPSK demodulator (after [3, Fig. 4.20(b)]). 28

2.10 The 16-QAM signaling constellation with Gray encoding (after [1, Fig.3]). The decision distance is denoted as d. 30

2.11 The 16-QAM I and Q bit Demappings (after [1, Fig.5]). 30

2.12 A QAM modulator (after [3, Fig. 8.8]). 31

2.13 A QAM demodulator. 32

4.1 New decision component set by the imperfect estimate. The parameters, α, θ are the amplitude and phase shift of the channel, respectively; $\hat{\theta}$ is the phase estimate and φ is the phase error between θ and $\hat{\theta}$. 49

4.2 New decision component set by the imperfect estimate and cross-quadrature interference. 53

4.3 New decision boundaries set by the imperfect estimate. The coordinates are those relative to the rotated signal constellation. 55

4.4 Cross-quadrature interferences due to imperfect estimation. 55

6.1 The BER performance of BPSK for $l = 8$ with a Hamming window applied to the sinc interpolator for $L = 15$, $K = 30$, and $f_D T_s = 0.03$; the parameter, l, is the symbol location in one frame. 71

6.2 The BER performance of QPSK for $l = 8$ with a Hamming window applied to the sinc interpolator for $L = 15$, $K = 30$, and $f_D T_s = 0.03$; the parameter, l, is the symbol location in one frame. 72

6.3 The BER performance of 16-QAM for $l = 8$ with a Hamming window applied to the sinc interpolator for $L = 15$, $K = 30$, and $f_D T_s = 0.03$; the parameter, l, is the symbol location in one frame. 73

6.4 Relationship between the covariance, Rc, and symbol location, l, for a Hamming window applied to the sinc interpolator. 77

6.5 Relationship between the square root of the variance of the channel estimate of 16-QAM, $\sigma_{\hat{x}}$, and symbol location, l, for a Hamming window applied to the sinc interpolator for fixed values of SNR per bit of 10 dB, 12 dB, 14 dB and 15 dB. 78

6.6 Relationship between the square root of the variance of the channel estimate of 16-QAM, $\sigma_{\hat{x}}$, and symbol location, l, for a Hamming window applied to the sinc interpolator for fixed values of SNR per bit of 35 dB, 37 dB, 39 dB and 40 dB. 79

6.7 Relationship between the correlation coefficient between the channel and the channel estimate of 16-QAM, ρ, and symbol location, l, for a Hamming window applied to the sinc interpolator for fixed values of SNR per bit of 10 dB, 12 dB, 14 dB and 15 dB. 80

6.8 Relationship between the correlation coefficient between the channel and the channel estimate of 16-QAM, ρ, and symbol location, l, for a Hamming window applied to the sinc interpolator for fixed values of SNR per bit of 35 dB, 37 dB, 39 dB and 40 dB. 81

6.9 The BER performance of 16-QAM for $l = 1$ and $l = 8$ with a Hamming windowing applied to the sinc interpolator for $L = 15$, $K = 30$, and $f_D T_s = 0.03$; M is the number of diversity branches and l is the symbol location in one frame. 82

6.10 The BER performance of BPSK for $l = 1$ and $l = 8$ with a Hamming window applied to the sinc interpolator for $L = 15$, $K = 30$, and $f_D T_s = 0.03$; the parameter, l, is the symbol location in one frame. 83

6.11 Relationship between the square root of the variance of the channel estimate of BPSK, $\sigma_{\hat{x}}$, and symbol location, l, for a Hamming window applied to the sinc interpolator for fixed values of SNR per bit of 10 dB, 12 dB, 14 dB and 15 dB. 84

6.12 Relationship between the square root of the variance of the channel estimate of BPSK, $\sigma_{\hat{x}}$, and symbol location, l, for a Hamming window applied to the sinc interpolator for fixed values of SNR per bit of 35 dB, 37 dB, 39 dB and 40 dB. 85

6.13 Relationship between the correlation coefficient between the channel and the channel estimate of BPSK, ρ, and symbol location, l, for a Hamming window applied to the sinc interpolator for fixed values of SNR per bit of 10 dB, 12 dB, 14 dB and 15 dB. 86

6.14 Relationship between the correlation coefficient between the channel and the channel estimate of BPSK, ρ, and symbol location, l, for a Hamming window applied to the sinc interpolator for fixed values of SNR per bit of 35 dB, 37 dB, 39 dB and 40 dB. 87

6.15 The BER performance of QPSK for $l = 1$ and $l = 8$ with a Hamming window applied to the sinc interpolator for $L = 15$, $K = 30$, and $f_D T_s = 0.03$; the parameter, l, is the symbol location in one frame. 88

6.16 Relationship between the square root of the variance of the channel estimate of QPSK, $\sigma_{\hat{x}}$, and symbol location, l, for a Hamming window applied to the sinc interpolator for fixed values of SNR per bit of 10 dB, 12 dB, 14 dB and 15 dB. 89

6.17 Relationship between the square root of the variance of the channel estimate of QPSK, $\sigma_{\hat{x}}$, and symbol location, l, for a Hamming window applied to the sinc interpolator for fixed values of SNR per bit of 35 dB, 37 dB, 39 dB and 40 dB. 90

6.18 Relationship between the correlation coefficient between the channel and the channel estimate of QPSK, ρ, and symbol location, l, for a Hamming window applied to the sinc interpolator for fixed values of SNR per bit of 10 dB, 12 dB, 14 dB and 15 dB. 91

6.19 Relationship between the correlation coefficient between the channel and the channel estimate of QPSK, ρ, and symbol location, l, for a Hamming window applied to the sinc interpolator for fixed values of SNR per bit of 35 dB, 37 dB, 39 dB and 40 dB. 92

6.20 Relationship between the covariance, Rc, and symbol location, l, for a rectangular window applied to the sinc interpolator for fixed values of SNR per bit of 15 dB, 20 dB, 30 dB and 40 dB. 95

6.21 Relationship between the correlation coefficient, ρ, and symbol location, l, for a rectangular window applied to the sinc interpolator for fixed values of SNR per bit of 15 dB, 20 dB, 30 dB and 40 dB. 96

6.22 Relationship between the correlation coefficient, ρ, and symbol location, l, for a Hamming window applied to the sinc interpolator for fixed values of SNR per bit of 30 dB, 32 dB, 35 dB and 40 dB. 97

6.23 The BER performance of 16-QAM with dual-branch diversity and a rectangular window applied to the sinc interpolator for $L = 15$, $K = 30$, and $f_D T_s = 0.03$; M is the number of diversity branches and l is the symbol location in one frame. 98

6.24 The BER performance of 16-QAM with dual-branch diversity and a Hamming window applied to the sinc interpolator for $L = 15$, $K = 30$, and $f_D T_s = 0.03$; M is the number of diversity branches and l is the symbol location in one frame. 99

6.25 The BER performance of single branch 16-QAM for $l = 8$ with different windows applied to the sinc interpolator for $L = 15$, $K = 30$, and $f_D T_s = 0.03$; the parameter, l, is the symbol location in one frame. 100

6.26 The BER performance of MRC 16-QAM for $l = 8$ with different windows applied to the sinc interpolator for $L = 15$, $K = 30$, and $f_D T_s = 0.03$; the parameter, l, is the symbol location in one frame. 101

Acronyms

Acronyms	Definition
AWGN	additive white Gaussian noise
BER	bit error rate
BPSK	binary phase shift keying
EGC	equal gain combining
GPRS	general packet radio service
JPDF	joint probability density function
LSB	least significant bit
MPSK	M-ary phase shift keying shift keying
M-QAM	M-ary quadrature amplitude modulation
MRC	maximal ratio combining
MSB	most significant bit
PDF	probability density function
PSAM	pilot symbol assisted modulation
PSK	phase shift keying
QAM	quadrature amplitude modulation
QPSK	quadrature phase shift keying
SC	selection combining
SER	symbol error rate
SNR	signal-to-noise ratio
TTIB	transparent tone-in-band

WCDMA	wide-band code division multiple access
WSS	wide-sense stationary

List of Symbols

Symbol	Definition
$a(t)$	transmitted binary sequence
A_c	the carrier amplitude
a_i, b_i	a pair of coordinates indicating the signal location in the constellation
B_d	Doppler spread
$cov(x,y)$	covariance of the random variables, x and y.
d	decision distance
$E(x)$	expectation of x
$erf(x)$	error function
E_b	energy per bit
E_{min}	lowest energy signal
E_p	pilot symbol energy
E_s	symbol energy
$f(x)$	pdf of x
f_c	carrier frequency
f_D	maximum Doppler frequency
$g(t)$	complex channel gain
g_k^l	complex channel gain sample at the l_{th} symbol lation in the k_{th} data frame
g_I	in-phase component of the complex channel gain sample
$g_I(t)$	in-phase component of the complex channel gain
g_m	complex channel gain sample of the m_{th} diversity branch

$g_m(t)$	complex channel gain of the m_{th} diversity branch
g_Q	quadrature component of the complex channel gain sample
$g_Q(t)$	quadrature component of the complex channel gain
$\hat{g}_k^l$	complex channel gain estimate sample at the l_{th} symbol location in the k_{th} data frame
$\hat{g}_I$	in-phase component of the complex channel gain estimate sample
$\hat{g}_m$	complex channel gain estimate sample of the m_{th} diversity branch
$\hat{g}_Q$	quadrature component of the complex channel gain estimate sample
h_k^l	interpolation coefficient of the estimation filter
I_k	bit transmitted on the in-phase channel
$J_o(\cdot)$	zero-order Bessel function
$\|J\|$	Jacobian
K	total number of the pilots used for one estimate
k_1	total number of the pilots from previous frames
k_2	total number of the pilots from subsequent frames
L	number of symbols in one frame
l	location of a symbol in one frame
m	index of the diversity branch
M	total number of diversity branches
$m(t)$	modulating signal
$m_I(t)$	modulating signal for the in-phase channel
$m_Q(t)$	modulating signal for the quadrature channel
$n(t)$	additive white Gaussian noise
n_k^0	noise sample at the 0_{th} symbol location in the k_{th} data frame
n_k^l	noise sample at the l_{th} symbol location in the k_{th} data frame
n_0	combiner noise output phasor
N_0	instantaneous output noise power
n_m	additive white Gaussian noise sample of the m_{th} diversity branch
$n_m(t)$	additive white Gaussian noise of the m_{th} diversity branch

$p(x,y,\ldots)$	jpdf of x , y and ...
$P_b(e)$	the average probability of bit error in an AWGN channel
$P_b(e\|x,\ldots)$	the probability of bit error conditioned on $x,\ldots$
P_e	the average probability of bit error on a fading channel
p_{Ik}	in-phase component of the channel gain sample of the pilot symbol in the k_{th} data frame
p_k	complex channel gain sample of the pilot symbol in the k_{th} data frame
p_{Qk}	quadrature component of the channel gain sample of the pilot symbol in the k_{th} data frame
$\hat{p}_k$	complex channel gain estimate sample of the pilot symbol in the k_{th} data frame
Q_k	bit transmitted on the quadrature channel
$Q(\cdot)$	Q-function, the area under the tail of the Gaussian pdf
r	received signal sample
R	covariance matrix
R_c	second order joint moment of $g_I(t)$ and $\hat{g}_I(t)$ or $g_Q(t)$ and $\hat{g}_Q(t)$
R_{cs}	second order joint moment of $g_I(t)$ and $\hat{g}_Q(t)$ or $\hat{g}_I(t)$ and $g_Q(t)$
$r(t)$	received signal
r_k^l	received symbol sample at the l_{th} symbol location in the k_{th} data frame
r_{1k}	received I channel component sample
r_{2k}	received Q channel component sample
r_m	received signal sample of the m_{th} diversity branch
$r_m(t)$	received signal of the m_{th} diversity branch
$s(t)$	transmitted signal
s_k^0	transmitted pilot symbol sample at the 0_{th} symbol location in the k_{th} data frame
s_k^l	transmitted symbol sample at the l_{th} symbol location in the k_{th} data frame
s_0	combiner signal output phasor
S_0	instantaneous output signal power
$s_1(t)$	transmitted signal 1
$s_2(t)$	transmitted signal 2

$s_{BPSK}(t)$	transmitted BPSK signal
$s_{QAM}(t)$	transmitted M-QAM signal
$s_{QPSK}(t)$	transmitted QPSK signal
s_w	w_{th} transmitted symbol sample
T	symbol duration
T_b	bit interval
T_m	reciprocal of the multipath spread
W	total number of symbols represented for one modulation scheme
x_{c1}, x_{c2}	in-phase component of the complex Gaussian variable at time t and $t+\tau$
x_{s1}, x_{s2}	quadrature component of the complex Gaussian variable at time t and $t+\tau$
α	channel attenuation sample
$\alpha(t)$	channel attenuation process
α_k^l	channel amplitude sample at the l_{th} symbol location in the k_{th} data frame
α_m	channel attenuation sample of the m_{th} diversity branch
α_t	channel attenuation sample at time t
$\alpha_{t+\tau}$	channel attenuation sample at time $t+\tau$
$\hat{\alpha}$	channel amplitude estimate sample
$\hat{\alpha}_m$	channel amplitude estimate sample of the m_{th} diversity branch
$\hat{\alpha}_k^l$	channel amplitude estimate sample at the l_{th} symbol location in the k_{th} data frame
γ	output SNR
γ_b	SNR per bit
γ_m	instantaneous SNR of the m_{th} diversity branch
$\bar{\gamma}_b$	average SNR per bit
$\bar{\gamma}_c$	average SNR per channel
$\hat{\theta}$	channel phase shift estimate sample
$\hat{\theta}_m$	channel phase shift estimate sample of the m_{th} diversity branch
$\hat{\theta}_k^l$	channel phase shift estimate sample at the l_{th} symbol location in the k_{th} data frame
θ	channel phase shift sample
$\theta(t)$	channel phase shift process

θ_k^l	channel phase shift sample at the l_{th} symbol location in the k_{th} data frame
θ_m	channel phase shift sample of the m_{th} diversity branch
θ_t	channel phase shift sample at time t
$\theta_{t+\tau}$	channel phase shift sample at time $t+\tau$
φ	phase difference between the channel phase shift and its estimate
φ_m	phase difference on the m_{th} diversity branch
$\phi_c(\tau)$	auto-correlation function of $g_I(t)$ and $g_Q(t)$
$\phi_{cs}(\tau)$	cross-correlation function of $g_I(t)$ and $g_Q(t)$
ρ	correlation coefficient between two random variables
$\sigma_{\hat{x}}^2$	variance of the channel estimate gain in both the real and the imaginary part
σ_{mn}^2	variance of AWGN in both the real and the imaginary part of the m_{th} diversity branch
σ_n^2	variance of AWGN in both the real and the imaginary part
σ_{x^2}	variance of the variable, x
σ_x^2	variance of the channel gain in both the real and the imaginary part
Δf_c	coherence bandwidth
Δt_c	coherence time

Chapter 1

Introduction

1.1 Background and Motivation

Since Dec. 12, 1901, when Marconi first successfully demonstrated that wireless signals could be transmitted across the Atlantic and Pacific Oceans, the wireless communication industry has experienced an exciting, fast growing and fertile century. However, the customers' requirements for wireless communication today are not merely long distance coverage, but rather flexibility, high data rate and high quality of service. In this market-driven and profit-driven world, these become an irresistible power and guide for the development of the wireless industry. Within just three decades, we have witnessed the births of a number of high technologies. The first generation(1G) wireless communication emerged in the early 1970's. It was analog and had limited quality voice service with fairly low data transmission speed, 9.6kbs(bit/sec). It is still used in some parts of the world. The second generation(2G) digital wireless system first came into service in the 1980's. It was widely spread throughout the world during the 1990's and offered good quality digital voice service. However it only supports a very low data transmission rate-14.4kbs. The so-called 2.5G wireless system (a wireless system that arose in the transition period between 2G and 3G) began commercial operation at the beginning of 21st century. It provides relatively a high data transmission rate. For example, GPRS(General Packet Radio Service),

one of the 2.5G systems, will deliver real world speeds between 30 kbps and 45 kbps. The third generation (3G) wireless system has been a hot topic since the late 1990's. It promises significantly higher data rates (up to 2Mbits/sec) with attractive multimedia services, such as web browsing, movie downloading and video conferencing. Researchers are now heading to 4G systems. However, there are huge challenges behind this fast-growing industry. Besides the demands of high-speed hardwares and other related technologies, the larger needs for larger capacity, better quality, more bandwidth, higher transmission rate and lower power consumption, etc. are always concerns for the development of wireless communication systems. All these problems mentioned remain as technical challenges due to the hostile wireless environment.

One of the critical technical bottlenecks in a wireless system is the unstable transmission quality due to the time variation of the channel, the multipath propagation and the severe interference from other users, neighboring cells and other sources. All of these affect the capacity of wireless channels. The bit error rate(BER) is an important parameter that indicates the quality of the system performance. It has been studied in many researches. Reference [4] gives the BER of 16-ary quadrature amplitude modulation(16-QAM) and 64-QAM over both the additive white Gaussian noise (AWGN) channel and the Rayleigh fading channel without diversity. A recursive algorithm for computing the BER of M-QAM constellations over an AWGN channel was given in [5]. More work has focused on the system performance with diversity techniques used to compensate for the fading caused by the multipath propagation. Reference [6] provided a unified and convenient method to derive the symbol error rate(SER) and BER for M-ary phase shift keying(MPSK) signals with maximal ratio combining(MRC) diversity and selection combining(SC) diversity. Reference [7] presented the SER of M-QAM with MRC diversity and SC diversity in Rayleigh fading channels. In [8], precise analytical expressions for the SER of MRC and equal gain combining (EGC) in Nakagami fading channels were derived. Reference [9] gave a thorough study of the performances of two-dimensional signaling schemes. The SER of MPSK and M-QAM on Rayleigh, Ricean and Nakagami fading channels with MRC, EGC and SC can be derived using the method proposed. A unified approach to performance analysis in

digital communication over generalized fading channels was presented in [10]. The SER for MPSK and M-QAM with MRC reception was given in terms of alternate forms of the Q-functions, widely used in communication theory [10].

Note that , references [4]- [10] assume that perfect channel state information is available to the receivers. Meanwhile, the performances of coherent demodulation and coherent combining can be severely degraded if good fading channel state information is not available as shown in [11]. Study of a variable-rate, variable-power M-QAM in [12] also showed the sensitivity of the error rate of M-QAM to estimation error. Thus, accurate channel estimation is required for proper system operation.

Performance analysis including consideration of estimation error is thus an open and important topic. Proakis, in 1968, proposed the method to calculate the BER performance for MPSK with MRC and estimation error in Rayleigh and Rician fading channel [13] . Reference [14] proposed a general form BER expression with MRC diversity including the effects of weighting errors. Pilot symbol assisted modulation (PSAM) has proved to be an effective method for channel estimation [15], [16] and there is some previous work on the system performance when using PSAM for channel estimation. Reference [15] obtains analytical expressions for the BER in binary phase shift keying(BPSK) and quadrature phase shift keying(QPSK), as well as a tight upper bound on the SER in 16-QAM. Reference [17] gives simple upper bounds for the SER of M-QAM over a Rayleigh fading channel in the presence of channel estimation error and the approximate BER of M-QAM with imperfect channel estimation has been derived in [1]. None of references [1], [11], [12] and [15]- [17] considered diversity.

In this thesis, we will study the system performance including consideration of the channel impairments, such as fading and multipath dispersion which can be characterized by the Doppler spread, (Rayleigh, Rician and Nakagami) amplitude probability densities, the coherence bandwidth and so on. The influence of diversity reception, one of the fundamental methods for tackling the fading problem, is also investigated with estimation error considered in both combining and demodulation. Besides the performance analysis of the basic modulation schemes, like BPSK and QPSK, we research high capacity M-QAM. Im-

portantly, M-QAM, as a higher-order modulation format, can transmit more information for a given bandwidth than do lower-order modulations, though its employment requires accurate channel state information. It is, therefore, a good choice for achieving high capacity in fading channels if the channel information can be accurately estimated

1.2 Thesis Outline and Contributions

This thesis is organized as follows. In Chapter 2, we review in detail all the required background knowledge needed in this thesis. The characteristics, including first-order distribution and second-order distribution, of the fading channel are introduced first. The principle of MRC diversity is presented second. The mechanism of the PSAM system is described afterwards, as well as that of the estimation error. Last, we introduce the modulation and demodulation schemes of BPSK, QPSK and M-QAM. The BER performance analysis associated with these modulation and demodulation schemes are also presented for both non-diversity and diversity cases with the assumption of coherent diversity combining and demodulation. To the best of the authors' knowledge, the BER expression for MRC 16-QAM with perfect estimation that is derived is new in the literature.

We will present reviews of the two papers, [1] and [14], in Chapter 3 to clarify the limitations and the approximate analytical approach used there. Reference [1] derives the BER of 16-QAM and 64-QAM using PSAM to provide the channel estimates for single branch reception in a Rayleigh fading channel, assuming that the joint probability density function(jpdf) of the channel amplitude and its estimate are independent of the jpdf of the channel phase shift and its estimate. Reference [14] gives a general form for the BER of an arbitrary modulation format with MRC in slow fading with weighting (channel estimation) errors, assuming that the conditional BER with channel estimation error depends only on the signa-to-noise ratio(SNR) of the received signal and is independent of the phase error. Both of these results are approximations.

In Chapter 4, we first describe the system model deployed in this thesis and derive some important parameters of the system. They are the second-order joint moment between the

channel and the channel estimate, the variance of the channel estimate, and the cross coefficient of the channel and the channel estimate. Then, the conditional probability of errors for BPSK, QPSK and 16-QAM with channel estimation error and quadrature interference caused by imperfect estimation are derived along with the jpdf of the channel amplitude, the channel amplitude estimate, and the phase error between the channel phase and its estimate. The performance analysis for single branch reception of BPSK, QPSK and 16-QAM with channel estimation error proceeds by averaging the conditional probability of error over the jpdf of the channel amplitude, the channel amplitude estimate, and the phase error between the channel phase and its estimate. A new method for calculating the BER for diversity combining with estimation error is presented in Chapter 5. The exact BER expressions for MRC BPSK, QPSK and 16-QAM with estimation error are derived. This method can be also used for M-QAM. To the best of the authors' knowledge, these results are new in the literature.

Some examples calculated using our theoretical results are presented and discussed in Chapter 6. Simulation results are also presented for verification. The effects of the imperfect channel estimation on the diversity system performance are studied. Both noise and estimator decorrelation effects on BER are examined for different symbol locations. Last, we investigate the influences on the BER of different selections of window functions for the channel interpolator.

Chapter 7 concludes the thesis with a summary of contributions.

Chapter 2

Literature Review

In this chapter, all the background knowledge needed in this thesis will be reviewed in detail. We first introduce the characteristics of the fading channels. MRC diversity, a well-known optimal diversity technique to mitigate the influence of fading, is described afterwards. The mechanism of the PSAM system is presented as well as the causes of estimation error. Following the introduction of the BPSK, QPSK, 16-QAM modulation and demodulation mechanisms, the BER performance analysis for both non-diversity and diversity BPSK, QPSK and 16-QAM are given with the assumption of coherent diversity combining and demodulation.

2.1 Fading channels

Propagation models that predict the mean signal strength for an arbitrary transmitter-receiver (T-R) separation distance are called large-scale propagation models. Propagation models that characterize the rapid fluctuations of the received signal strength over very short time durations are called small-scale or fading models [18]. In this thesis, we will focus on the small-scale, simply, the fading models. When a steady-state, single-frequency radio wave is transmitted over a long path, due to the reflection, scattering and diffraction from various objects, there will be two or more versions of the transmitted signal which arrive at the receiver at slightly different times. These waves are called multipath waves [19], [20].

Constructive or destructive summation of the multipath waves at the receiver side that leads to the fluctuation of the envelope amplitude of the received signal in time is called fading. It is primarily caused by the time variations in the phases [2]. Associated with each path is a phase shift and a amplitude attenuation factor. Both of them are time-variant as a result of changes in the structure of the medium.

The fading can be categorized into four different types, flat fading, frequency selective fading, slow fading and fast fading. Depending on how fast the transmitted signal changes as compared to the changes of the channel, a channel can be classified either as slow fading or fast fading. The time dispersion due to the transmission delay of the multipath waves determines whether the transmitted signal experiences flat or frequency selective fading. Importantly, time selectivity and frequency selectivity of the fading channel are independent of each other [18].

Slow fading and fast fading, both are small scale fading based on the Doppler spread. There are clear explanations of the origins of them, but no accurate threshold to distinguish slow fading from fast fading. The most common explanations of the terms can be found in several references [18], [2], [21]. When the channel impulse response changes at a rate much slower than the transmitted baseband signal, it is called slow fading [18], otherwise, fast fading. There is an alternative explanation in [2]. When the condition $T << (\Delta t)_c$ holds, the channel is called a slow fading channel, where T is the duration of the signal interval, and $(\Delta t)_c$ is the coherence time over which the fading is considered approximately constant. The parameter, $(\Delta t)_c$ is the reciprocal of the Doppler spread, B_d. Since T is smaller than the coherence time of the channel, the channel attenuation and phase shift are essentially fixed for the duration of at least one signal interval. In a fast fading channel, the channel impulse response changes rapidly within the symbol duration. So a signal undergoes fast fading if $T > (\Delta t)_c$. Fast fading can also be called as time selective fading. In this thesis, we assume slow fading in our system model according to the second definition but our models also assume the decorrelation of the channel complex gain from symbol to symbol, which is called moderate fading model in [22].

Flat and frequency selective fading are distinguished by the coherence bandwidth. The

coherence bandwidth, also known as the reciprocal of the multipath spread, T_m, is defined as the bandwidth over which all the frequency components experience the same channel response. The channel is said to be a flat channel when a signal is transmitted through a channel and the bandwidth of the transmitted signal is smaller than the coherence bandwidth, Δf_c; if the bandwidth of the transmitted signal is larger than Δf_c, the channel is said to be a frequency selective channel. A frequency selective channel causes severe distortion to the transmitted signal [2].

The flat fading channel can be referred to as a narrow-band [1] system. When fading affects the narrow-band system, the amplitude of the received signal is mainly decided by the fading attenuation and the transmitted signal. There are many different models for describing the statistical behavior of the multipath fading envelope. The most well known are the Rayleigh model, the Ricean model and the Nakagami-m model. Rayleigh fading models the urban transmission environments and the fading is most commonly caused by random scatterers. Ricean fading models environments that have fading plus a steady line-of-sight signal component, usually caused by fixed scatterers or signal reflectors in the medium in addition to the random ones [2]. The Nakagami model is used to characterize rapid fading in long distance HF channels and it is known to provide a closer match to some empirical data than either the Rayleigh or Ricean [24]. In this thesis, our work is based on the Rayleigh model. In the following subsections, the first-order distribution and second-order distribution of the Rayleigh fading channel are introduced.

2.1.1 First-Order Distributions

The Rayleigh fading distribution is the most commonly used fading distribution in the wireless communication literature. It have been reported that the envelope of the radio signal is Rayleigh distributed over frequencies from 50 to 11,2000 MHz for some channels

[1] A random process is said to be a narrow-band random process if the width, Δf, of the significant region of its spectral density is small compared to the center frequency f_c of the region [23]

[25]. This empirical data suggests the assumption that the received signal,

$$r(t) = g(t)s(t) + n(t) \tag{2.1}$$

where $g(t)$ is the complex channel gain, $s(t)$ is the transmitted signal and $n(t)$ is the AWGN which is independent of the fading, can be modeled as narrow-band Gaussian random process when there are a large number of paths; thus, the central limit theorem is applied [2]. This will be shown in the following. This also means that the fading channel process, $g(t)$, can be considered as a complex Gaussian random process. Further, $n(t)$ is Gaussian and independent of $g(t)$. It is known that the pdf of the envelop of a narrow-band Gaussian random process satisfies the Rayleigh pdf [23], which is in consistent with the empirical data. The first-order statistical properties of the envelope and the phase of the narrow-band random Gaussian process are studied here. The process, $g(t)$ can be expressed as [24]

$$g(t) = \alpha(t)e^{j\theta(t)} = g_I(t) + jg_Q(t) \tag{2.2}$$

where $\alpha(t)$ is the channel attenuation and $\theta(t)$ is the channel phase shift. It represents the process within the time duration, $0 \leq t \leq T$.

Assumed that the random variables g_I and g_Q, which refer to the possible values of $g_I(t)$ and $g_Q(t)$, are independent Gaussian variables and have zero means and the same variance, σ_x^2. The jpdf is then [23]

$$p(g_I, g_Q) = \frac{1}{2\pi\sigma_x^2} exp\left(-\frac{g_I^2 + g_Q^2}{2\sigma_x^2}\right) \tag{2.3}$$

and

$$E(g_I) = E(g_Q) = 0 \tag{2.4a}$$

$$E(g_I^2) = E(g_Q^2) \triangleq \sigma_x^2. \tag{2.4b}$$

The jpdf of the envelope and phase variables, α and θ, can be obtained by the variable transformation,

$$\alpha = (g_I^2 + g_Q^2)^{1/2} \tag{2.5a}$$

$$\theta = tan^{-1}(g_I, g_Q) \tag{2.5b}$$

$$|J| = \alpha \tag{2.5c}$$

where $tan^{-1}(\cdot,\cdot)$ is the inverse tangent function of two arguments which returns a value of θ in the correct quadrant. Therefore, the joint pdf of α and θ is

$$p(\alpha,\theta) = \begin{cases} \frac{\alpha}{2\pi\sigma_x^2} exp\left(-\frac{\alpha^2}{2\sigma_x^2}\right), & for\ \alpha \geq 0\ and\ 0 \leq \theta < 2\pi \\ 0 & otherwise. \end{cases} \tag{2.6}$$

The pdf's of α and θ are the marginal distribution functions of (2.6), given by

$$f(\alpha) = \begin{cases} \frac{\alpha}{\sigma_x^2} exp\left(-\frac{\alpha^2}{2\sigma_x^2}\right), & for\ \alpha \geq 0 \\ 0 & otherwise \end{cases} \tag{2.7a}$$

$$f(\theta) = \begin{cases} \frac{1}{2\pi} & for\ 0 \leq \theta < 2\pi, \\ 0 & otherwise. \end{cases} \tag{2.7b}$$

The pdf of the envelope, α, is Rayleigh distributed and the pdf of the phase, θ, is uniformly distributed in the range of 0 to 2π. Observing (2.6) and (2.7a), we note that

$$p(\alpha,\theta) = f(\alpha)f(\theta). \tag{2.8}$$

Hence, for the narrow-band Gaussian random process, the envelope and phase are independent random variables.

2.1.2 Second-Order Distributions

In the previous subsection, we studied first-order statistical properties of a narrow-band Gaussian random process. In this subsection, we will introduce the second-order distributions of a Gaussian random process in which we consider the envelope and phase random process at two fixed times. We first define, α_t and $\alpha_{t+\tau}$, θ_t and $\theta_{t+\tau}$ which are envelope and phase variables at time t and $t+\tau$, respectively, in a wide-sense stationary (WSS) gaussian random process. Again, we define four gaussian variables, x_{c1}, x_{s1}, x_{c2} and x_{s2}, where x_{c1} and x_{c2} refer to the values of $g_I(t)$ at time t and $t+\tau$, respectively; x_{s1} and x_{s2} refer to the values of $g_Q(t)$ at time t and $t+\tau$, respectively. The relationships between α_t and θ_t with

x_{c1} and x_{s1}, $\alpha_{t+\tau}$ and $\theta_{t+\tau}$ with x_{c2} and x_{s2} are the same as those of α and θ with g_I and g_Q as shown in (2.5a) and (2.5b). The jpdf of α_t, $\alpha_{t+\tau}$, θ_t and $\theta_{t+\tau}$ can be derived from the jpdf of the four real random variables, x_{c1}, x_{s1}, x_{c2} and x_{s2}, from a complex random process. It is, in fact, a 4-dimensional Gaussian jpdf, which can be expressed as [23, eqn. (8-101)]

$$p(x_{c1},x_{s1},x_{c2},x_{s2}) = \frac{1}{4\pi^2|\wedge|^{1/2}}$$
$$exp\left\{-\frac{[\sigma_x^2(x_{c1}^2+x_{s1}^2+x_{c2}^2+x_{s2}^2)-2\phi_c(\tau)(x_{c1}x_{c2}+x_{s1}x_{s2})-2\phi_{cs}(\tau)(x_{c1}x_{s2}-x_{s1}x_{c2})]}{2|\wedge|^{1/2}}\right\} \tag{2.9a}$$

$$\sigma_x^2 = E[x_{c1}^2] = E[x_{s1}^2] = E[x_{c2}^2] = E[x_{s2}^2] \tag{2.9b}$$

$$\phi_c(\tau) = E[x_{c1}x_{c2}] = E[x_{s1}x_{s2}] \tag{2.9c}$$

$$\phi_{cs}(\tau) = E[x_{c1}x_{s2}] = -E[x_{s1}x_{c2}] \tag{2.9d}$$

$$|\wedge| = [\sigma_x^4 - \phi_c^2(\tau) - \phi_{cs}^2(\tau)]^2 \tag{2.9e}$$

where x_{c1}, x_{s1}, x_{c2} and x_{s2} have same variance, and $\phi_c(\tau)$ and $\phi_{cs}(\tau)$ is the auto-correlation and cross-correlation function, respectively. By the transformation of variables, we can get the jpdf of α_t, $\alpha_{t+\tau}$, θ_t and $\theta_{t+\tau}$. The Jacobian of the transformation from x_{c1}, x_{s1}, x_{c2} and x_{s2} to α_t, $\alpha_{t+\tau}$, θ_t and $\theta_{t+\tau}$ is then [23, eqn. (8-102)]

$$|J| = \alpha_t\alpha_{t+\tau} \tag{2.10}$$

and the jpdf is [23, eqn. (8-102)]

$$p(\alpha_t,\alpha_{t+\tau},\theta_t,\theta_{t+\tau}) = \frac{\alpha_t\alpha_{t+\tau}}{4\pi^2|\wedge|^{1/2}}$$
$$exp\left\{-\frac{[\sigma_x^2(\alpha_t^2+\alpha_{t+\tau}^2)-2\phi_c(\tau)\alpha_t\alpha_{t+\tau}cos(\theta_t-\theta_{t+\tau})-2\phi_{cs}(\tau)\alpha_t\alpha_{t+\tau}sin(\theta_t-\theta_{t+\tau})]}{2|\wedge|^{1/2}}\right\}. \tag{2.11}$$

As we know, the fading channel is time-varying due to the time spreading properties. More practically, it is caused by the motion between the transmitter and the receiver that

results in propagation-path changes [21]. In this thesis, we adopt Clark's 2-D isotropic scattering model [26], so the second-order statistics for fading channel are given by the auto-correlation function and the cross-correlation function [24] [26]

$$\phi_c(\tau) = E[x_{c1}x_{c2}] = E[x_{s1}x_{s2}] = \sigma_x^2 J_0(2\pi f_D \tau) \tag{2.12a}$$

and

$$\phi_{cs}(\tau) = E[x_{c1}x_{s2}] = -E[x_{c2}x_{s1}] = 0 \tag{2.12b}$$

respectively, where $J_0(\cdot)$ is the zero-order Bessel function of the first kind [27] and f_D is the maximum Doppler frequency.

The joint pdf of α_t and $\alpha_{t+\tau}$ can be obtained by integrating (2.11) over θ_t and $\theta_{t+\tau}$; the joint pdf of θ_t and $\theta_{t+\tau}$ can be obtained by integrating (2.11) over α_t and $\alpha_{t+\tau}$. The results are as follows [23, eqn. (8-103), eqn. (8-104)and (8-106)]

$$p(\alpha_t, \alpha_{t+\tau}) = \frac{\alpha_t \alpha_{t+\tau}}{|\wedge|^{1/2}} I_0\left(\frac{\alpha_t \alpha_{t+\tau}(\phi_c(\tau)^2 + \phi_{cs}(\tau)^2)}{|\wedge|^{1/2}}\right) exp\left[-\frac{\sigma_x^2(\alpha_t^2 + \alpha_{t+\tau}^2)^{1/2}}{2|\wedge|^{1/2}}\right] \tag{2.13a}$$

$$p(\theta_t, \theta_{t+\tau}) = \frac{|\wedge|^{1/2}}{4\pi^2\sigma_x^2}\left[\frac{(1-\beta^2)^{1/2} + \beta(\pi - cos^{-1}\beta)}{(1-\beta^2)^{3/2}}\right] \tag{2.13b}$$

$$\beta = \frac{R_c}{\sigma_x^2} cos(\theta_t - \theta_{t+\tau}) + \frac{R_{cs}}{\sigma_x^2} sin(\theta_t - \theta_{t+\tau}) \tag{2.13c}$$

where $I_0(z)$ is the zero-order modified Bessel function of the first kind [27], $\alpha_t, \alpha_{t+\tau} \geq 0$, $0 \leq \theta_t, \theta_{t+\tau} \leq 2\pi$.

Eqn. (2.11), (2.13a) and (2.13b) show that

$$p(\alpha_t, \alpha_{t+\tau}, \theta_t, \theta_{t+\tau}) \neq p(\alpha_t, \alpha_{t+\tau}) p(\theta_t, \theta_{t+\tau}). \tag{2.14}$$

Thus, (α_t, $\alpha_{t+\tau}$) and (θ_t, $\theta_{t+\tau}$) are not independent. In other words, the envelope process, $\alpha(t)$, and the phase processes, $\theta(t)$, are not independent random process [23] . More importantly, the second-order distribution can be generalized and applied to any two jointly gaussian processes. Here we give two examples of applications, one of which is used in this thesis later. Reference [25] gives the jpdf of the envelopes and the phases for two signals

with different frequencies but transmitting on the same path within a certain time. If the frequency separation is within the coherence bandwidth, the two signals are correlated, otherwise independent. The statistical studies of this model are useful for the analysis of the correlation of the envelopes and the correlation of the phases in terms of the delay spreads and frequency separation. Further, it can be used to assess the performance and limitations of different modulation and diversity schemes [25]. In this thesis, we derive a jpdf of two Gaussian complex variables, $\hat{g}_I$ and $\hat{g}_Q$, from the complex channel estimation and two Gaussian complex variables, g_I and g_Q, from the complex fading channel gain, which are jointly Gaussian with different variances. It can be used for calculating the performance of different modulation schemes with imperfect channel estimation.

Denote

$$\hat{\alpha} = (\hat{g}_I^2 + \hat{g}_Q^2)^{1/2} \tag{2.15a}$$

$$\hat{\theta} = tan^{-1}(\hat{g}_I, \hat{g}_Q) \tag{2.15b}$$

$$\varphi = \theta - \hat{\theta} \tag{2.15c}$$

and assume that

$$E(\hat{g}_I) = E(\hat{g}_Q) = 0 \tag{2.16a}$$

$$E(\hat{g}_I^2) = E(\hat{g}_Q^2) = \sigma_{\hat{x}}^2 \tag{2.16b}$$

where $\hat{\alpha}$ is the amplitude of the channel estimation sample, α is the amplitude of the fading channel sample, φ is the phase difference between the channel estimation phase, $\hat{\theta}$, and the fading channel phase, θ. The parameters, α and θ follow the definitions in (2.5a), (2.5b). Following the derivation for the jpdf of N Gaussian real random variables [23, eqn. (8-46)] and the same method for the jpdf of the amplitude and the phase random process, we derive the jpdf of the envelopes and phases for the channel estimation and the fading channel. The

jpdf of g_I, g_Q, $\hat{g}_I$ and $\hat{g}_Q$ is

$$p(g_I, g_Q, \hat{g}_I, \hat{g}_Q) = \frac{1}{4\pi^2 |\wedge|^{1/2}}$$
$$exp\left\{ -\frac{\left[\sigma_{\hat{x}}^2(g_I^2 + g_Q^2) + \sigma_x^2(\hat{g}_I^2 + \hat{g}_Q^2) - 2R_c(g_I\hat{g}_I + g_Q\hat{g}_Q) - 2R_{cs}(g_I\hat{g}_Q - \hat{g}_I g_Q)\right]}{2|\wedge|^{1/2}} \right\} \tag{2.17a}$$

where

$$R_c = E[g_I\hat{g}_I] = E[g_Q\hat{g}_Q] \tag{2.17b}$$
$$R_{cs} = E[g_I\hat{g}_Q] = -E[\hat{g}_I g_Q] \tag{2.17c}$$
$$|\wedge| = [\sigma_x^2\sigma_{\hat{x}}^2 - R_c^2 - R_{cs}^2]^2, \tag{2.17d}$$

where R_c is the second-order joint moment(or cross moment) of the joint probability distribution of the random variables [23], g_I and $\hat{g}_I$, and g_Q and $\hat{g}_Q$, R_{cs} is the second-order joint moment of the variables, g_I and $\hat{g}_Q$, and the negative value of that of $\hat{g}_I$ and g_Q. As we know, if the random variables have zero means, their covariances are equal to their second-order joint moments. In this thesis, all the Gaussian variables are zero mean due to Rayleigh fading assumption. Thus, calculating the second-order joint moments equivalent calculating the covariances, which are required for the jpdf for the N Gaussian random variables. Applying the variable transformation from g_I, g_Q, $\hat{g}_I$ and $\hat{g}_Q$ to $\hat{\alpha}$, $\hat{\alpha}$ and φ, the Jocobian is $|J| = \alpha\hat{\alpha}$. The jpdf of $\hat{\alpha}$, $\hat{\alpha}$ and φ is then

$$p(\alpha, \hat{\alpha}, \varphi) = \frac{\alpha\hat{\alpha}}{2\pi|\wedge|^{1/2}} exp\left\{ -\frac{\left[\sigma_{\hat{x}}^2\alpha^2 + \sigma_x^2\hat{\alpha}^2 - 2R_c\alpha\hat{\alpha}cos\varphi - 2R_{cs}\alpha\hat{\alpha}sin\varphi\right]}{2|\wedge|^{1/2}} \right\}. \tag{2.18}$$

2.2 Diversity

In the previous section, we introduced the fading channel, a very important phenomena in wireless communication, which causes a severe performance degradation especially in the Rayleigh fading case. Diversity combining techniques are, thus, adopted and later widely studied and used in order to overcome the system degradation caused by deep fades.

Generally speaking, the term "diversity" refers to a system in which several closely similar copies of desired signals are available, all of which experience independent fading to avoid the deep fades, thus to improve the system performance as well as the SNR. It can be classified as microscopic diversity and macroscopic diversity corresponding to the small-scale fading and large-scale fading, respectively. Microscopic diversity deals with the rapidly changing signal to mitigate the deep fades caused by multiple reflections [18]; macroscopic diversity is used to overcome the long term log-normal shadowing. In this thesis, we concentrate on microscopic diversity. An alternative to classify the diversity technique is based on the propagation mechanisms. There are space diversity, frequency diversity, time diversity and polarization diversity. The most common diversity technique is space diversity [28]. It is achieved by using multiple receiver antennas. The spatial separations between the multiple antennas are chosen so that the diversity branches experience uncorrelated fading. Frequency diversity transmits the same signal by using multiple channels that are separated by at least the coherence bandwidth of the channel [3]. Time diversity is obtained by using multiple time slots that are separated by at least the coherence time of the channel [10]. Polarization diversity exploits the property that a scattering environment tends to depolarize a signal; receiver antennas having different polarizations can be used to obtain diversity [3].

Diversity combining refers to the method by which the signals from the diversity branches are combined. It can be classed in two groups, predetection diversity and postdetection diversity [19]. Diversity combining that takes place before detection refers to predetection diversity; diversity combining that takes place after detection is named postdetection diversity. Alternatively, we can say that the diversity combining that takes place at RF is called predetection combining and that takes place at baseband is called postdetection combining [24]. Each can use one of the combining methods, like SC, MRC, and EGC. With ideal coherent detection, there is no difference in performance between predetection diversity and postdetection diversity. However, in real systems, the performance will be different due to different factors. In this thesis, we consider the baseband signals. The received

baseband equivalent signal for the m_{th} diversity branch can be expressed as

$$r_m(t) = g_m(t)s(t) + n_m(t) \tag{2.19}$$

where $g_m(t)$ is the complex channel gain, $s(t)$ is the transmitted signal and $n_m(t)$ is AWGN. Assuming perfect symbol timing recovery, the received signal sample on the m_{th} diversity branch is then

$$r_m = g_m s + n_m \tag{2.20a}$$

$$g_m = \alpha_m e^{j\theta_m} \tag{2.20b}$$

where g_m is the complex channel gain sample with the amplitude sample, α_m, and phase sample, θ_m, s is the transmitted signal sample and n_m is the AWGN sample. The most general linear combining output of M diversity branches can be expressed as [29]

$$r(t) = \sum_{m=0}^{M-1} \hat{g}_m^* r_m(t) \tag{2.21}$$

where the $\hat{g}_m$ are complex weighting factors. The received signal sample as a sum of M branches is

$$r = \sum_{m=0}^{M-1} \hat{g}_m^* r_m = \sum_{m=0}^{M-1} \hat{g}_m^* g_m s + \sum_{m=0}^{M-1} \hat{g}_m^* n_m \tag{2.22}$$

Define the combiner signal output phasor s_0 and the noise output phasor n_0

$$s_0 = \sum_{m=0}^{M-1} \hat{g}_m^* g_m s \tag{2.23a}$$

$$n_0 = \sum_{m=0}^{M-1} \hat{g}_m^* n_m. \tag{2.23b}$$

In this thesis, we assume that the fadings of all the diversity branches are independent of each other and the noise of each branch is independent of the signal as well as of the noise on other branches. As MRC is used for the performance analysis in this thesis, we will introduce MRC in detail in the following subsection.

2.2.1 Maximal ratio Combining

Maximal ratio combining has been proved to be the optimum combiner [28] in the sense of maximum combiner output SNR under conditions of perfect channel estimation. It was proven in [19] using the Schwarz inequality that (4.9) achieves the maximum when

$$\hat{g}_m = \frac{\alpha_m e^{j\theta_m}}{2\sigma_{mn}^2} \tag{2.24}$$

where σ_{mn}^2 is the noise power (equivalent to the variance) of the m_{th} branch in both the real and imaginary parts. Eqn.(2.24) indicates that the channel information is perfectly known. Further, we assume the noise power of all the branches are equal, defined as σ_n^2. Putting (2.20b) and (2.24) in (2.23a), we get

$$s_0 = \sum_{m=0}^{M-1} \frac{\alpha_m^2 s}{2\sigma_n^2} \tag{2.25a}$$

$$n_0 = \sum_{m=0}^{M-1} \frac{\alpha_m e^{-j\theta_m}}{2\sigma_n^2} n_m \tag{2.25b}$$

so that the instantaneous output signal and noise powers are

$$S_0 = \frac{1}{2}\left(\sum_{m=0}^{M-1} \frac{\alpha_m^2 s}{2\sigma_n^2}\right)^2 \tag{2.26a}$$

$$N_0 = \sigma_n^2 \sum_{m=0}^{M-1} \left(\frac{\alpha_m}{2\sigma_n^2}\right)^2. \tag{2.26b}$$

Thus, the output SNR is given by

$$\gamma = \frac{S_0}{N_0} = \sum_{m=0}^{M-1} \frac{(\alpha_m s)^2}{2\sigma_n^2} = \sum_{m=0}^{M-1} \gamma_m \tag{2.27}$$

where γ_m is the instantaneous SNR of the m_{th} diversity branch. Practically, the fading gains of the various diversity branches typically have some degree of correlation. For analytical convenience, it is assumed that the diversity branches are uncorrelated. However, branch correlation reduces the achievable diversity gain and therefore, the uncorrelated branch assumption gives optimistic results [24].

In a Rayleigh fading channel, the output SNR for MRC with perfectly known channel attenuation and phase shift has a chi-square distribution with $2M$ degrees of freedom. The pdf of the output SNR is given in [2, eqn.(14.3-7)] as

$$p(\gamma) = \frac{1}{(M-1)!\bar{\gamma}_c^M}\gamma^{M-1}e^{-\gamma/\bar{\gamma}_c} \tag{2.28}$$

where $\bar{\gamma}_c$ is the average SNR per channel.

2.3 Channel Estimation

Channel fading is a crucial problem in digital communication. If the state the channel fading is not known, coherent demodulation and diversity combining are severely impaired. Thus, channel estimation turns out to be important. It helps to reduce the BER and attenuate the error floor caused by fading. There are two practical and powerful methods proposed and used in the field, one is transparent tone-in-band (TTIB), the other is PSAM. The TTIB scheme inserts a pilot tone within the spectrum of the transmitted signal [4]. The pilot tone is assigned with the carrier frequency and thus provides the receiver a relatively straightforward recovery frequency for the receiver. Moreover, it offers the information of the channel attenuation and phase shift to the receiver. However, it is only workable when the pilot tone and the additional transmitted signal experience a flat fading channel. Other disadvantages are the extra bandwith required, extra power required and complicated implementation. On the other hand, PSAM has proved to be an effective method for channel estimation. In PSAM, the receiver estimates the channel state by using pilot symbols periodically inserted into the data sequence, thus reducing the effect of channel fading in digital communication. However, inserting the pilot symbols introduces some side effects, such as reduced data throughput due to the overhead for the pilot symbols, less energy for the information symbols due to energy consumed for the pilot symbols and computation complexity. This has lead to to the studies and researches on the optimization of the PSAM parameters as well as on good performance interpolation methods with relatively simple implementations. In the following subsection, an introduction of PSAM will be given.

2.3.1 Pilot Symbol Assisted Modulation

A block diagram of the PSAM system structure considered here is shown in Fig. (2.1). The transmitter periodically inserts the known pilot symbols into the data sequence via a multiplexer. Let s_k^l denote the sample of the l_{th} symbol transmitted in the k_{th} data frame. The symbols are formatted into frames of L symbols with the first pilot symbol ($l = 0$) followed by $(L-1)$ data symbols ($1 \le l \le L-1$) as depicted in Fig. (2.2). At the receiver side, the pilot symbols are extracted and input to an estimation/interpolator filter. Thus, knowledge of the channel amplitude and phase at the times of the pilot symbols is used to estimate the channel amplitude and phase at the times of other symbols.

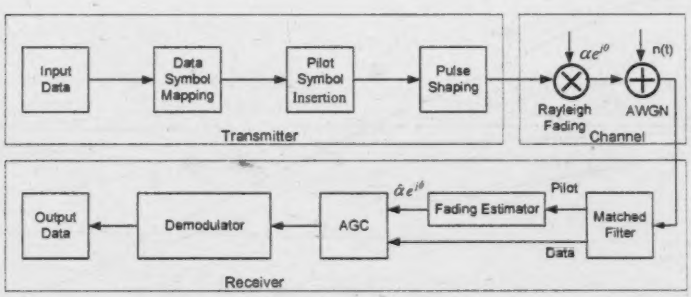

Fig. 2.1. The PSAM system block diagram (after [1, Fig. 1]).

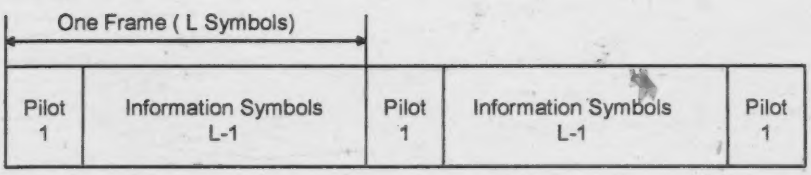

Fig. 2.2. The PSAM system frame format (after [1, Fig. 7]) .

With the symbol interval, T, and perfect symbol timing recovery, the received signal sample at the l_{th} symbol in the k_{th} frame, r_k^l, is given by

$$r_k^l = g_k^l s_k^l + n_k^l \tag{2.29}$$

where $g_k^l = \alpha_k^l e^{j\theta_k^l}$ is the complex channel gain sample with Rayleigh-distributed amplitude sample, α_k^l, and phase sample , θ_k^l, uniformly distributed on $[0, 2\pi)$; s_k^l is the transmitted signal sample and n_k^l is the AWGN sample with variance σ_n in both the real and imaginary parts and is indepedent of the fading. The channel estimate for the k_{th} pilot symbol is given by

$$\hat{p}_k = p_k + \frac{n_k^0}{s_k^0} \tag{2.30}$$

where s_k^0 is the known symbol in the k_{th} frame. The fading at the l_{th} symbol in the k_{th} frame is estimated from K adjacent pilot symbols with k_1 pilot symbols from previous frames, one from the current frame and k_2 pilot symbols from subsequent frames where $k_1 + k_2 + 1 = K$. The estimate is given by

$$\hat{g}_k^l = \hat{\alpha}_k^l e^{j\hat{\theta}_k^l} = \sum_{x=-k_1+k}^{k_2+k} h_x^l \hat{p}_x \tag{2.31}$$

where $h_x^l, l = 0, 1, \ldots, L-1, x = -k_1 + k, \ldots, 0, \ldots, k_2 + k$ are the interpolation coefficients of the estimation filter [16].

From the theory of PSAM, the system graph(Fig. 2.1) as well as eqn. (2.31), we can see that the PSAM technique encounters delay due to prediction and interpolation. It is known that a better channel estimation can be obtained by optimally updating the interpolator's coefficients as well as getting more pilot samples; that means the receiver has to wait and buffer information to give the final result. So, there is a tradeoff between accuracy and processing delay. Several optimal methods have been proposed, which can be categorized into two groups, optimize through: 1) fading estimator (interpolation filter) by changing interpolator size or interpolation coefficients; 2) frame structure by changing the insertion location of the pilot symbol or the frame size.

Most of the studies are based on specific interpolation methods, then deriving the symbol error probability and giving a performance analysis with optimum parameters. Among the proposed first-order linear, low pass, polynomial, Caver's minimum mean squared error linear, and Kim's sinc interpolation schemes, Caver's scheme achieves the optimal performance, but it requires a priori information of the autocorrelation function of the channel gain, Doppler frequency and SNR as well as a huge number of computations [16]. In

contrast, Kim's scheme has close to optimum performance with simple implementations in [30].

2.3.2 Estimator Error

The estimation errors of PSAM are mainly from AWGN and decorrelation between an information symbol and the pilot symbols caused by the time varying fading. The channel information is first obtained from a pilot signal at location $l = 0$ in a frame. Eqn. (2.30) shows the channel estimate for the pilot symbols is corrupted by AWGN. Then, the channel estimate for the l_{th} information symbol in the k_{th} frame is a linear sum of channel estimates for the pilot symbols shown in (2.31). According to (2.12a), there is a cross-correlation between symbols at different locations which is dependent on the location of the information symbols, the transmission rate and the Doppler frequency. Note importantly, that the true value of the channel information for the transmitted symbol has a decorrelation from the pilot symbol without considering the AWGN. Thus, the decorrelation between the channel estimate for the pilot symbol and the true value of the channel information for the transmitted symbol affects the final channel estimate shown in (2.12a) and (2.31) in certain degree.

2.4 Modulation and Demodulation Scheme

Digital modulation is the process by which a baseband signal is moved into a high frequency band that is compatible with the characteristics of the channel [21]. In Fig. 2.3, we can see the digital modulator is the interface that transforms the digital signals into the analog signals that match the channel characteristics [2]. Then, at the receiver side, the transmitted signal must be demodulated to a baseband signal first. Obviously, the function of the digital modulator is to process the channel-corrupted analog signals and recover them into a sequence of numbers [2]. There are several benefits to using digital modulation in the process of signal transmission. For example, it helps to minimize the antenna size by

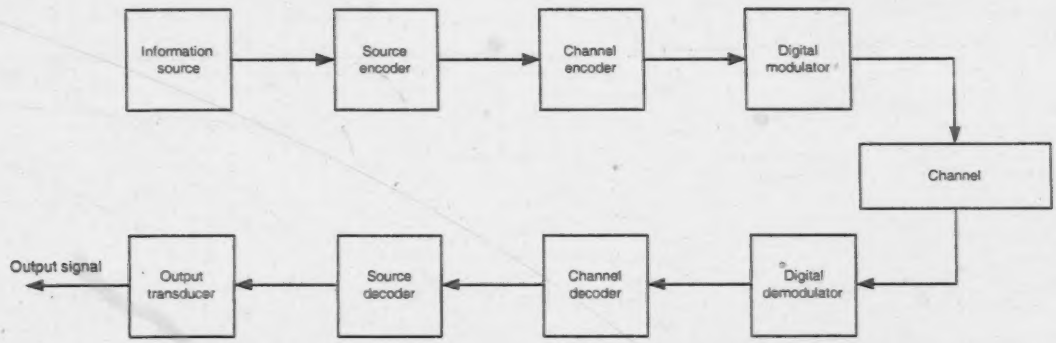

Fig. 2.3. Basic elements of a digital communication system (after [2, Fig. 1-1-1]).

transmitting a signal at high frequency. Also, it can be used to fulfill the frequency division multiplexing by modulating information signals on different carrier frequencies [21]. Here we will introduce two phase shift keying(PSK) modulation schemes, BPSK and QPSK and one multilevel modulation scheme, M-QAM. All of them are linear modulations. Digital modulation techniques can be broadly classified as linear and nonlinear. Linearity of a modulation scheme requires that the amplitude of the transmitted signal varies linearly with the modulating signal [18]. As linear modulation schemes offer high bandwidth and power efficiency, they are very attractive for use in wireless communication. Note that PSK holds a very important role in digital modulation schemes; BPSK and QPSK are the most widely used PSK schemes due to their simplicity and high efficiency [3]. For example, BPSK is adopted as the reverse link modulation for cdma2000 and QPSK is adopted in various systems, like IS-95, wide-band code division multiple access(WCDMA) and the forward link of cdma2000 [24]. Also, M-QAM has gained increasing interest for use in mobile and cellular systems in recent years. It is now used in the WLAN(wireless LAN) netwok. As we know, higher-order, or higher-dimensional modulation formats transmit more information for a given bandwidth than do lower-order modulations. Hence, M-QAM as a two-dimensional modulation scheme provides high capacity which is essential to high transmission rate network.

In the following subsections, both the modulation and demodulation of BPSK, QPSK

and M-QAM will be reviewed. Coherent demodulation is considered which requires the information of the carrier frequency and phase in an AWGN channel. Moreover, channel attenuation and phase shift are required for the fading channel.

2.4.1 Binary Phase Shift Keying

In BPSK, the binary data '1' and '0' can be represented by two signals with constant amplitude but different phases, '0' and 'π', respectively. The signals are [3]

$$s_1(t) = \sqrt{\frac{2E_b}{T_b}} cos 2\pi f_c t, \qquad 0 \le t \le T_b, \text{ for binary '1'} \tag{2.32a}$$

$$\begin{aligned} s_2(t) &= \sqrt{\frac{2E_b}{T_b}} cos(2\pi f_c t + \pi) \\ &= -\sqrt{\frac{2E_b}{T_b}} cos 2\pi f_c t, \qquad 0 \le t \le T_b, \text{for binary '0'} \end{aligned} \tag{2.32b}$$

where $E_b = \frac{1}{2} A_c^2 T_b$ is the energy per bit, A_c is the carrier amplitude, f_c is the carrier frequency and T_b is the bit interval. The constellation is shown in Fig. 2.4. Since $s_1(t) = -s_2(t)$, these signals are called antipodal. They have the same frequency and energy. Besides, another important characteristic of antipodal signals is that they have a correlation coefficient, $\rho = -1$, which leads to a minimum error probability [3].

The implementation of BPSK is very simple. Figs. 2.5 and 2.6 show clearly the modulation and demodulation mechanisms. Denoting the transmitted binary sequence as $a(t)$, where logic '1' maps to binary '1' and logic '-1' maps to binary '0', the resulting signal, $s(t)$ obtained after $a(t)$ passes the modulator can be expressed as

$$s_{BPSK}(t) = a(t)m(t) \tag{2.33}$$

where the modulating signal, $m(t) = \sqrt{\frac{2E_b}{T_b}} cos 2\pi f_c t$, is a sinusoidal function. The received signal can be expressed as

$$r(t) = s(t) + n(t). \tag{2.34}$$

At the receiver side, it first passes the coherent demodulator by multiplying a sinusoidal function with the same frequency as the carrier and then is input to a matched filter or

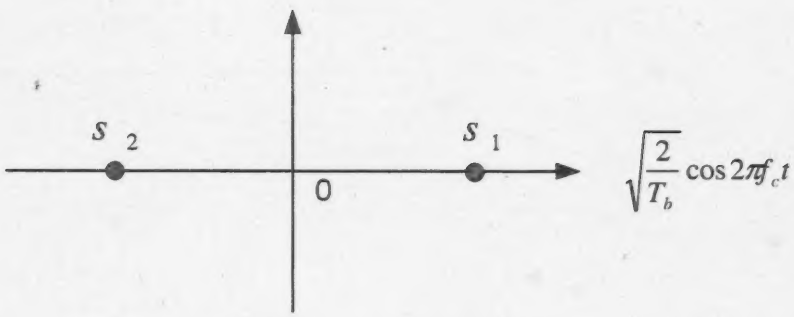

Fig. 2.4. A BPSK signal constellation (after [3, Fig. 4.1]).

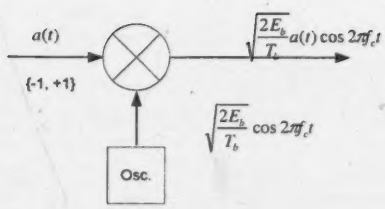

Fig. 2.5. A BPSK modulator (after [3, Fig. 4.3(a)]).

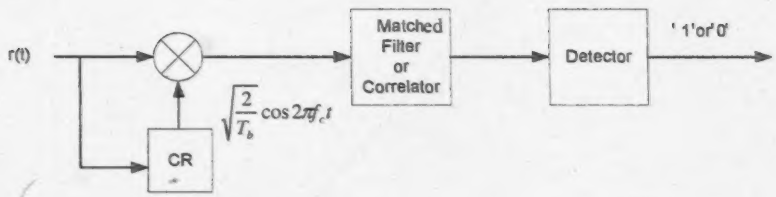

Fig. 2.6. A BPSK demodulator (after [3, Fig. 4.3(b)]).

correlator. The received signal sample is obtained afterwards as

$$r = \sqrt{E_b} + n, \text{ if binary '1' is sent} \tag{2.35a}$$

$$r = -\sqrt{E_b} + n, \text{ if binary '0' is sent} \tag{2.35b}$$

where n is the AWGN sample with variance, σ_n^2, in both the real and imaginary parts. If $r \geq 0$, a binary '1' is declared sent, otherwise a binary '0' is declared sent.

2.4.2 Quadrature Phase Shift Keying

In practice, QPSK is one of the most often used modulation schemes due to its high spectrum efficiency and strong resistance to interference. It can represent four signals with two bits, '00', '01', '11' and '10' corresponding to four different phases, $\pi/4$, $3\pi/4$, $5\pi/4$ and $7\pi/4$. The signals can be expressed as [18]

$$\begin{aligned} s_{QPSK}(t) &= \sqrt{\frac{2E_s}{T}} cos\left[2\pi f_c t + (2i-1)\frac{\pi}{4}\right] \\ &= \sqrt{\frac{2E_s}{T}} cos\left[(2i-1)\frac{\pi}{4}\right] cos(2\pi f_c t) - \sqrt{\frac{2E_s}{T}} sin\left[(2i-1)\frac{\pi}{4}\right] sin(2\pi f_c t), \\ &0 \leq t < T_b,\ i = 1,2,3,4 \end{aligned} \tag{2.36}$$

where E_s is the symbol energy, T is the symbol duration. As

$$cos(2i-1)\frac{\pi}{4} = \pm\frac{1}{\sqrt{2}} \tag{2.37a}$$

$$sin(2i-1)\frac{\pi}{4} = \pm\frac{1}{\sqrt{2}} \tag{2.37b}$$

and denoting

$$I_k = \pm 1 \tag{2.38a}$$

$$Q_k = \pm 1 \tag{2.38b}$$

$$m_I(t) = \sqrt{\frac{E_s}{T}} cos(2\pi f_c t) \tag{2.38c}$$

$$m_Q(t) = \sqrt{\frac{E_s}{T}} sin(2\pi f_c t) \tag{2.38d}$$

where I_k represents the bit transmits on the in-phase(I) channel, Q_k represents the bit transmits on the quadrature(Q) channel and the logic '1' maps to the binary '1', the logic '-1' maps to the binary '0', $m_I(t)$ is the modulating signal for the I channel and $m_Q(t)$ is the modulating signal for the Q channel. Thus, (2.36) can be rewritten as

$$s_{QPSK} = I_k m_I(t) - Q_k m_Q(t). \tag{2.39}$$

The constellation of QPSK with the signal points arranged according to Grey coding is shown in Fig. 6.2. The basic principle of QPSK is very similar to that of BPSK as can be observed by both the constellation and eqn. (2.39). It can be considered as transmitting two BPSK signals at the same time on the in-phase and quadrature channels. As the in-phase and quadrature components are orthogonal to each other, they do not interfere with each other. Thus, QPSK and BPSK have the same bandwidth efficiency and same bit error rate with perfect channel estimation but twice the transmitting rate.

The modulator and demodulator are exhibited in Figs. 2.8 and 2.9. As a QPSK symbol is represented by two bits, tthe bit stream is split into two streams and mapped onto the I and Q channels by multiplying with cosine and sine carriers. At the receiver side, the coherent demodulator demodulates the received signal by multiplying with a cosine and

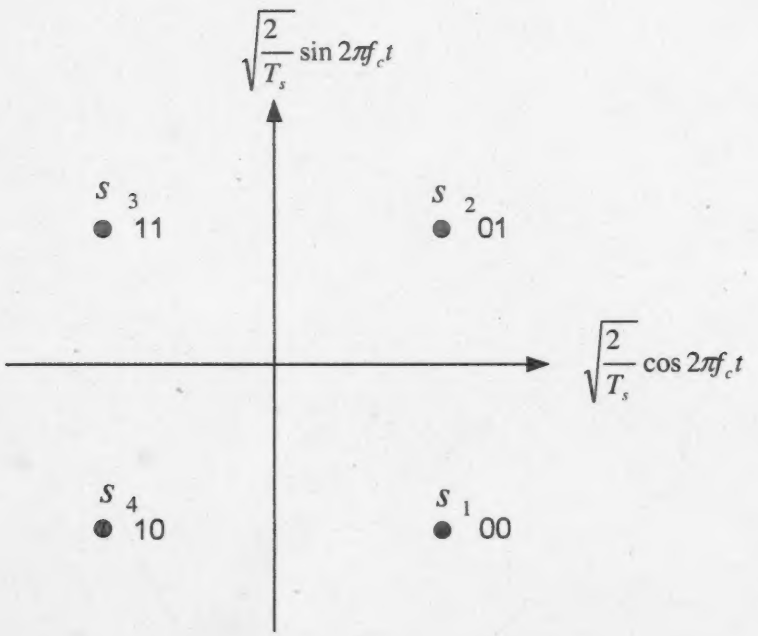

Fig. 2.7. A QPSK signal constellation (after [3, Fig. 4.18]).

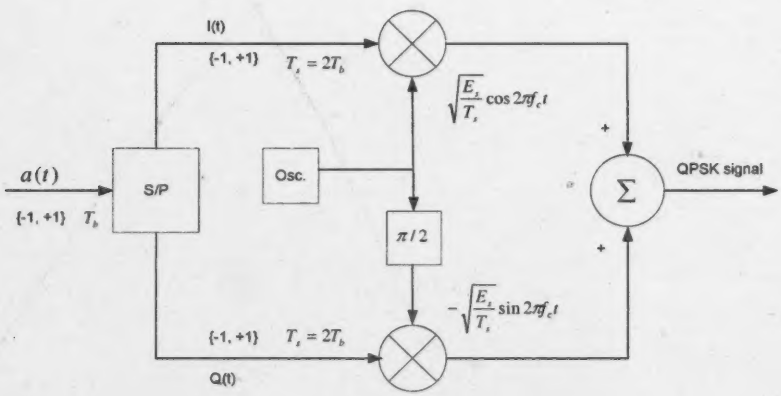

Fig. 2.8. A QPSK modulator (after [3, Fig. 4.20(a)]).

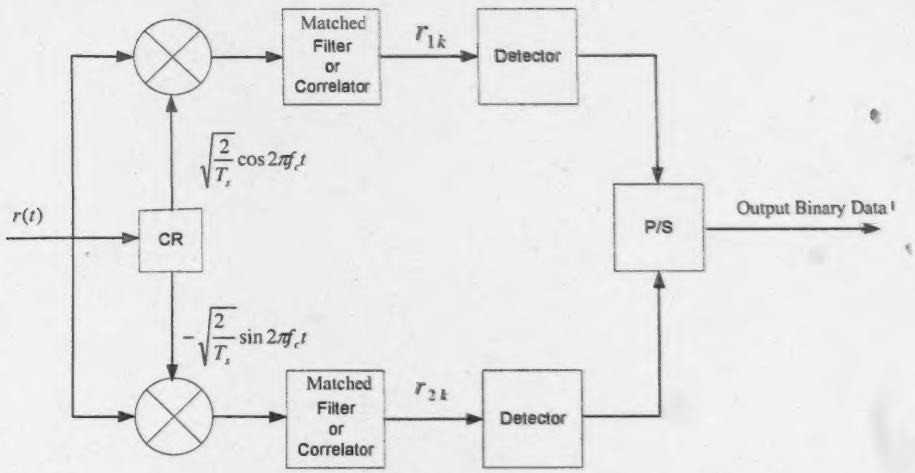

Fig. 2.9. A QPSK demodulator (after [3, Fig. 4.20(b)]).

sine function with the same frequency as the carrier to extract the I and Q components. Since the I channel signal and the Q channel signal are BPSK signals [3], the modulation and demodulation on each channel is exactly the same as for BPSK which can been seen through Figs. 2.8 and 2.9.

2.4.3 M-ary Quadrature Amplitude Modulation

Compared to PSK modulation, QAM doesn't have a constant envelope but achieves high bandwidth efficiency. It is desirable in systems where bandwidth is more crucial. Reference [4] describes the modulation and demodulation of square M-QAM in great detail. The M-QAM signal can be expressed as [18]

$$s_{QAM}(t) = \sqrt{\frac{E_{min}}{T}} a_i cos(2\pi f_c t) + \sqrt{\frac{E_{min}}{T}} b_i sin(2\pi f_c t) \tag{2.40}$$

where $0 \leq t \leq T$, $i = 1, 2 \ldots, M$, E_{min} is the lowest energy signal and a_i and b_i are a pair of integers indicating the location of the signal in the constellation. The signaling constellation and the Gray code mapping of the transmitted bits is shown in Fig. 6.3.

Define

$$I_k = a_i \tag{2.41a}$$

$$Q_k = b_i \tag{2.41b}$$

$$m_I(t) = \sqrt{\frac{E_{min}}{T}} cos(2\pi f_c t) \tag{2.41c}$$

$$m_Q(t) = \sqrt{\frac{E_{min}}{T}} sin(2\pi f_c t) \tag{2.41d}$$

where I_k is the I component which represents i_1 and i_2 and transmits on the I channel and Q_k is the Q component which represents q_1 and q_2 and transmits on the Q channel; $m_I(t)$ is the modulating signal for the I channel and $m_Q(t)$ is the modulating signal for the Q channel. Thus (2.40) can be rewritten as

$$s_{QAM} = I_k m_I(t) - Q_k m_Q(t). \tag{2.42}$$

Fig. 2.12 shows the modulation of QAM. The transmitted bits are first split into I and Q bit streams and go through the level generator which decides the transmitting signal level of I and Q components, I_k and Q_k, by the symbol location in the constellation. That will make the detection a little more complicated. Then I_k and Q_k are modulated by the I and Q carriers.

The demodulation of the received signal shown in Fig. 2.13 is implemented by extracting the I and Q components separately and deciding the transmitted bits according to the decision boundaries. The received I and Q components samples, r_{1k} and r_{2k} can be expressed as

$$r_{1k} = a_i \sqrt{\frac{E_{min}}{2}} + n \tag{2.43}$$

$$r_{2k} = b_i \sqrt{\frac{E_{min}}{2}} + n. \tag{2.44}$$

As the performance of 16-QAM will be studied later, we use 16-QAM as an example to explain QAM modulation and demodulation in more detail. Every 16-QAM symbol is represented by 4 bits, two most significant bits (MSB's), i_1 and q_1 and two least significant

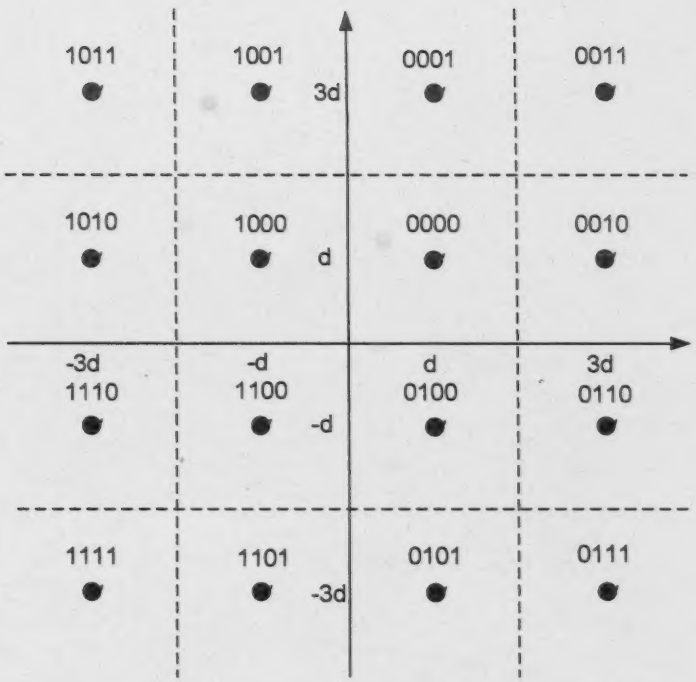

Fig. 2.10. The 16-QAM signaling constellation with Gray encoding (after [1, Fig.3]). The decision distance is denoted as *d*.

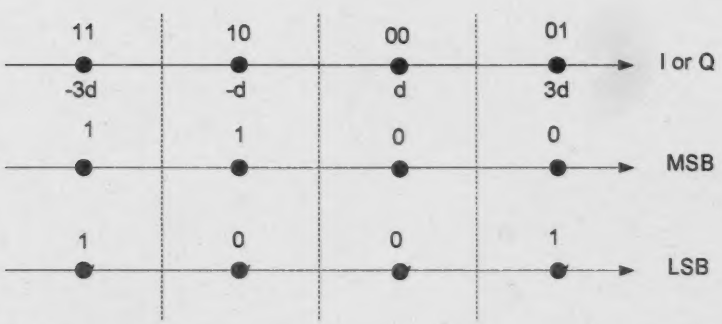

Fig. 2.11. The 16-QAM I and Q bit Demappings (after [1, Fig.5]).

bits (LSB's), i_2 and q_2, in the sequence of i_1, q_1, i_2, q_2, where i_1 and i_2 are the in-phase bits and q_1 and q_2 are the quadrature bits. The I and Q bit streams are Gray encoded by assigning the bits 01, 00, 10, 11 to the levels $3d, d, -d,$ and $-3d$, respectively, where d is the decision distance, shown in Fig. 2.11, denoted as $\sqrt{\frac{E_{min}}{2}}$. Thus the combinations of a_i and b_i are listed as follows: {1,1}, {1,3}, {3,1}, {3,3}, {-1,1},{-1,3}, {-3,1}, {-3,3}, {1,-1}, {1,-3}, {3,-1}, {3,-3}, {-1,-1}, {-1,-3}, {-3,-1}, {-3,-3} according to the signal constellation. Eqn. (2.43) can be rewritten in terms of d

$$r_{1k} = a_i d + n \tag{2.45}$$

$$r_{2k} = b_i d + n. \tag{2.46}$$

Due to the symmetry of the constellation, the demodulation is same for the I and Q components and similar to QPSK but the detection is much more complicated due to the multi-level decision boundaries, which will be covered in Subsection 2.5.3 for the AWGN case with perfect channel estimation and Subsection 4.4 for the imperfect channel estimation case.

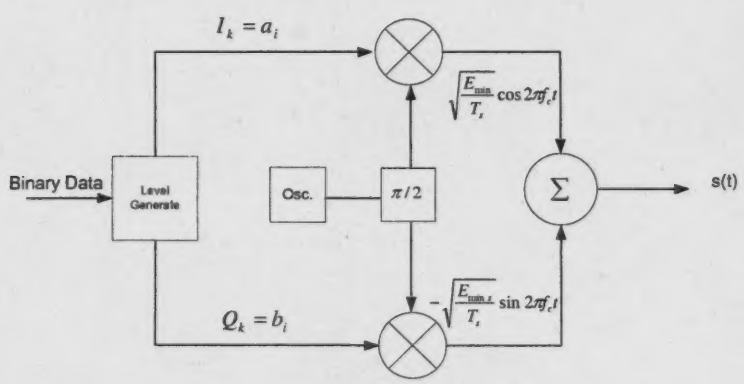

Fig. 2.12. A QAM modulator (after [3, Fig. 8.8]).

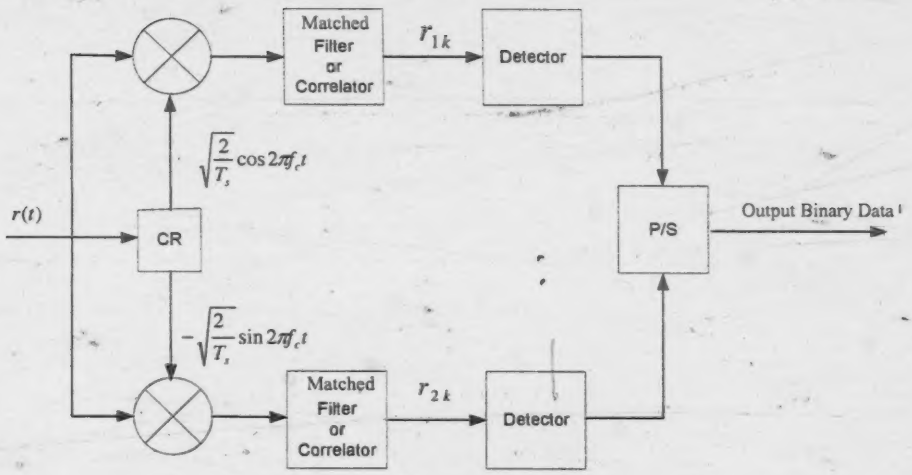

Fig. 2.13. A QAM demodulator.

2.5 Performance Analysis of Different Modulations with Perfect Channel Estimation

In this section, we deal with the performance analysis of different modulation schemes. It is well known that for the case of perfect channel estimation, the MRC output signal is real and, thus, the conditional BER depends only on the SNR [2], [19]. The performance will be degraded by lots of factors including the Doppler spreading , fading, delay spreading , co-channel and adjacent channel interference [24]. We start with a simple system model which only considers the corruption by the AWGN and then extend the model to a fading channel with perfect channel estimation. The basic idea behind it is the foundation for the complicated system model which will be introduced in later chapters. Meanwhile, the transmitted signal is assumed to pass through the AWGN channel and be received by the optimum receiver with perfect synchronization and timing recovery. The received signal sample from the demodulator (matched filter or correlator) can be expressed as

$$r = s_w + n \tag{2.47}$$

where r is the received signal sample, s_w is the transmitted signal sample and n is the AWGN sample with zero mean and variance σ_n^2. Generally, the probability of a decision bit error given that $s_w(t)$ is transmitted is denoted as $P_b(e|s_w)$. Under the assumption that all the W signals have the equal transmission probability, the average probability of bit error is ,

$$P_b(e) = \sum_{w=1}^{W} \frac{1}{W} P_b(e|s_w). \tag{2.48}$$

If the BER of every symbol is same, the average BER is equal to the BER of any of the W signals, for example the w_{th} symbol. Thus, (2.48) can be rewritten as

$$P_b(e) = P_b(e|s_w). \tag{2.49}$$

As, we will see later, the average BER in AWGN channel is only determined by the SNR per bit, γ_b, the average BER in Rayleigh fading with perfect channel estimation can be obtained by averaging the conditional BER (conditioned on the SNR per bit) with respect to the SNR per bit according to

$$P_e = \int_0^\infty P_b(e|\gamma_b) f(\gamma_b) d\gamma_b \tag{2.50}$$

where P_e is the average BER in slow fading, $P_b(e|\gamma_b)$ is the BER conditioned on the SNR per bit, γ_b, and $f(\gamma_b)$ is the pdf of the fading signal's SNR per bit. If γ_b is the diversity output SNR, P_e is the average BER with diveristy reception. Note that the only diversity technique considered in this thesis is MRC.

2.5.1 BER of BPSK

In BPSK, every symbol is represented by 1 bit, so the BER is equivalent to the SER. The transmitted signal samples, s_1 and s_2, are equal to $\sqrt{E_b}$ and $-\sqrt{E_b}$, respectively, corresponding to the transmitted signals $s_1(t)$ and $s_2(t)$ and the received signal sample is r, expressed in (4.9). As shown in Fig. 2.4, s_1 and s_2 are symmetrical and their BER's are the same. The decision threshold is zero as shown in Fig. 2.4. Assuming $s_1(t) = 1$ is sent, the transmitted signal sample, s_1, after matched filter equals is $\sqrt{E_b}$. If the received sample,

$r \geq 0$, the decision is made that $s_1(t)$ is transmitted. Otherwise, the decision is wrong. As n is Gaussian distributed with zero mean and s_1 is fixed, the conditional pdf of r is [2, Eqn. (5-2-3)]

$$p(r|s_1) = \frac{1}{\sqrt{2\pi}\sigma_n} e^{-(r-\sqrt{E_b})^2/2\sigma_n^2}. \tag{2.51}$$

The BER is the probability that $r < 0$,

$$\begin{aligned} P_b(e) &= \int_{-\infty}^{0} p(r|s_1)dr \\ &= Q(\sqrt{2\gamma_b}) \end{aligned} \tag{2.52}$$

where $\gamma_b = \frac{E_b}{2\sigma_n^2}$ is the SNR per bit and $Q(\cdot)$ is the Q-function, usually used for the area under the tail of the Gaussian pdf [2]. Due to the equal probability of the transmitted signals, the average BER for transmiting '0' and '1' has the same expression. Thus, the average BER of BPSK is the expression in (2.52).

The average BER for Rayleigh fading with or without MRC diversity can be obtained according to (2.50). The pdf of output SNR with single branch reception is chi-square distributed with two degrees of freedom, while the pdf of output SNR with M diversity branch reception is chi-square distributed with $2M$ degrees of freedom [2, eqns. (2-1-126) and (14-4-13)]

$$f(\gamma_b) = \left\{ \begin{array}{ll} \frac{1}{\bar{\gamma}_b} exp\left(-\frac{\gamma_b}{\bar{\gamma}_b}\right) & \text{single branch} \\ \frac{1}{(M-1)!\bar{\gamma}_c^M} \gamma_b^{M-1} e^{-\gamma_b/\bar{\gamma}_c} & M \text{ branch MRC diversity} \end{array} \right\} \tag{2.53}$$

where $\gamma_b = \frac{\alpha^2 E_b}{2\sigma_n^2}$, is the output SNR, $\bar{\gamma}_b = \frac{\sigma_x^2 E_b}{\sigma_n^2}$, is the average output SNR, $E(\alpha^2) = \sigma_x^2$, σ_x^2 is the complex fading channel variance both in the real and imaginary part, and $\bar{\gamma}_c$ is the average SNR per channel. Then, (2.52) combined with (2.50) and (2.53) gives [2, eqn. (14-3-7) and (14-4-15)]

$$P_e = \left\{ \begin{array}{ll} \frac{1}{2}\left(1 - \sqrt{\frac{\bar{\gamma}_b}{1+\bar{\gamma}_b}}\right) & \text{single branch} \\ \left[\frac{1}{2}(1-\mu)\right]^M \sum_{m=0}^{M-1} \binom{M-1+m}{m} \left[\frac{1}{2}(1+\mu)\right]^m & M \text{ branch MRC diversity} \end{array} \right\} \tag{2.54}$$

where $\mu = \sqrt{\frac{\bar{\gamma}_c}{1+\bar{\gamma}_c}}$.

2.5.2 BER of QPSK

It is shown in (2.42) and Fig. 6.3 that QPSK is actually two BPSK signals modulated on in-phase and quadrature carriers. In such case, the BER's of QPSK for an AWGN channel or a fading channel with perfect channel estimation are identical to those of BPSK.

2.5.3 BER of Quadrature Amplitude Modulation

Since QAM is a multi-level modulation scheme, the detection is more complicated than BPSK and QPSK. The derivation of the BER's for 16-QAM with single branch reception in both AWGN channel and fading channel with perfect channel estimation are explained in detail following the method used in [4] and extended to the diversity case. The method introduced can be applied to M-QAM.

A 16-QAM symbol is represented by 4 bits, each of which has two most significant bits (MSB's), i_1 and q_1, and two least significant bits (LSB's), i_2 and q_2, shown in Fig. 2.11. We calculate the MSB BER, P_M, and the LSB BER, P_L, separately. Then, the BER, P_e, of 16-QAM is the average of P_M and P_L. That is,

$$P_e = \frac{1}{2}(P_M + P_L). \tag{2.55}$$

In the case of an AWGN channel, the detection is achieved by using the decision boundaries shown in Fig. 2.11. For the MSB bits, i_1 and q_1 [4, eqn. (5.13)] ,

$$\begin{aligned} &\text{if } I, Q \geq 0, \text{ then } i_1, q_1\text{=0}, \\ &\text{if } I, Q < 0, \text{ then } i_1, q_1\text{=1}. \end{aligned} \tag{2.56}$$

For the LSB bits, i_2 and q_2 [4, eqn. (5.14)],

$$\begin{aligned} &\text{if } I, Q \geq 2d \text{ or } I, Q < -2d, \text{ then } i_2,\ q_2\text{=1}, \\ &\text{if } -2d \geq I, Q < 2d, \text{ then } i_2,\ q_2\text{=0}. \end{aligned} \tag{2.57}$$

As the received signal samples, r_{1k} and r_{2k}, shown in (2.43) consist of a constant value, $a_i d$ or $b_i d$ plus the AWGN sample, the MSB and LSB BER can be derived using the same method described in Subsection 2.5.1 with the decision boundaries known. Due to the symmetry of the constellation, we only consider the I components with $I \geq 0$ case. Observing Fig. 2.11, for the MSB, it has a decision distance d if a d-level '0' is transmitted and a decision distance $3d$ if a $3d$-level '0' is transmitted. With the same symbol transmission probability,

$$P_M(e) = \frac{1}{2}\left[Q\left(\frac{d}{\sigma_n}\right) + Q\left(\frac{3d}{\sigma_n}\right)\right]. \tag{2.58}$$

For the LSB, in the case of '0' transmitted, if the noise exceeds the distance of either 'd' or '3d' in the opposite direction, an error will occur; in the case of '1' transmitted, if the noise exceeds the distance of 'd' but less than '5d', an error will occur, and

$$P_L(e) = \frac{1}{2}\left[Q\left(\frac{d}{\sigma_n}\right) + Q\left(\frac{3d}{\sigma_n}\right)\right] + \frac{1}{2}\left[Q\left(\frac{d}{\sigma_n}\right) - Q\left(\frac{5d}{\sigma_n}\right)\right]. \tag{2.59}$$

The average symbol energy of a 16-QAM symbol is

$$E_0 = 4\bar{E}_b = 10d^2 \tag{2.60}$$

and the SNR per bit is

$$\gamma_b = \frac{\bar{E}_b}{\sigma_n^2}. \tag{2.61}$$

Thus, we have

$$\frac{d}{\sigma_n} = \sqrt{\frac{2\bar{\gamma}_b}{5}}. \tag{2.62}$$

Eqn. (2.55) combined with (2.58), (2.59) and (2.62) yield the BER of 16-QAM in an AWGN channel

$$P_{QAM}(e) = \frac{1}{4}\left[Q(\sqrt{2\gamma_b/5}) + Q(3\sqrt{2\gamma_b/5}) + Q\left(\sqrt{2\gamma_b/5}\right) + Q\left(3\sqrt{2\gamma_b/5}\right) + Q\left(\sqrt{2\gamma_b/5}\right) - Q\left(5\sqrt{2\gamma_b/5}\right)\right]. \tag{2.63}$$

In the case of a Rayleigh fading channel, the average BER with perfect channel information can be obtained by averaging $P_{QAM}(e)$ over the pdf of γ_b which has the same expression as (2.53). Combining (2.63) with (2.50) and (2.53), we obtain the average BER

of 16-QAM in a Rayleigh fading channel with perfect estimation for single branch and MRC . The BER for a single branch reception is

$$\begin{aligned} P_e = & \frac{1}{2}\left\{\frac{1}{2}\left[\frac{1}{2}(1-\mu_1)+\frac{1}{2}(1-\mu_2)\right]\right. \\ & +\frac{1}{2}\left[\frac{1}{2}(1-\mu_1)-\frac{1}{2}(1-\mu_3)\right. \\ & \left.\left.+\frac{1}{2}(1-\mu_1)+\frac{1}{2}(1-\mu_2)\right]\right\}. \end{aligned} \tag{2.64a}$$

The BER for MRC diversity is

$$\begin{aligned} P_{div}(e) = & \frac{1}{2}\left[\frac{1}{2}\left\{\left[\frac{1}{2}(1-\mu_1)\right]^M \sum_{m=0}^{M-1}\binom{M-1+m}{m}\left[\frac{1}{2}(1+\mu_1)\right]^m\right.\right. \\ & \left.+\left[\frac{1}{2}(1-\mu_2)\right]^M \sum_{m=0}^{M-1}\binom{M-1+m}{m}\left[\frac{1}{2}(1+\mu_2)\right]^m\right\} \\ & +\frac{1}{2}\left\{\left[\frac{1}{2}(1-\mu_1)\right]^M \sum_{m=0}^{M-1}\binom{M-1+m}{m}\left[\frac{1}{2}(1+\mu_1)\right]^m\right. \\ & -\left[\frac{1}{2}(1-\mu_3)\right]^M \sum_{m=0}^{M-1}\binom{M-1+m}{m}\left[\frac{1}{2}(1+\mu_3)\right]^m \\ & +\left[\frac{1}{2}(1-\mu_1)\right]^M \sum_{m=0}^{M-1}\binom{M-1+m}{m}\left[\frac{1}{2}(1+\mu_1)\right]^m \\ & \left.\left.\left.+\left[\frac{1}{2}(1-\mu_2)\right]^M \sum_{m=0}^{M-1}\binom{M-1+m}{m}\left[\frac{1}{2}(1+\mu_2)\right]^m\right\}\right] \end{aligned} \tag{2.64b}$$

where, by definition,

$$\mu_1 = \sqrt{\frac{2\bar{\gamma}_c}{5+2\bar{\gamma}_c}} \tag{2.64c}$$

$$\mu_2 = \sqrt{\frac{18\bar{\gamma}_c}{5+18\bar{\gamma}_c}} \tag{2.64d}$$

$$\mu_3 = \sqrt{\frac{50\bar{\gamma}_c}{5+50\bar{\gamma}_c}} \tag{2.64e}$$

and $\bar{\gamma}_c = \frac{\sigma_x^2 E_b}{\sigma_n^2}$.

Note that (2.64a) and (2.64b) assume perfect channel estimation both for the demodulation and for the channel weighting in the maximal ratio diversity combining. To the best

of the authors' knowledge, this expression is new and different from other results in the literature.

Chapter 3

Approximate Analysis of the BER Performance with Channel Estimation Error

Most of the previous works on performance analysis of two-dimensional modulations in fading channels are based on the perfect channel estimation. Some work [11], [12], [17] and [1] considers the estimation errors but without diversity included. Reference [1] derives the BER of M-QAM using PSAM to provide estimates of the channel amplitude and phase in the receiver demodulation process for AWGN and Rayleigh fading channels with a single receiver branch and estimation errors considered. Reference [14] gives a general form for the BER of an arbitrary modulation format when used with MRC in slow fading with weighting (channel estimation) errors. But both of the results in [1] and [14] are approximations. As each of reference [1] and reference [14] neither identifies nor justifies that the analyses are approximations and as the methods have been used in other subsequel research works, we will present the reviews of those two papers in the following sections to clarify the approximate analytical approaches used there. Problems in [14] that are related to [29] will also be clarified.

3.1 Review of Tang et. al's Results

In Tang et al's paper, the BER's of 16-QAM and 64-QAM in flat fading with imperfect channel estimation are derived. The channel estimation method used in the system is PSAM. The estimation errors in PSAM are from the decorrelation between the pilot and the data symbol as well as from AWGN. There are two techniques involved in the paper that make the results approximate. We will go through those in detail to make the problems clear.

Generally, the average BER can be calculated by averaging the conditional BER, $P(e|\alpha,\hat{\alpha},\varphi)$, for the AWGN channel over the fading represented by the variables α, $\hat{\alpha}$ and φ,

$$P_e = \int_0^\infty \int_0^\infty \int_0^{2\pi} P(e|\alpha,\hat{\alpha},\varphi)p(\alpha,\hat{\alpha},\varphi)d\varphi d\alpha d\hat{\alpha}. \tag{3.1}$$

where $p(\alpha,\hat{\alpha},\varphi)$ is the jpdf of α, $\hat{\alpha}$ and φ. First, note that it is well-known that the amplitude and the phase of the Rayleigh fading channel are independent random variables. It is shown in Subsection 2.1.1 that

$$p(\alpha,\theta) = p(\alpha)p(\theta), \tag{3.2}$$

so that the first order jpdf factors into the product of the amplitude pdf and the phase pdf. However, and importantly, the envelope and phase random processes are not independent random processes, which is shown and demonstrated in Subsection 2.1.2 and [23, Chapter 8]. In [1], the analysis and results are based on treating the phase errors and the amplitude fades independently. The distribution of the amplitude and its estimate and the distribution of the phase and its estimate are given in [1]. This treatment is equivalent to using the following equation,

$$P_e = \int_0^\infty \int_0^\infty \int_0^{2\pi} \int_0^{2\pi} P(e|\alpha,\hat{\alpha},\theta,\hat{\theta})p(\alpha,\hat{\alpha})p(\theta,\hat{\theta})d\theta d\hat{\theta} d\alpha d\hat{\alpha} \tag{3.3}$$

which is only approximate. The exact form is

$$P_e = \int_0^\infty \int_0^\infty \int_0^{2\pi} \int_0^{2\pi} P(e|\alpha,\hat{\alpha},\theta,\hat{\theta})p(\alpha,\hat{\alpha},\theta,\hat{\theta})d\theta d\hat{\theta} d\alpha d\hat{\alpha}. \tag{3.4}$$

In [1] the jpdf $p(\alpha, \hat{\alpha}, \theta, \hat{\theta})$ has effectively been replaced by the product $p(\alpha, \hat{\alpha})p(\theta, \hat{\theta})$. This conclusion can be drawn by careful scrutiny of [1, eqn. (40)] and [1, eqn. (38)]. This replacement requires that the amplitude samples (α, $\hat{\alpha}$) are independent of the phase samples (θ, $\hat{\theta}$). It is clear from the analysis in Subsection 2.1.2 and [23, Ch. 8] that (α, $\hat{\alpha}$) and (θ, $\hat{\theta}$) are not independent.

There is a second reason for which the BER results in [1] are only approximate. Even in the absence of noise and other system errors (for example, carrier recovery error or symbol timing error) the channel estimate is corrupted by an error that is Gaussian distributed. This error has its origin in the fact that the fading at an information symbol's time is decorrelated from the fading at a pilot symbol's time. Note particularly, that the BER depends on the location of the information symbol since the decorrelation depends on the location (in addition, other error sources may also depend on the location of the information symbol). These errors cause an error-rate floor which will determine the BER when the SNR is large. The analysis in [1] averages the parameters r ($r = \sigma_{\hat{x}}^2/\sigma_x^2$) and ρ (the correlation coefficient between α^2 and $\hat{\alpha}^2$) over l, the location of a symbol in a data symbol frame and then uses these averaged parameters in the BER equation. This approach is an approximation. The precise BER is obtained by averaging the BER conditioned on these parameters over the probabilities of these parameters, a more complex computation. The average BER can be obtained by averaging the conditional BER's over the locations of the information symbols in the frame.

3.2 Review of Tomiuk's Result

Tomiuk's paper provides a general form for MRC diversity with weighting errors. This result and the reasoning used to derive this result have been used in subsequent research [31]. It is, therefore, important to report that these results, which originate from [14] and [32], are incorrect.

The analysis in [14], [32] is based on the concept that the BER of maximal ratio combining (MRC) diversity when used with a particular modulation format in slow fading can

be obtained by averaging the conditional BER for AWGN channel (conditioned on the SNR) with respect to the SNR. Recall (2.50),

$$P_e = \int_0^\infty P(e|\gamma) f(\gamma) d\gamma. \tag{3.5}$$

The distribution of the output SNR, γ, considering the channel estimation errors and MRC, is obtained from [29]. But the conditional BER , $P(e|\gamma)$, being dependent on γ and no other parameters is only true for the case of perfect channel estimation. The expression of the conditional BER with channel estimation error will be derived in the later sections. It can be shown that generally, with imperfect estimation, the conditional BER is conditional on the channel amplitude, the amplitude estimate, and the phase difference, φ between the channel phase shift and its estimate in addition to the the SNR . The single branch case for BPSK with imperfect channel estimation will be used as an example to clarify the erroneous reasoning in Section 4.2 of Chapter 4. Thus, (2.50) can not be used for the calculation of the BER for either a single receiver branch or MRC diversity with estimation error. The single branch BER's with perfect estimation for different modulation schemes will be derived correctly in Chapter 4. A method to derive the BER with MRC diversity based on the concept of (3.1) will be included in Chapter 5.

3.2.1 Problems in Tomiuk's Paper Related to Gans' Results

The Gaussian weighting errors model employed in [14], [32] is taken from the paper by Gans [29]. This model applies to channel estimation errors originating from decorrelation of the channel state and the channel state estimate due to displacement in time or in frequency of the pilot used to estimate the channel and the instantaneous channel state. It is explicitly stated in [14], [32] that Gans' model can be used to model any situation where the channel estimation is corrupted by complex Gaussian errors, and this assumption is used in the analysis. This is incorrect. Gans' model exclusively applies to Gaussian errors caused by time or frequency displacement of the pilot signal(or symbol) from the instantaneous channel state. Specifically, Gans' model can not be correctly used to model the effects of

independent noise corrupting an estimator as stated and employed in [14], [32]. Mathematical contradictions arise if Gans' model is used to model independent estimator noise. This is proved as follows.

Consider the case where the estimator is corrupted by independent zero-mean additive Gaussian noise, i.e.,

$$\hat{g_k} = g_k + n_k \tag{3.6}$$

where $\hat{g_k}$ is the complex channel estimate, g_k is the complex channel gain and n_k is complex Gaussian noise. Then, since n_k and g_k are independent,

$$E[Re\{\hat{g_k}^2\}] = E[Re\{g_k^2\}] + E[Re\{n_k^2\}] \tag{3.7a}$$

$$E[Im\{\hat{g_k}^2\}] = E[Im\{g_k^2\}] + E[Im\{n_k^2\}]. \tag{3.7b}$$

Unless the noise power is zero, this contradicts one of the basic assumptions of Gans' model [29, eqn.(12)] that

$$E[Re\{\hat{g_k}^2\}] = E[Re\{g_k^2\}] = E[Im\{\hat{g_k}^2\}] = E[Im\{g_k^2\}]. \tag{3.8}$$

Thus, application of Gans' model to the case of independent Gaussian estimator noise is incorrect. Alternatively, one can write $\Delta = \hat{g_k} - g_k$ where the complex Gaussian error in Gans' model is denoted Δ. Then,

$$\sigma_\Delta^2 = \sigma_{\hat{g_k}}^2 + \sigma_{g_k}^2 - 2\sigma_{\hat{g_k}}\sigma_{g_k}\rho. \tag{3.9}$$

Eqn.(3.9) shows that the Gaussian errors in Gans' model depend on the correlation, ρ, between the channel gain and its estimate, and thus, Gans' model can not be used for independent estimator noise. For very slow fading, $\rho = 1$ and $\sigma_\Delta^2 = 0$, necessarily [4].

Chapter 4

BER Analysis with Channel Estimation Error

In this chapter, we establish the system and channel model. The jpdf of the channel amplitude, channel amplitude estimate, and the phase difference between the channel phase shift and the channel phase estimate are derived along with some related parameters. The performance analysis for single branch BPSK, QPSK and 16-QAM with channel estimation error in Rayleigh fading channel will be introduced afterwards. The information symbols are assumed to be transmitted with the same probability.

4.1 System and Channel Model

Following the discussion of the second-order distribution of the fading channel and the estimation system-PSAM in Chapter 2, we would like to extend the system and channel model in this section. In our system, we consider the channel estimates are corrupted by both the AWGN and the decorrelations between an information symbol and the pilot symbols caused by the time varying fading. We also account for the cross-quadrature-carrier intersymbol interference that occurs because of the phase error for QPSK and 16-QAM. In the case of perfect channel estimation, the receiver can construct the decision

boundaries perfectly. However, in the case of imperfect channel estimation, the decision boundaries are set with the imperfect channel estimate. These will be illustrated in the later analysis associated with different modulation schemes.

As introduced in previous chapters, the BER with channel estimation error is determined by averaging the conditional error rate, conditioned on the channel amplitude, channel amplitude estimate, and channel phase estimate error, across the channel amplitude, channel amplitude estimate and channel phase estimate error. The channel fading and the noise are independent complex Gaussian random variables. The channel estimate, $\hat{g}_k^l$, show in (2.31), is a weighted sum of zero-mean independent complex Gaussian random variables. Thus, it is also a zero-mean complex Gaussian random variable. Since g_k^l and $\hat{g}_k^l$ are correlated complex Gaussian random variables, the jpdf of their amplitudes, α_k^l and $\hat{\alpha}_k^l$, and their phase difference, φ_k^l, can be obtained from (2.18) in Subsection 2.1.2 as (The subscripts for the complex channel gain and its estimate have been omitted in the following discussion when ambiguity can not arise, for notational simplicity.),

$$p(\alpha,\hat{\alpha},\varphi)=\frac{\alpha\hat{\alpha}}{2\pi|\wedge|^{1/2}}exp\left\{-\frac{[\sigma_{\hat{x}}^2\alpha^2+\sigma_x^2\hat{\alpha}^2-2R_c\alpha\hat{\alpha}cos\varphi-2R_{cs}\alpha\hat{\alpha}sin\varphi]}{2|\wedge|^{1/2}}\right\}. \quad (4.1)$$

The second moments, R_c and R_{cs}, will be derived in Subsection 4.1.1 and $\sigma_{\hat{x}}^2$ will be derived in Subsection 4.1.2.

4.1.1 Derivation of the Second-Order Joint Moment of g and $\hat{g}$

The samples of the complex fading gain and its estimate can be expressed in terms of quadrature components as

$$g=g_I+jg_Q \quad (4.2a)$$

$$\hat{g}=\hat{g}_I+j\hat{g}_Q \quad (4.2b)$$

where g_I and g_Q are the in-phase component and the quadrature component of the fading channel, respectively; $\hat{g}_I$ and $\hat{g}_Q$ are the in-phase components and the quadrature component of the fading channel estimate, respectively. The statistics of an omnidirectional

scattering Rayleigh fading channel are give by (2.12a) and (2.12b) in Subsection 2.1.2. Using (2.30), (2.31), (2.12a) and (2.12b) in (2.17b), (2.17c), the second-order joint moments of the variables, g_I and g_Q, from the fading channel, and of $\hat{g}_I$ and $\hat{g}_Q$, from the channel estimation, are determined as

$$\begin{aligned} R_c =& E[g_I\hat{g}_I] = E[g_Q\hat{g}_Q] \\ =& \sum_{k=-k_1}^{k_2} h_k^l E\left[g_I\left(p_{Ik}+\frac{n_{Ik}^0}{s_{Ik}^0}\right)\right] \\ =& \sum_{k=-k_1}^{k_2} \sigma_x^2 h_k^l J_0(2\pi f_D|kL-l|T_s) \end{aligned} \tag{4.3a}$$

$$\begin{aligned} R_{cs} =& E[g_I\hat{g}_Q] = -E[g_Q\hat{g}_I] \\ =& \sum_{k=-k_1}^{k_2} h_k^l E\left[g_I\left(p_{Qk}+\frac{n_{Qk}^0}{s_{Qk}^0}\right)\right] = 0. \end{aligned} \tag{4.3b}$$

4.1.2 Derivation of the variance of the channel estimate, $\sigma_{\hat{x}}^2$

The variance of each component of the complex Gaussian fading estimate is obtained by using the definition (2.4b) with (2.30) and (2.31). It is given by

$$\begin{aligned} \sigma_{\hat{x}}^2 =& E[\hat{g}_I^2] = E[\hat{g}_Q^2] = E\left[\left(\sum_{-k_1}^{k_2} h_k^l(p_{Ik}+\frac{n_{Ik^0}}{s_k^0})\right)^2\right] \\ =& \sum_k \sum_m h_k^l h_m^l cov(p_{Ik}p_{Im}) + \sum_k (h_k^l)^2 \frac{\sigma_n^2}{|s_k^0|^2}. \end{aligned} \tag{4.4}$$

From (2.9c) and (2.12a) ,

$$cov(g_{Ipk}g_{Ipm}) = \sigma_x^2 J_0(2\pi f_D|k-m|LT_s) \tag{4.5}$$

and assuming that the pilot symbol energy E_p is equal to the average data symbol energy E_s, one can rewrite (4.4) as,

$$\begin{aligned} \sigma_{\hat{x}}^2 =& \sum_k \sum_m h_k^l h_m^l cov(g_{Ipk}g_{Ipm}) + \sum_k (h_k^l)^2 \frac{\sigma_n^2}{E_s} \\ =& H_l R H_l' + |H_l|^2 \frac{\sigma_n^2}{E_s} \end{aligned} \tag{4.6}$$

where R is the covariance matrix. The results of (4.3a), (4.3b) and (4.6) are used in the jpdf (4.1) of the amplitudes and phase difference of the channel fading and its estimate.

4.1.3 Derivation of Correlation Coefficient of g and $\hat{g}$

The correlation coefficient, ρ, is defined as

$$\rho = \frac{R_c}{\sigma_x \sigma_{\hat{x}}}. \tag{4.7}$$

Using (4.7) combined with (4.3a) and (4.4), the correlation coefficient, ρ, can be expressed as

$$\rho = \frac{\sum_{k=-k_1}^{k_2} \sigma_x^2 h_k^l J_0(2\pi f_D |kL-l|T_s)}{\sigma_x (H_l R H_l' + |H_l|^2 \frac{\sigma_n^2}{E_s})^{1/2}}. \tag{4.8}$$

4.2 BER Analysis of BPSK with Channel Estimation Error

The received signal sample output from the matched filter can be expressed as

$$r = g\sqrt{E_b} + n = \alpha e^{j\theta}\sqrt{E_b} + n. \tag{4.9}$$

By multiplying (4.9) with the conjugate of the channel estimate, $\hat{g}^* = \hat{\alpha} e^{-j\hat{\theta}}$, we get w as

$$w = s_{w0} + n_{w0} = \alpha\hat{\alpha}\sqrt{E_b} e^{j(\theta-\hat{\theta})} + \hat{\alpha} n e^{-j\hat{\theta}}. \tag{4.10}$$

The instantaneous SNR per bit, γ_b and the average SNR per bit, $\bar{\gamma}_b$ are give as ,

$$\gamma_b = \frac{s_{w0}{}^* s_{w0}}{n_{s0}{}^* n_{w0}} = \frac{\hat{\alpha}^2\alpha^2 E_b}{2\hat{\alpha}^2\sigma_n^2} = \frac{\alpha^2 E_b}{2\sigma_n^2} \tag{4.11a}$$

$$\bar{\gamma}_b = \frac{E[\alpha^2]E_b}{2\sigma_n^2} = \frac{\sigma_x^2 E_b}{\sigma_n^2}. \tag{4.11b}$$

The real part of w, wr, is used for decision as shown in Fig. 4.1,

$$\begin{aligned} w_r = Re\{w\} &= Re\left\{\alpha\hat{\alpha}\sqrt{E_b} e^{j(\theta-\hat{\theta})}\right\} + Re\left\{\hat{\alpha} n e^{-j\hat{\theta}}\right\} \\ &= \alpha\hat{\alpha}\cos\varphi\sqrt{E_b} + n' \end{aligned} \tag{4.12}$$

where φ is the phase error between θ and $\hat{\theta}$. As n has a Gaussian distribution and $\hat{g}$ is considered fixed, the parameter, n' is then Gaussian with zero mean and the variance of n', $\sigma_{n'}^2 = \hat{\alpha}^2\sigma_n^2$. In BPSK modulation, $\{1,-1\}$ is the signal set. Assuming $s_i = 1$ is transmitted, the conditional pdf of wr can be expressed as

$$p(w_r|s_1,\alpha,\varphi) = \frac{1}{\sqrt{2\pi\sigma_{n'}^2}} e^{\frac{-(wr-\alpha\hat{\alpha}cos\varphi\sqrt{E_b})^2}{2\sigma_{n'}^2}}. \tag{4.13}$$

Shown in Fig. 4.1, the decision threshold for wr is '0'. If wr is detected less than 0, the decision is wrong. Thus, given s_1 is transmitted, the probability of error is the probability that wr is less than 0, i.e.,

$$\begin{aligned} P(e|s_1,\alpha,\varphi) &= \int_{-\infty}^{0} p(w_r|s_1,\alpha,\hat{\alpha},\varphi)dwr \\ &= Q\left(\sqrt{\frac{\alpha^2 E_b}{\sigma_n^2}}cos\varphi\right). \end{aligned} \tag{4.14}$$

Assuming the signals are equally probable, then

$$P(e|\alpha,\varphi) = P(e|s_1,\alpha,\varphi). \tag{4.15}$$

Combining (4.15) with (2.55) and (4.11), the conditional BER of BPSK is

$$P(e|\alpha,\varphi) = Q\left(\sqrt{2\gamma_b}cos\varphi\right) \tag{4.16a}$$

or

$$P(e|\alpha,\varphi) = Q\left(\sqrt{\frac{\bar{\gamma}_b}{\sigma_x^2}}\alpha cos\varphi\right). \tag{4.16b}$$

Eqn. (4.16) tells us that the BER of BPSK with estimation error depends on the instantaneous SNR per bit, γ_b, or equivalently, the channel amplitude, α, and the phase error, φ. Thus, it is obvious that the BER obtained by averaging the conditional BER over the instantaneous SNR per bit, γ_b, is only an approximation. Defined by [2, eqn.(2-1-95) and eqn.(2-1-98)] that $Q(x)$ can be expressed by the error function, $erf(x)$

$$Q(x) = \frac{1}{2}\left[1 - erf\left(\frac{x}{\sqrt{2}}\right)\right]. \tag{4.17}$$

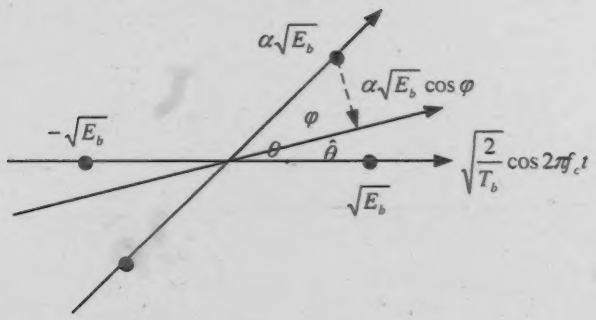

Fig. 4.1. New decision component set by the imperfect estimate. The parameters, α, θ are the amplitude and phase shift of the channel, respectively; $\hat{\theta}$ is the phase estimate and φ is the phase error between θ and $\hat{\theta}$.

We use

$$P(e|\alpha,\varphi) = \frac{1}{2}\left[1 - erf\left(\sqrt{\frac{\bar{\gamma}_b}{2\sigma_x^2}}\alpha cos\varphi\right)\right] \tag{4.18}$$

to calculate the average BPSK BER by averaging $P(e|\alpha,\varphi)$ over α, $\hat{\alpha}$ *and* φ,

$$
\begin{aligned}
Pe =& \frac{1}{2} - \frac{1}{2}\int_0^{\infty}\int_0^{2\pi}\int_0^{\infty} P(e|\alpha,\varphi)p(\alpha,\hat{\alpha},\varphi)d\hat{\alpha}d\varphi d\alpha \\
=& \frac{1}{2} - \frac{1}{2}\int_0^{\infty}\int_0^{2\pi}\int_0^{\infty} erf\left(\sqrt{\frac{\bar{\gamma}_b}{2\sigma_x^2}}\alpha cos\varphi\right)\frac{\alpha\hat{\alpha}}{2\pi|\wedge|^{1/2}} \\
& exp\left\{-\frac{1}{2|\wedge|^{1/2}}\left[(\hat{\sigma}_x^2\alpha^2+\sigma_x^2\hat{\alpha}^2)-2R_c\alpha\hat{\alpha}cos\varphi\right]\right\}d\hat{\alpha}d\varphi d\alpha \\
=& \frac{1}{2} - \frac{1}{2}\left\{\int_0^{\infty}\int_{-\frac{\pi}{2}}^{\frac{\pi}{2}}\int_0^{\infty} erf\left(\sqrt{\frac{\bar{\gamma}_b}{2\sigma_x^2}}\alpha cos\varphi\right)\frac{\alpha\hat{\alpha}}{2\pi|\wedge|^{1/2}}\right. \\
& exp\left\{-\frac{1}{2|\wedge|^{1/2}}\left[(\hat{\sigma}_x^2\alpha^2+\sigma_x^2\hat{\alpha}^2)-2R_c\alpha\hat{\alpha}cos\varphi\right]\right\}d\hat{\alpha}d\varphi d\alpha \\
& +\int_0^{\infty}\int_{\frac{\pi}{2}}^{\frac{3\pi}{2}}\int_0^{\infty} erf\left(\sqrt{\frac{\bar{\gamma}_b}{2\sigma_x^2}}\alpha cos\varphi\right)\frac{\alpha\hat{\alpha}}{2\pi|\wedge|^{1/2}} \\
& \left. exp\left\{-\frac{1}{2|\wedge|^{1/2}}\left[(\hat{\sigma}_x^2\alpha^2+\sigma_x^2\hat{\alpha}^2)-2R_c\alpha\hat{\alpha}cos\varphi\right]\right\}d\hat{\alpha}d\varphi d\alpha\right\} \\
=& \frac{1}{2} - \frac{1}{2}\left\{\int_0^{\infty}\int_{-\frac{\pi}{2}}^{\frac{\pi}{2}}\int_0^{\infty} erf\left(\sqrt{\frac{\bar{\gamma}_b}{2\sigma_x^2}}\alpha cos\varphi\right)\frac{\alpha\hat{\alpha}}{2\pi|\wedge|^{1/2}}\right. \\
& exp\left\{-\frac{1}{2|\wedge|^{1/2}}\left[(\hat{\sigma}_x^2\alpha^2+\sigma_x^2\hat{\alpha}^2)-2R_c\alpha\hat{\alpha}cos\varphi\right]\right\}d\hat{\alpha}d\varphi d\alpha \\
& +\int_0^{\infty}\int_{-\frac{\pi}{2}}^{\frac{\pi}{2}}\int_0^{\infty} erf\left(\sqrt{\frac{\bar{\gamma}_b}{2\sigma_x^2}}\alpha cos(\varphi+\pi)\right)\frac{\alpha\hat{\alpha}}{2\pi|\wedge|^{1/2}} \\
& \left. exp\left\{-\frac{1}{2|\wedge|^{1/2}}\left[(\hat{\sigma}_x^2\alpha^2+\sigma_x^2\hat{\alpha}^2)-2R_c\alpha\hat{\alpha}cos(\varphi+\pi)\right]\right\}d\hat{\alpha}d\varphi d\alpha\right\}. \qquad (4.19)
\end{aligned}
$$

As

$$cos(\varphi+\pi) = -cos\varphi \qquad (4.20a)$$

$$erf(-x) = -erf(x) \qquad (4.20b)$$

$$sinh(z) = \frac{e^z - e^{-z}}{2}, \qquad (4.20c)$$

(4.19) turns into

$$
\begin{aligned}
Pe =& \frac{1}{2} - \frac{1}{2}\left\{\int_0^{\infty}\int_{-\frac{\pi}{2}}^{\frac{\pi}{2}}\int_0^{\infty} erf\left(\sqrt{\frac{\bar{\gamma}_b}{2\sigma_x^2}}\alpha cos\varphi\right)\frac{\alpha\hat{\alpha}}{2\pi|\wedge|^{1/2}}\right. \\
& exp\left\{-\frac{1}{2|\wedge|^{1/2}}\left[(\hat{\sigma}_x^2\alpha^2+\sigma_x^2\hat{\alpha}^2)-2R_c\alpha\hat{\alpha}cos\varphi\right]\right\}d\hat{\alpha}d\varphi d\alpha \\
& + \int_0^{\infty}\int_{-\frac{\pi}{2}}^{\frac{\pi}{2}}\int_0^{\infty} erf\left(-\sqrt{\frac{\bar{\gamma}_b}{2\sigma_x^2}}\alpha cos\varphi\right)\frac{\alpha\hat{\alpha}}{2\pi|\wedge|^{1/2}} \\
& \left. exp\left\{-\frac{1}{2|\wedge|^{1/2}}\left[(\hat{\sigma}_x^2\alpha^2+\sigma_x^2\hat{\alpha}^2)+2R_c\alpha\hat{\alpha}cos\varphi\right]\right\}d\hat{\alpha}d\varphi d\alpha\right\} \\
=& \frac{1}{2} - \frac{1}{2}\int_0^{\infty}\int_{-\frac{\pi}{2}}^{\frac{\pi}{2}}\int_0^{\infty} erf\left(\sqrt{\frac{\bar{\gamma}_b}{2\sigma_x^2}}\alpha cos\varphi\right)\frac{\alpha\hat{\alpha}}{2\pi|\wedge|^{1/2}} \\
& exp\left\{-\frac{1}{2|\wedge|^{1/2}}\left[(\hat{\sigma}_x^2\alpha^2+\sigma_x^2\hat{\alpha}^2)\right]\right\} \\
& \left[exp\left(\frac{R_c\alpha\hat{\alpha}cos\varphi}{|\wedge|^{1/2}}\frac{1}{2}\right)-exp\left(-\frac{R_c\alpha\hat{\alpha}cos\varphi}{|\wedge|^{1/2}}\right)\right]d\hat{\alpha}d\varphi d\alpha \\
=& \frac{1}{2} - \int_0^{\infty} erf\left(\sqrt{\frac{\bar{\gamma}_b}{2\sigma_x^2}}\alpha cos\varphi\right)\frac{\alpha}{2\pi|\wedge|^{1/2}}exp(-\mu_1\alpha^2) \\
& \int_{-\pi/2}^{\pi/2}\int_0^{\infty}\hat{\alpha}exp(-\mu_2\hat{\alpha}^2)sinh(\nu\alpha\hat{\alpha}cos\varphi)d\hat{\alpha}d\varphi d\alpha \\
=& \frac{1}{2} - \int_0^{\infty}\int_{-\pi/2}^{\pi/2} erf\left(\sqrt{\frac{\bar{\gamma}_b}{2\sigma_x^2}}\alpha cos\varphi\right) \\
& \frac{\alpha}{2\pi|\wedge|^{1/2}}exp(-\mu_1\alpha^2)\frac{\nu\alpha cos\varphi}{4\mu_2}\sqrt{\frac{\pi}{\mu_2}}e^{\frac{(\nu\alpha cos\varphi)^2}{4\mu_2}}d\varphi d\alpha \\
=& \frac{1}{2} - \int_{-\pi/2}^{\pi/2}\frac{\nu cos\varphi}{8\pi|\wedge|^{1/2}\mu_2}\sqrt{\frac{\pi}{\mu_2}} \\
& \int_0^{\infty}\alpha^2 erf\left(\sqrt{\frac{\bar{\gamma}_b}{2\sigma_x^2}}\alpha cos\varphi\right)exp\left\{-\left[\mu_1-\frac{(\nu cos\varphi)^2}{4\mu_2}\right]\alpha^2\right\}d\alpha d\varphi \\
=& \frac{1}{2} - \int_{-\pi/2}^{\pi/2}\frac{\nu cos\varphi}{8\pi|\wedge|^{1/2}\mu_2}\sqrt{\frac{\pi}{\mu_2}}\left\{\frac{\sqrt{\pi}}{4b^3}-\frac{1}{4\sqrt{\pi}}\left[\frac{1}{b^3}tan^{-1}\frac{b}{a}-\frac{a}{b^2(a^2+b^2)}\right]\right\}d\varphi \quad (4.21)
\end{aligned}
$$

where

$$\mu_1 = \frac{\sigma_{\hat{x}}^2}{2|\wedge|^{1/2}} \tag{4.22a}$$

$$\mu_2 = \frac{\sigma_x^2}{2|\wedge|^{1/2}} \tag{4.22b}$$

$$\nu = \frac{R_c}{|\wedge|^{1/2}} \tag{4.22c}$$

$$a = \sqrt{\frac{\gamma_b}{2\sigma_x^2}} cos\varphi \tag{4.22d}$$

$$b^2 = \mu_1 - \frac{(\nu cos\varphi)^2}{4\mu_2}. \tag{4.22e}$$

The integration of $\hat{\alpha}$ is by [33, pp.384 eqn.(3.562 3)]

$$\int_0^\infty x e^{-\mu x^2} sinh\nu x dx = \frac{\nu}{4\mu}\sqrt{\frac{\pi}{\mu}} exp\left(\frac{\nu^2}{4\mu}\right). \tag{4.23}$$

The integration of α is by [34, eqn.(4.36)].

$$\int_0^\infty erf(ax) e^{-b^2x^2} x^2 dx = \left\{\frac{\sqrt{\pi}}{4b^3} - \frac{1}{4\sqrt{\pi}}\left[\frac{1}{b^3} tan^{-1}\frac{b}{a} - \frac{a}{b^2(a^2+b^2)}\right]\right\} \tag{4.24}$$

where $|arg(a)| < \frac{\pi}{4}$.

4.3 BER Analysis of QPSK with Channel Estimation Error

The derivation of the BER for QPSK with channel estimation error is very similar to that of BPSK. Observing Fig. 4.2, we can see there is a cross-quadrature interference, $\alpha sin\varphi$, added to the decision component. Since the parameter, φ, will be averaged over $[0, 2\pi]$ and the constellation is symmetrical, the result is the same using either $\alpha cos\varphi + \alpha sin\varphi$ or $\alpha cos\varphi - \alpha sin\varphi$ for the BER calculation. Thus, the conditional BER is expressed as

$$P(e|\alpha, \varphi) = Q\left[\sqrt{\frac{\gamma_b}{\sigma_x^2}}\alpha(cos\varphi + sin\varphi)\right]. \tag{4.25}$$

The average BER is obtained by averaging the conditional BER over the jpdf of α, $\hat{\alpha}$ and

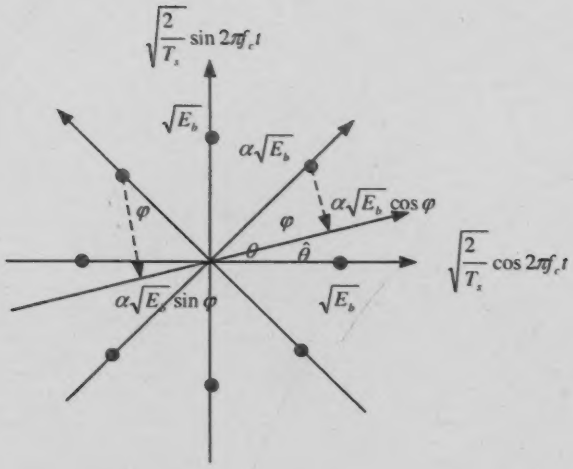

Fig. 4.2. New decision component set by the imperfect estimate and cross-quadrature interference.

φ,

$$
\begin{aligned}
Pe &= \int_0^{\infty}\int_0^{2\pi}\int_0^{\infty} P(e|\alpha,\varphi)p(\alpha,\hat{\alpha},\varphi)d\hat{\alpha}d\varphi d\alpha \\
&= \int_0^{\infty}\int_0^{2\pi}\int_0^{\infty} Q\left[\sqrt{\frac{\bar{\gamma}_b}{\sigma_x^2}}\alpha(cos\varphi+sin\varphi)\right]\frac{\alpha\hat{\alpha}}{2\pi|\wedge|^{1/2}} \\
&\quad exp\left\{-\frac{1}{2|\wedge|^{1/2}}\left[(\hat{\sigma}_x^2\alpha^2+\sigma_x^2\hat{\alpha}^2)-2R_c\alpha\hat{\alpha}cos\varphi\right]\right\}d\hat{\alpha}d\varphi d\alpha \\
&= 0.5-\int_{-\frac{3\pi}{4}}^{\frac{\pi}{4}}\frac{\nu cos\varphi}{8\pi|\wedge|^{1/2}\mu_2}\sqrt{\frac{\pi}{\mu_2}}\left\{\frac{\sqrt{\pi}}{4b^3}-\frac{1}{4\sqrt{\pi}}\left[\frac{1}{b^3}tan^{-1}\frac{b}{a}-\frac{a}{b^2(a^2+b^2)}\right]\right\}d\varphi
\end{aligned}
\tag{4.26a}
$$

where

$$
a=\sqrt{\frac{\gamma_b}{2\sigma_x^2}}(cos\varphi+sin\varphi). \tag{4.26b}
$$

4.4 BER Analysis of 16-QAM with Channel Estimation Error

The performance analysis of 16-QAM is more complicated than that of BPSK and QPSK due to the detection of the multilevel modulated information bits. In the case of perfect channel estimation, the receiver can construct the decision boundaries perfectly. However, in the case of imperfect channel estimation, the decision boundaries are set with the imperfect channel estimate. Fig. 4.3 illustrates that the phase error causes rotation of the decision boundaries. Further clarification is provided in Fig. 4.4; the true phase is θ and the estimated phase is $\hat{\theta}$; so, there is a phase error, φ. The phase error causes a signal amplitude degradation, replacing, for example, $3\alpha d$ by $3\alpha d cos\varphi$. The phase error also causes cross-quadrature-intersymbol interference with values $\pm 3d\alpha sin\varphi$ or $\pm d\alpha sin\varphi$. Note further that due to the symmetries and sign changes of $(+3d\alpha sin\varphi, -3d\alpha sin\varphi)$ and $(+d\alpha sin\varphi, -d\alpha sin\varphi)$, it suffices to include only the values $(3d\alpha sin\varphi, d\alpha sin\varphi)$ in the bit error rate averaging.

It is informative to compare these with the decision boundaries shown in Fig. 2.11 for the case of perfect channel estimation. As seen in Fig. 2.11, the decision boundary for the MSB bits is 0 with perfect estimation. This decision boundary is the same with imperfect estimation as the fading amplitude does not affect the decision boundary in the MSB case as also seen in Fig. 4.3. The BER of the MSB conditioned on α, $\hat{\alpha}$ and φ and accounting for the intersymbol interference from the cross-quadrature components is

$$P_M(e|\alpha,\hat{\alpha},\varphi) = \frac{1}{4}\left\{Q\left[\frac{d}{\sigma_n}(3\alpha cos\varphi + 3\alpha sin\varphi)\right] + Q\left[\frac{d}{\sigma_n}(3\alpha cos\varphi + \alpha sin\varphi)\right] + Q\left[\frac{d}{\sigma_n}(\alpha cos\varphi + 3\alpha sin\varphi)\right] + Q\left[\frac{d}{\sigma_n}(\alpha cos\varphi + \alpha sin\varphi)\right]\right\}. \quad (4.27)$$

As seen in Fig. 2.11, the decision boundaries for the LSB bits are located at $\pm 2\alpha d$ under the assumption that the channel information is perfectly known. In the presence of channel estimation error, the decision boundaries are located at $\pm 2\hat{\alpha}d$ as shown in Fig. 4.3. If a demodulated quadrature sample amplitude is greater than $|2\hat{\alpha}d|$, it is mapped to "1"; if it is greater than $-2\hat{\alpha}d$ and less than $+2\hat{\alpha}d$, it is mapped to "0". Thus, when a logical

"1" is transmitted, the conditional BER can be expressed as $Q[(3\alpha d\cos\varphi - 2\hat{\alpha}d)/\sigma_n]$ - $Q[(3\alpha d\cos\varphi + 2\hat{\alpha}d)/\sigma_n]$; when a logical "0" is transmitted, the conditional BER is given by $Q[(2\hat{\alpha}d - \alpha d\cos\varphi)/\sigma_n] + Q[(2\hat{\alpha}d + \alpha d\cos\varphi)/\sigma_n]$. The BER of the LSB conditioned

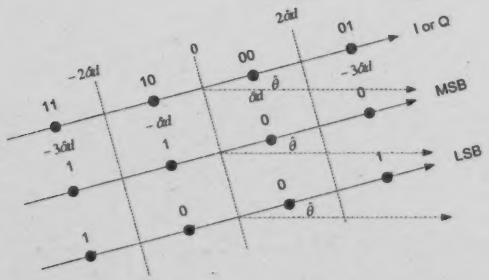

Fig. 4.3. New decision boundaries set by the imperfect estimate. The coordinates are those relative to the rotated signal constellation.

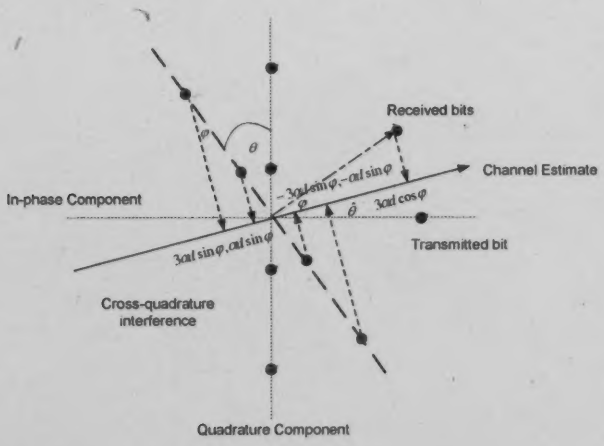

Fig. 4.4. Cross-quadrature interferences due to imperfect estimation.

on α, $\hat{\alpha}$ and φ and accounting for the cross-quadrature interference is then

$$P_L(e|\alpha,\hat{\alpha},\varphi) = \frac{1}{4}\left\{Q\left[\frac{d}{\sigma_n}(3\alpha cos\varphi + 3\alpha sin\varphi - 2\hat{\alpha})\right] - Q\left[\frac{d}{\sigma_n}(3\alpha cos\varphi + 3\alpha sin\varphi + 2\hat{\alpha})\right]\right.$$
$$+Q\left[\frac{d}{\sigma_n}(3\alpha cos\varphi + \alpha sin\varphi - 2\hat{\alpha})\right] - Q\left[\frac{d}{\sigma_n}(3\alpha cos\varphi + \alpha sin\varphi + 2\hat{\alpha})\right]$$
$$+Q\left[\frac{d}{\sigma_n}(-\alpha cos\varphi + 3\alpha sin\varphi + 2\hat{\alpha})\right] + Q\left[\frac{d}{\sigma_n}(\alpha cos\varphi + 3\alpha sin\varphi + 2\hat{\alpha})\right]$$
$$\left.+Q\left[\frac{d}{\sigma_n}(-\alpha cos\varphi + \alpha sin\varphi + 2\hat{\alpha})\right] + Q\left[\frac{d}{\sigma_n}(\alpha cos\varphi + \alpha sin\varphi + 2\hat{\alpha})\right]\right\} \tag{4.28a}$$

$$10d^2 = E_s \tag{4.28b}$$

$$E_s = 4E_b \tag{4.28c}$$

$$\bar{\gamma}_b = \frac{2\sigma_x^2 E_b}{2\sigma_n^2} \tag{4.28d}$$

$$\left(\frac{d}{\sigma_n}\right)^2 = \sqrt{\frac{E_s/10}{\sigma_n^2}} = \frac{2\bar{\gamma}_b}{5\sigma_x^2} \tag{4.28e}$$

where E_b is the energy per bit and $\bar{\gamma}_b$ is the average SNR per bit. Define the integral

$$I(x,y,z,\bar{\gamma}_b) =$$
$$\int_0^\infty \int_0^\infty \int_0^{2\pi} Q\left[\sqrt{\frac{2\bar{\gamma}_b}{5\sigma_x^2}}(x\alpha cos\varphi + y\alpha sin\varphi + z\hat{\alpha})\right] p(\alpha,\hat{\alpha},\varphi)d\varphi d\alpha d\hat{\alpha}. \tag{4.29}$$

Then, (4.29) combined with (2.55), (4.27) and (4.28) gives

$$P_e = \frac{1}{8}\sum_{i=1}^{12} w_i I(x_i,y_i,z_i) \tag{4.30}$$

where the coefficients w_i, x_i, y_i, z_i are listed in Table 4.1.

For $z_i = 0$, the function $I(x_i,y_i,0)$ can be simplified by the same method used in the

TABLE 4.1

Coefficients in the BER Expression (4.30) and (5.26) for 16-QAM

i	w_i	x_i	y_i	z_i	i	w_i	x_i	y_i	z_i
1	1	3	3	0	7	-1	3	3	2
2	1	3	1	0	8	-1	3	1	2
3	1	1	3	0	9	1	-1	3	2
4	1	1	1	0	10	1	-1	1	2
5	1	3	3	-2	11	1	1	3	2
6	1	3	1	-2	12	1	1	1	2

calculation of single branch QPSK case. Define the integral, $W1((x_i,y_i) = I(x_i,y_i,0)$,

$$
\begin{aligned}
W1(x_i,y_i) &= \int_0^{\infty}\int_0^{2\pi}\int_0^{\infty} P(e|\alpha,\varphi)p(\alpha,\hat{\alpha},\varphi)d\hat{\alpha}d\varphi d\alpha \\
&= \int_0^{\infty}\int_0^{2\pi}\int_0^{\infty} Q\left[\sqrt{\frac{2\bar{\gamma}_b}{5\sigma_x^2}}\alpha(x_i cos\varphi + y_i sin\varphi)\right]\frac{\alpha\hat{\alpha}}{2\pi|\wedge|^{1/2}} \\
&\quad exp\left\{-\frac{1}{2|\wedge|^{1/2}}\left[(\hat{\sigma}_x^2\alpha^2+\sigma_x^2\hat{\alpha}^2)-2R_c\alpha\hat{\alpha}cos\varphi\right]\right\}d\hat{\alpha}d\varphi d\alpha \\
&= 0.5 - \int_{-\frac{\pi}{2}-arctan^{-1}\frac{y_i}{x_i}}^{\frac{\pi}{2}-arctan^{-1}\frac{y_i}{x_i}} \frac{vcos\varphi}{8\pi|\wedge|^{1/2}\mu_2}\sqrt{\frac{\pi}{\mu_2}} \\
&\quad \left\{\frac{\sqrt{\pi}}{4b^3} - \frac{1}{4\sqrt{\pi}}\left[\frac{1}{b^3}tan^{-1}\frac{b}{a} - \frac{a}{b^2(a^2+b^2)}\right]\right\}d\varphi
\end{aligned}
\tag{4.31a}
$$

where

$$
a = \sqrt{\frac{\gamma_b}{5\sigma_x^2}}(x_i cos\varphi + y_i sin\varphi). \tag{4.31b}
$$

For $z_i \neq 0$, we introduce a different method for simplification of the integration. Make a change of variables. Let $\alpha = rcos\theta$, $\hat{\alpha} = rsin\theta$, where $0 \leq \theta \leq \pi/2$, $0 \leq r \leq \infty$; the corresponding Jacobian transformation is $J = r$. Define the integral, $W2((x_i,y_i,z_i) = I(x_i,y_i,z_i)$,

$$
\begin{aligned}
W2(x_i,y_i,z_i) &= \int_0^{2\pi}\int_0^{\infty}\int_0^{\infty} P(e|s_1,\alpha,\hat{\alpha}\varphi)p(\alpha,\hat{\alpha},\phi)d\alpha d\hat{\alpha}d\phi \\
&= \int_0^{2\pi}\int_0^{\infty}\int_0^{\infty} Q\left\{\sqrt{\frac{2\bar{\gamma}_b}{5\sigma_x^2}}\left[\alpha(x_i cos\varphi + y_i sin\varphi) + z_i\hat{\alpha}\right]\right\}\frac{\alpha\hat{\alpha}}{2\pi|\wedge|^{1/2}} \\
&\quad exp\left\{-\frac{1}{2|\wedge|^{1/2}}\left[(\hat{\sigma}_x^2\alpha^2 + \sigma_x^2\hat{\alpha}^2) - 2R_c\alpha\hat{\alpha}cos\varphi\right]\right\} d\hat{\alpha}d\alpha d\varphi \\
&= \int_0^{2\pi}\int_0^{\pi/2}\int_0^{\infty} Q\left\{\sqrt{\frac{2\bar{\gamma}_b}{5\sigma_x^2}}\left[cos\theta(x_i cos\varphi + y_i sin\varphi) + z_i sin\theta\right] r\right\} \\
&\quad \frac{r^3 sin2\theta exp\left\{-\frac{r^2}{2|\wedge|^{1/2}}\left[(\hat{\sigma}_x^2 cos^2\theta + \sigma_x^2 sin^2\theta) - R_c sin2\theta cos\phi\right]\right\}}{4\pi|\wedge|^{1/2}} dr d\theta d\phi \\
&= \int_0^{2\pi}\int_0^{\pi/2} \frac{sin2\theta}{4\pi|\wedge|^{1/2}} G(p_i,q_i)d\theta d\phi
\end{aligned}
\tag{4.32a}
$$

where by definition,

$$
\begin{aligned}
G(p,q) &= \int_0^{\infty} e^{-px^2}x^3 Q(qx)dx \\
&= \int_0^{\infty} 0.5e^{-py}yQ(q\sqrt{y})dy \\
&= \frac{1}{2p^2}\left(\frac{1}{2} - \frac{3q}{4\sqrt{2p+q^2}} - \frac{q^3}{4(2p+q^2)^{3/2}}\right)
\end{aligned}
\tag{4.32b}
$$

$$
p_i = \frac{(\hat{\sigma}_x^2 cos^2\theta + \sigma_x^2 sin^2\theta) - R_c sin2\theta cos\phi}{2|\wedge|^{1/2}} \tag{4.32c}
$$

$$
q_i = \frac{2\bar{\gamma}_b}{5\sigma_x^2}\left[cos\theta(x_i cos\varphi + y_i sin\varphi) + z_i sin\theta\right]. \tag{4.32d}
$$

Combining (4.30) with (4.31) and(4.32), the BER for single branch 16-QAM with decorrelation error can be expressed as

$$
\begin{aligned}
Pe &= \frac{1}{8}\sum_{i=1}^{12} w_i I(x_i,y_i,z_i) \\
&= \frac{1}{8}\left[\sum_{i=1}^{4} w_i W1(x_i,y_i) + \sum_{i=1}^{8} w_i W2(x_i,y_i,z_i)\right].
\end{aligned}
\tag{4.33}
$$

In this chapter, we derived the BERs' expressions for single branch BPSK, QPSK and 16-QAM with estimation error. In the following chapter, we will extend the results with the consideration of the MRC diversity combining.

Chapter 5

BER Analysis of Diversity with Channel Estimation Error

In this chapter, we start to derive the BER for MRC BPSK, QPSK and 16-QAM with estimation error. In the case of diversity, imperfect channel estimation degrades the performance of the demodulation *and* degrades the performance of the diversity combining (recall that the weighting of the diversity branches in MRC requires estimates of the complex channel gains [19]). It is desired to find the BER with MRC in Rayleigh fading accounting both for the effect of imperfect channel estimation on the demodulation process and on the diversity combining. We assume that all the diversity branches are independent of each other. The basic idea for deriving the average BER of MRC diversity is same as the single branch. It is obtained by averaged the conditional BER for MRC with estimation error over the jpdf of the related parameters.

5.1 BER Analysis of Diversity BPSK with Channel Estimation Error

Assuming '1' is transmitted, the combiner output sample is given as (2.22),

$$w = \sum_{m=0}^{M-1} \hat{g}_m^* g_m \sqrt{E_b} + \sum_{m=0}^{M-1} \hat{g}_m^* n_m \tag{5.1}$$

The real part of it is then,

$$w_r = Re\{w\} = \sum_{m=0}^{M-1} \hat{\alpha}_m^* \alpha_m \sqrt{E_b} cos\varphi_m + \sum_{m=0}^{M-1} \hat{\alpha}_m^* n'_m \tag{5.2}$$

where α_m, $\hat{\alpha}_m$ and φ_m is the fading channel amplitude, channel amplitude estimate and the phase error on the m_{th} diversity branch, respectively, M is the number of diversity branches. The conditional probability of bit error can be derived using the same method described in Section. 4.2,

$$\begin{aligned} P(e|t) &= Q\left(\sqrt{\frac{\bar{\gamma}_b}{\sigma_x^2}} \frac{\sum_{m=0}^{M-1} \alpha_m \hat{\alpha}_m cos\varphi_m}{\sqrt{\sum_{m=0}^{M-1} \hat{\alpha}_m^2}}\right) \\ &= Q\left(t\sqrt{\frac{\bar{\gamma}_b}{\sigma_x^2}}\right) \end{aligned} \tag{5.3}$$

where $t = \frac{\sum_{m=0}^{M-1} \hat{\alpha}_m \alpha_m cos\varphi_m}{\sqrt{\sum_{m=0}^{M-1} \hat{\alpha}_m^2}}$.

We need the pdf of t to calculate the BER. The derivation of the pdf of t follows the analysis described in [29], but in contrast to the analysis in [29] where the variances of a fading quadrature component and its estimate are equal, here the variances of a fading quadrature component and its estimate are different. The case where they are equal models noiseless estimation and, thus, only the effects of decorrelation are accounted for in the analysis of [29]. We extend the analysis of [29] to include channel estimation error originating from both decorrelation and noise. Let the variance of a fading quadrature component and its estimate be σ_x and $\sigma_{\hat{x}}$, respectively. Recall from (4.1) that the joint distribution of

amplitudes α_m, $\hat{\alpha}_m$ and their phase difference φ_m is

$$p(\alpha_m, \hat{\alpha}_m, \varphi_m) = \frac{\alpha_m \hat{\alpha}_m}{2\pi|\wedge|^{1/2}}$$
$$\times exp\left\{ -\frac{[\sigma_{\hat{x}}^2 \alpha_m^2 + \sigma_x^2 \hat{\alpha}_m^2 - 2R_c \alpha_m \hat{\alpha}_m cos\varphi_m - 2R_{cs} \alpha_m \hat{\alpha}_m sin\varphi_m]}{2|\wedge|^{1/2}} \right\}. \quad (5.4)$$

The amplitude of the estimate, $\hat{\alpha}_m$, is Rayleigh distributed, its pdf is given by [2, eqn. (2-1-128)].

$$p(\hat{\alpha}_m) = \frac{\hat{\alpha}_m}{\sigma_{\hat{x}}^2} exp\left(-\frac{\hat{\alpha}_m^2}{2\sigma_{\hat{x}}^2}\right). \quad (5.5)$$

So the conditional pdf of α_m, φ_m given $\hat{\alpha}_m$ is

$$p(\alpha_m, \varphi_m|\hat{\alpha}_m) = \frac{p(\alpha_m, \hat{\alpha}_m, \varphi_m)}{p(\hat{\alpha}_m)}. \quad (5.6)$$

Define,

$$\alpha_m cos\varphi_m = u_m + \frac{R_c \hat{\alpha}_m}{\sigma_{\hat{x}}^2} \quad (5.7a)$$

$$\alpha_m sin\varphi_m = v_m + \frac{R_{cs} \hat{\alpha}_m}{\sigma_{\hat{x}}^2} \quad (5.7b)$$

$$du_m dv_m = \alpha_m d\alpha_m d\varphi_m \quad (5.7c)$$

and (5.4)-(5.7) yield

$$p(u_m, v_m|\hat{\alpha}_m) = \frac{\sigma_{\hat{x}}^2}{2\pi\wedge^{\frac{1}{2}}} exp\left[-\frac{\sigma_{\hat{x}}^2}{2\wedge^{\frac{1}{2}}}(u_m^2 + y_m^2)\right] \quad (5.8)$$

where R_c, R_{cs} and $\wedge$ are defined in (4.3a), (4.3b) and (2.17d). It can be shown from (5.8) that u_m and v_m are independent of each other , and independent of $\hat{\alpha}_m$ [29]. Each of them has a zero-mean Gaussian distribution with variance, $\frac{\wedge^{\frac{1}{2}}}{\sigma_{\hat{x}}^2}$. Now define,

$$u = \frac{\sum_{m=0}^{M-1} \hat{\alpha}_m u_m}{\sqrt{\sum_{m=0}^{M-1} \hat{\alpha}_m^2}} \quad (5.9a)$$

$$v = \frac{\sum_{m=0}^{M-1} \hat{\alpha}_m v_m}{\sqrt{\sum_{m=0}^{M-1} \hat{\alpha}_m^2}} \quad (5.9b)$$

$$U = \frac{R_c}{\sigma_{\hat{x}}^2} \left(\sum_{m=0}^{M-1} \hat{\alpha}_m^2 \right)^{1/2}. \quad (5.9c)$$

It is shown in [29] that u and v are also Gaussian distributed with variance, $\frac{\Lambda^{\frac{1}{2}}}{\sigma_{\hat{x}}^2}$, and are independent of $\hat{\alpha}_m$. The parameter, U, has a chi density [35, eqn. (5-25)] with $2M$ degrees of freedom and each degree of freedom has a variance σ^2. Note that u and U are independent of each other [29]. Summarizing, the pdf's of u, U and v are given by

$$p(u) = \frac{\sigma_{\hat{x}}}{\sqrt{2\pi\Lambda^{1/2}}} exp\left[-\frac{\sigma_{\hat{x}}^2}{2\Lambda^{1/2}}u^2\right] \tag{5.10a}$$

$$p(v) = \frac{\sigma_{\hat{x}}}{\sqrt{2\pi\Lambda^{1/2}}} exp\left[-\frac{\sigma_{\hat{x}}^2}{2\Lambda^{1/2}}v^2\right] \tag{5.10b}$$

$$p(U) = \frac{2U^{2M-1}exp(-U^2/2\sigma^2)}{2^M\sigma^{2M}\Gamma(M)} \tag{5.10c}$$

where $\sigma^2 = \frac{R_c^2}{\sigma_{\hat{x}}^2}$.

Thus, the pdf of $t = u + U$ is

$$\begin{aligned} p_{u+U}(t) &= \int_0^\infty p_u(t-U)p_U(U)dU \\ &= \frac{\sqrt{2}\sigma_{\hat{x}}exp(-\sigma_{\hat{x}}^2t^2/2\Lambda^{1/2})}{2^M\sqrt{\pi}\sigma^{2M}\Gamma(M)} \int_0^\infty U^{2M-1}exp\left(-\beta U^2 - \lambda U\right)dU \end{aligned} \tag{5.11a}$$

where

$$\beta = \frac{1}{2\sigma^2} + \frac{\sigma_{\hat{x}}^2}{2\Lambda^{1/2}} \tag{5.11b}$$

$$\lambda = -\frac{\sigma_{\hat{x}}^2 t}{\Lambda^{1/2}}. \tag{5.11c}$$

Eqn. (5.11a) can be simplified using [33, eqn. (3.462)]. Thus,

$$p(t) = \frac{\sqrt{2}\sigma_{\hat{x}}\Gamma(2M)}{2^{2M}\sqrt{\pi\Lambda^{1/2}}\sigma^{2M}\beta^M\Gamma(M)} exp\left[-\left(\frac{1}{2} - \frac{\sigma_{\hat{x}}^2}{8\Lambda^{1/2}\beta}\right)\frac{\sigma_{\hat{x}}^2t^2}{\Lambda^{1/2}}\right] D_{-2M}\left(\frac{-\sigma_{\hat{x}}^2 t}{\sqrt{2\Lambda\beta}}\right) \tag{5.12}$$

where $D_v(x)$ is the parabolic cylinder function defined at [29, eqn. (42)]. So the BER for

MRC BPSK with estimation error is

$$
\begin{aligned}
Pe &= \int_{-\infty}^{\infty} Q\left(t\sqrt{\frac{\bar{\gamma}_b}{\sigma_x^2}}\right) p(t)dt \\
&= \frac{\sqrt{2}\sigma_{\hat{x}}\Gamma(2M)}{2^{2M}\sqrt{\pi}\Lambda^{1/2}\sigma^{2M}\beta^M\Gamma(M)} \\
&\quad \int_{-\infty}^{\infty} Q\left(t\sqrt{\frac{\bar{\gamma}_b}{\sigma_x^2}}\right) exp\left[-\left(\frac{1}{2}-\frac{\sigma_{\hat{x}}^2}{8\Lambda^{1/2}\beta}\right)\frac{\sigma_{\hat{x}}^2 t^2}{\Lambda^{1/2}}\right] D_{-2M}\left(\frac{-\sigma_{\hat{x}}^2 t}{\sqrt{2\Lambda\beta}}\right) dt.
\end{aligned} \tag{5.13}
$$

Using (5.13), P_e can be calculated numerically for a given order of diversity, M, and given frame length, L, as well as given symbol location, l.

5.2 BER Analysis of Diversity QPSK with Channel Estimation Error

Recalling the conditional BER for single branch QPSK with estimation error from Section 4.3 and combining with the derivation in Section 5.1, the conditional BER for MRC diversity QPSK with estimation error is expressed as

$$
\begin{aligned}
P(e|t) &= Q\left(\sqrt{\frac{\bar{\gamma}_b}{\sigma_x^2}}\frac{\sum_{m=0}^{M-1}\alpha_m\hat{\alpha}_m(cos\varphi_m+sin\varphi_m)}{\sqrt{\sum_{m=0}^{M-1}\hat{\alpha}_m^2}}\right) \\
&= Q\left(t\sqrt{\frac{\bar{\gamma}_b}{\sigma_x^2}}\right).
\end{aligned} \tag{5.14}
$$

where $t = \frac{\sum_{m=0}^{M-1}\hat{\alpha}_m\alpha_m(cos\varphi_m+sin\varphi_m)}{\sqrt{\sum_{m=0}^{M-1}\hat{\alpha}_m^2}}$.

Define t_1 and t_2,

$$
t_1 = \frac{\sum_{m=0}^{M-1}\hat{\alpha}_m\alpha_m cos\varphi_m}{\sqrt{\sum_{m=0}^{M-1}\hat{\alpha}_m^2}} \tag{5.15a}
$$

$$
t_2 = \frac{\sum_{m=0}^{M-1}\hat{\alpha}_m\alpha_m sin\varphi_m}{\sqrt{\sum_{m=0}^{M-1}\hat{\alpha}_m^2}}. \tag{5.15b}
$$

Then $t = t_1 + t_2$. The pdf of t_1 is as given in (5.12),

$$p(t_1) = \frac{\sqrt{2}\sigma_{\hat{x}}\Gamma(2M)}{2^{2M}\sqrt{\pi}\wedge^{1/2}\sigma^{2M}\beta^M\Gamma(M)} exp\left[-\left(\frac{1}{2} - \frac{\sigma_{\hat{x}}^2}{8\wedge^{1/2}\beta}\right)\frac{\sigma_{\hat{x}}^2 t_1^2}{\wedge^{1/2}}\right] D_{-2M}\left(\frac{-\sigma_{\hat{x}}^2 t_1}{\sqrt{2\wedge\beta}}\right) \tag{5.16}$$

As $R_{cs} = 0$, the pdf of t_2 is obtained by combining (5.7b), (5.9b) and (5.10b) yielding

$$p(t_2) = \frac{\sigma_{\hat{x}}}{\sqrt{2\pi}\wedge^{1/2}} exp\left(-\frac{\sigma_{\hat{x}}^2}{2\wedge^{1/2}} t_2^2\right). \tag{5.17}$$

So the BER for MRC QPSK with estimation error is

$$Pe = \int_{-\infty}^{\infty}\int_{-\infty}^{\infty} Q\left[(t_1 + t_2)\sqrt{\frac{\bar{\gamma}_b}{\sigma_x^2}}\right] p(t_1)p(t_2)dt_1 dt_2 \tag{5.18}$$

Make a change of variables. Let $t_1 = rcos\theta$, $t_2 = rsin\theta$, where $0 \leq \theta \leq 2\pi$, $0 \leq r \leq \infty$; the corresponding Jacobian transformation is $J = r$. Then Pe becomes

$$Pe = \int_0^{\infty}\int_0^{2\pi} rQ\left[(rcos\theta + rsin\theta)\sqrt{\frac{\bar{\gamma}_b}{\sigma_x^2}}\right] p_{t_1}(rcos\theta)p_{t_2}(rsin\theta)d\theta dr. \tag{5.19}$$

Using (5.19), P_e can be calculated numerically for a given order of diversity, M, and given frame length, L, as well as given symbol location, l.

5.3 BER Analysis of Diversity 16-QAM with Channel Estimation Error

We start from (4.27) and (4.28) and alter these equations to account for diversity, fading and channel estimation error as well as intersymbol interference. To do so, we define a useful ancillary parameter t_i and then condition the BER on t_i giving

$$\begin{aligned} P(e|t_i) &= \frac{1}{8}\sum_{i=1}^{12} w_i Q(At_i) \\ &= \frac{1}{8}\sum_{i=1}^{12} w_i Q\left(A\frac{\sum_{m=0}^{M-1}\alpha_m\hat{\alpha}_m(x_i cos\varphi_m + y_i sin\varphi_m) + z_i\hat{\alpha}_m^2}{\sqrt{\sum_{m=0}^{M-1}\hat{\alpha}_m^2}}\right) \end{aligned} \tag{5.20a}$$

$$A = \frac{d}{\sigma_n} = \sqrt{\frac{2\bar{\gamma}_b}{5\sigma_x^2}} \tag{5.20b}$$

$$t_i = \frac{\sum_{m=0}^{M-1} \hat{\alpha}_m \left[(\alpha_m x_i cos\varphi_m + \alpha_m y_i sin\varphi_m) + z_i \hat{\alpha}_m \right]}{\sqrt{\sum_{m=0}^{M-1} \hat{\alpha}_m^2}}. \tag{5.20c}$$

The coefficients w_i, x_i, y_i, z_i are again listed in Table 4.1. The parameter, t_i, is clarified as follows. In the single branch reception case, $M = 1$ and the BER of the 16-QAM in the absence of fading is given by (4.27) and (4.28). In the case of diversity, $M > 1$ and t_i corresponds to the i_{th} term in a sum of weighted terms, each term being a $Q(\cdot)$ function as in (4.27) and (4.28). The decision statistic of the m_{th} diversity branch includes the transmitted signal distorted by the phase error, $\alpha_m x_i cos\varphi_m$, the intersymbol interference, $\alpha_m y_i sin\varphi_m$, caused by phase error and the decision boundary information represented by $z_i \hat{\alpha}_m$, which is determined by the amplitude estimate. The derivation is very similar to the earlier derivation given in Section 4.4 and illustrated in Figs. 4.3 and 4.4, but includes the effect of MRC diversity.

We rewrite t_i from (5.20c) as

$$\begin{aligned} t_i &= x_i(u+U) + y_i v + z_i \left(\sum_{m=0}^{M-1} \hat{\alpha}_m^2 \right)^{1/2} \\ &= x_i(u+U_i') + y_i v \\ &= x_i \mu_i + y_i v \end{aligned} \tag{5.21a}$$

where

$$U_i' = \left(\frac{R_c}{\sigma_{\hat{x}}^2} + z_i/x_i\right)\left(\sum_{m=0}^{M-1} \hat{\alpha}_m^2\right)^{1/2}. \tag{5.21b}$$

The pdf of U'_i is given by

$$p(U_i') = \frac{2U_i'^{2M-1} exp(-U_i'^2/2\sigma_i^2)}{2^L \sigma_i^{2M} \Gamma(M)} \tag{5.22a}$$

$$\sigma_i^2 = \left(\frac{R_c}{\sigma^2} + \frac{z_i}{x_i}\right)^2 \sigma_{\hat{x}}^2. \tag{5.22b}$$

The pdf of $\mu_i = u + U'_i$ is derived using the same method for the derivation of $t = u + U$ in Subsection. 5.1,

$$p_{\mu_i}(\mu_i) = \int_0^\infty p_u(\mu_i - U'_i) p_{U'_i}(U'_i) dU'_i$$
$$= \frac{\sqrt{2}\sigma_{\hat{x}} exp(-\sigma_{\hat{x}}^2 \mu_i^2 / 2\wedge^{1/2})}{2^L \sqrt{\pi} \sigma_i^{2M} \Gamma(M)} \int_0^\infty U'^{2M-1}_i exp\left(-\beta_i U'^2_i - \lambda_i U'_i\right) dU'_i \quad (5.23a)$$

where

$$\beta_i = \frac{1}{2\sigma_i^2} + \frac{\sigma_{\hat{x}}^2}{2\wedge^{1/2}} \quad (5.23b)$$

$$\lambda_i = -\frac{\sigma_{\hat{x}}^2 \mu_i}{\wedge^{1/2}}. \quad (5.23c)$$

Eqn. (5.23a) can be simplified using [33, eqn. (3.462)]. Thus,

$$p_{\mu_i}(\mu_i) = \frac{\sqrt{2}\sigma_{\hat{x}} \Gamma(2M)}{2^{2M} \sqrt{\pi} \sigma_i^{2L\beta_i^M} \Gamma(M)} exp\left[-\left(\frac{1}{2} - \frac{\sigma_{\hat{x}}^2}{8\wedge^{1/2}\beta_i}\right) \frac{\sigma_{\hat{x}}^2 \mu_i^2}{\wedge^{1/2}}\right] D_{-2M}\left(\frac{-\sigma_{\hat{x}}^2 \mu_i}{\sqrt{2\wedge\beta_i}}\right). \quad (5.24)$$

Since x_i, y_i and z_i are real numbers and μ_i and v are independent, the BER of 16-QAM with MRC can be written as,

$$Pe = \frac{1}{8} \sum_{i=1}^{12} \int_{-\infty}^{\infty} \int_{-\infty}^{\infty} P(e|\mu_i, v) p_{\mu_i}(\mu_i) p_v(v) d\mu_i dv$$
$$= \frac{1}{8} \sum_{i=1}^{12} \int_{-\infty}^{\infty} \int_{-\infty}^{\infty} w_i Q\left[A(x_i \mu_i + y_i v)\right] p_{\mu_i}(\mu_i) p_v(v) d\mu_i dv. \quad (5.25)$$

Eqn. (5.25) is a double integral in two variables each of which has doubly infinite range. Making the variable changes, $\mu_i = r_i cos\theta_i$ and $v = r_i sin\theta_i$, where $0 \leq \theta_i \leq 2\pi$, $0 \leq r_i \leq \infty$, the corresponding Jacobian of the transformation is $J = r_i$. Then (5.25) can be written as

$$Pe = \frac{1}{8} \sum_{i=1}^{12} \int_0^{\infty} \int_0^{2\pi} w_i r_i Q\left[A(x_i r_i cos\theta_i + y_i r_i sin\theta_i)\right] p_{\mu_i}(r_i cos\theta_i) p_v(r_i sin\theta_i) d\theta_i dr_i \quad (5.26)$$

with the coefficients w_i, x_i, y_i and z_i given in Table 4.1. Using (5.26), P_e can be calculated numerically for a given order of diversity, M, and given frame length, L, as well as given symbol location, l.

We derived the BER MRC BPSK, QPSK and 16-QAM with estimation errors in this chapter. The numerical examples will be shown in the next chapter. We will also consider the BERs' associated with different information symbol locations, the sensitivity of the BER results to the choice of windows used in the pilot symbol interpolation filter and the sensitivity of diversity systems to channel estimation errors.

Chapter 6

Numerical Examples and Discussion

In this chapter, the BER performances of BPSK, QPSK and 16-QAM at symbol location, $l = 8$, with or without diversity are first illustrated. Afterwards, two interesting topics will be discussed. One is about the relationships among the average BER, the correlation coefficient and the symbol locations. The other is related to the sensitivity of the BER performance, or say, the the estimate quality, to the windows applied to the sinc interpolator.

All the numerical results were obtained using Mathematica and the simulations were implemented in Matlab. The simulator in [36] was used to generate complex gain samples from a Rayleigh flat fading channel with Doppler shift. The high statistical quality of this simulator is certified in [36] and [37]. We set the system parameters for both numerical calculation and simulation as frame length, $L = 15$, interpolation order, $K = 30$ with $k_1 = 14$ and $k_2 = 15$, normalized Doppler spread, $f_D T = 0.03$ and fading variance, $\sigma_x^2 = 1$.

6.1 Numerical Examples

Fig. 6.1, Fig. 6.2 and Fig. 6.3 show the BER as a function of the average SNR per bit of BPSK, QPSK and 16-QAM, respectively, for single branch ($M = 1$) reception as well as dual branch ($M = 2$) diversity with a Hamming window applied to the sinc interpolator . Both theoretical and simulation results for the BER's at the symbol location, $l = 8$, as well as the BER's for perfect channel estimation are presented. Note first that our theoretical

results and simulation results are in excellent agreement. This gives confidence that our theoretical expressions for the BER's are correct.

The BER performance with MRC is much better than without diversity, as expected. In particular, at $\gamma_b = 40$ dB, the BER's of BPSK, QPSK and 16-QAM are lowered by almost two orders of magnitude by the use of dual diversity. However, the performance with diversity degrades, compared with the perfect estimation case, more than that of a single branch system due to the channel estimation error. For example, in Fig. 6.3, at γ_b =30 dB, the BER is increased by a factor of 1.90 (from 9.43×10^{-4} to 4.96×10^{-4}) for the system without diversity, while the BER is increased by a factor of 3.92 (from 3.46×10^{-6} to 8.82×10^{-7}) for the dual diversity system. This is expected since the channel estimation error degrades the diversity combining as well as degrading the coherent demodulation. Similar conclusions can be drawn from Fig. 6.1 and Fig. 6.2, associated with BPSK and QPSK modulation, respectively.

6.2 Discussion of the Relationships Among the Average BER, the Correlation Coefficient and the Symbol Locations

The accuracy of the channel estimate, in fact, determines the degradation of the BER from that of perfect estimation. The better the estimate, the smaller the BER and vice versa. Based on the mathematical point of view, the correlation coefficient, $\rho = \frac{R_c}{\sigma_x \sigma_{\hat{x}}}$, in fact, is the normalized covariance of the in-phase/quadrature component samples of the channel and the channel estimate. It illustrates the dependency or say similarity , of the samples of the real channel and its estimate. In turn, it determines the behavior of the BER performance. By carefully scrutiny of all the equations for the BER's of BPSK, QPSK and 16-QAM, with or without diversity, all the occurrences of Rc, σ_x and $\sigma_{\hat{x}}$ in the equations can be expressed in terms of ρ. In the view of communication, there are two factors, decorrelation and AWGN, mainly affecting the estimation. As we adopt moderate fading

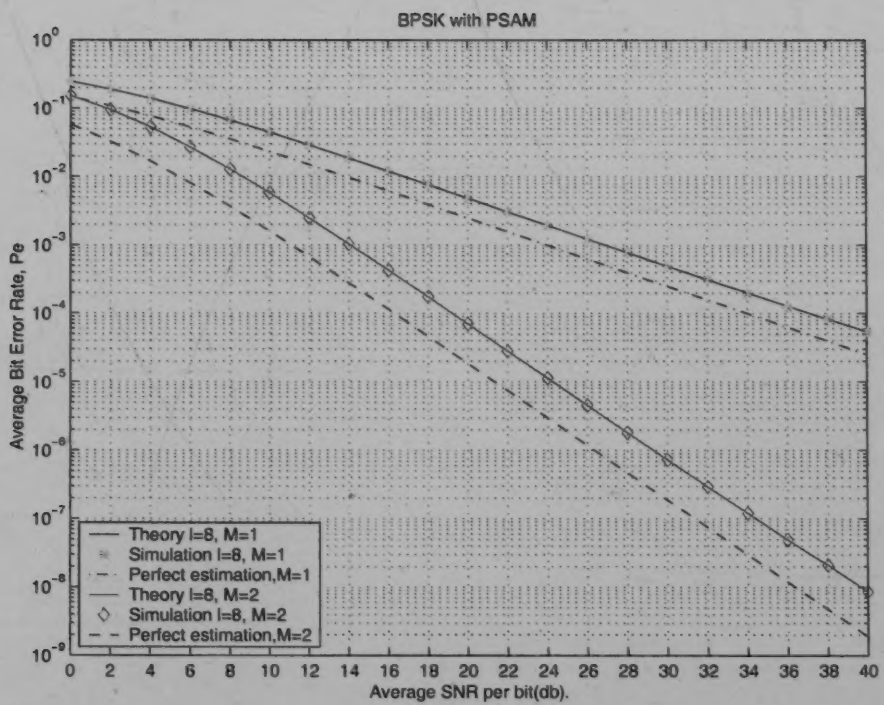

Fig. 6.1. The BER performance of BPSK for $l = 8$ with a Hamming window applied to the sinc interpolator for $L = 15$, $K = 30$, and $f_D T_s = 0.03$; the parameter, l, is the symbol location in one frame.

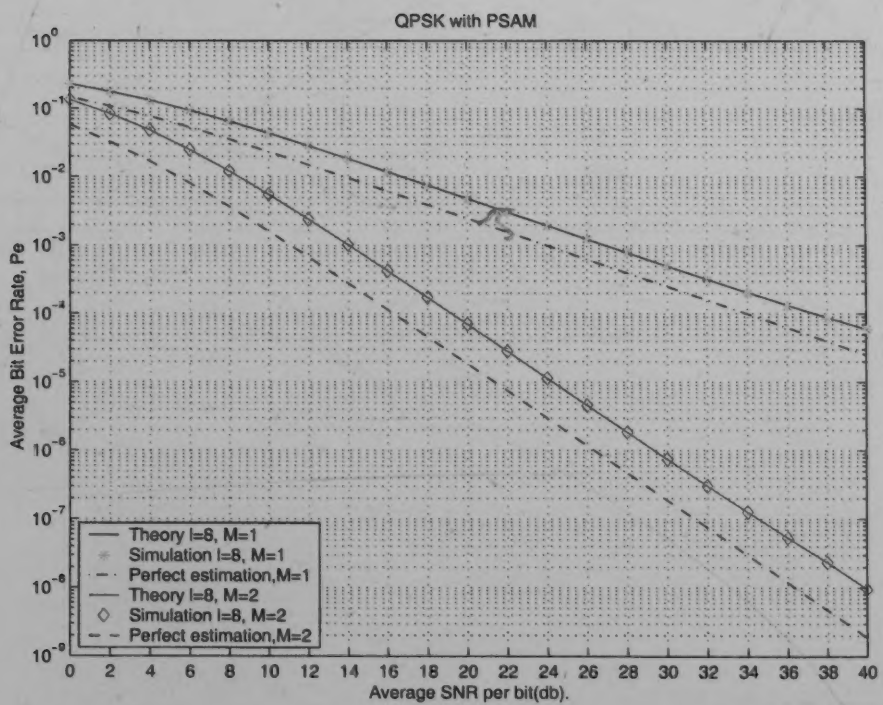

Fig. 6.2. The BER performance of QPSK for $l = 8$ with a Hamming window applied to the sinc interpolator for $L = 15$, $K = 30$, and $f_D T_s = 0.03$; the parameter, l, is the symbol location in one frame.

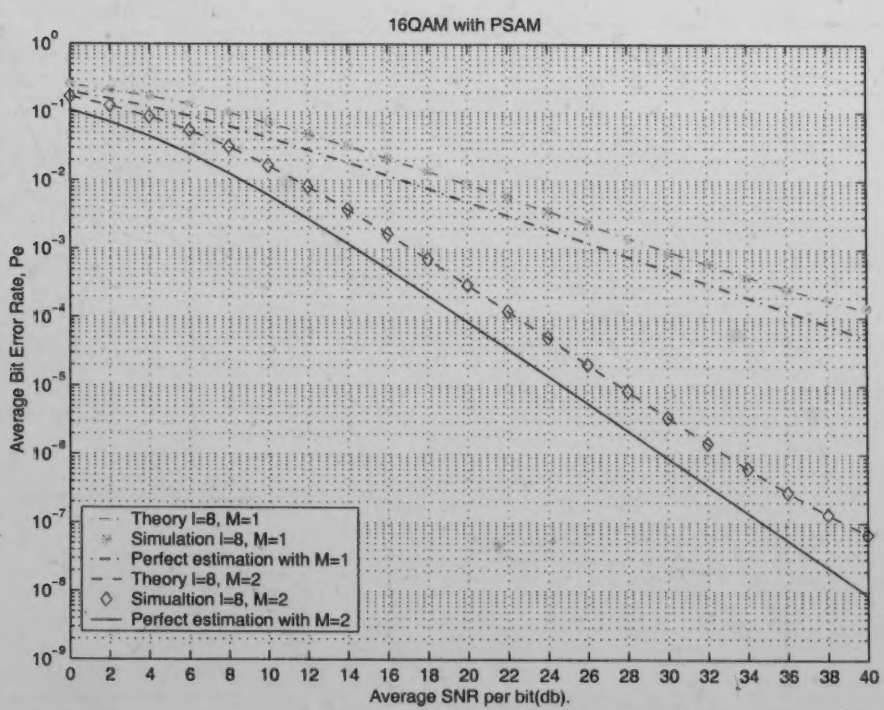

Fig. 6.3. The BER performance of 16-QAM for $l = 8$ with a Hamming window applied to the sinc interpolator for $L = 15$, $K = 30$, and $f_D T_s = 0.03$; the parameter, l, is the symbol location in one frame.

model in our system, the fading is changing among the successive symbols but remains unchanged during a symbol period. In a PSAM system, the further a symbol from the pilot, the larger the decorrelation between the real channel state of the current symbol and that of the pilot and the larger the decorrelation between the channel and the channel estimate, which leads to less accurate estimation. This is demonstrated by Fig. 6.4, corresponding to (4.3a), which shows the covariance between the in-phase/quadrature component samples of the channel and the channel estimate for 16-QAM. In this thesis, the covariance is equivalent to the second order joint moment of those random variables because they are all zero means according to the characteristics of Rayleigh fading. In Fig. 6.4, the second order joint moment, Rc, achieves its largest value at $l = 1$ and $l = 14$, is symmetrical for $1 \leq l \leq 14$ about $l = 7$ and $l = 8$ and achieves the smallest value at $l = 7$ and $l = 8$, which is in the middle of a frame. Besides the parameter, Rc, there is another parameter, the deviation of the channel estimate, $\sigma_{\hat{x}}$, which is related to the position of the symbol. Fig. 6.5 and Fig. 6.6 for 16-QAM, corresponding to (4.4), show that the parameter, $\sigma_{\hat{x}}$, achieves its largest value at $l = 1$ and $l = 14$, is symmetrical for $1 \leq l \leq 14$ about $l = 7$ and $l = 8$ and achieves its smallest value at $l = 7$ and $l = 8$, which is in the middle of a frame. Simply speaking, the further the symbol from the pilot, the smaller the variance of the channel estimate. Similar conclusions apply to the results for BPSK and QPSK that are shown in Fig. 6.11, Fig. 6.12, Fig. 6.16 and Fig. 6.17. A good channel estimate should be achieved with a large covariance and a small deviation. However, in this system, the influences of the parameters, Rc and $\sigma_{\hat{x}}$ on the accuracy of the channel estimate operate in opposite ways as the location of the symbol changes. Thus, the accuracy of the channel estimate should depend on the ratio of these two parameters, which can be expressed as, $\rho = \frac{R_c}{\sigma_x \sigma_{\hat{x}}}$, since $\sigma_{\hat{x}}^2 = 1$. So the mathematical analysis is consistent with the communication explanation.

All the numerical and simulation results for BER's prove our analysis that the BER's change with the symbol location, l, and have an inverse dependency on ρ. We use 16-QAM as an example for further discussion. Fig.6.7 and Fig.6.8 are plots of the parameter, ρ, which changes with both the symbol location and the SNR per bit. This is because Rc varies only with the symbol location since it is independent of the SNR per bit when

the other PSAM parameters are held constant. In contrast, $\sigma_{\hat{x}}$ varies with both the symbol location and the SNR per bit. Fig. 6.9 illustrates the BER's of 16-QAM for $l = 1$ and $l = 8$ with a Hamming window applied to the sinc interpolator. The behavior of the BER in Fig. 6.9 and Table 6.1 can be seen to correspondent to the behavior of ρ in Fig.6.7 and Fig.6.8. Fig. 6.8 shows that ρ (at fixed $\gamma_b = 35$ dB, 37 dB, 39 dB, 40 dB) achieves its largest value at $l = 1$ and $l = 14$, is symmetrical for $1 \leq l \leq 14$ about $l = 7$ and $l = 8$ and achieves its smallest value at $l = 7$ and $l = 8$, which is in the middle of a frame. Meanwhile, Fig. 6.9 clearly shows that at large SNR per bit ($\gamma_b \geq 34$ dB), the BER performance is better at $l = 1$ than that at $l = 8$, so the value of BER is larger at $l = 8$ than that at $l = 1$, which is opposite the behavior of ρ. Furthermore, the error rate floor is greater for information symbols more distant from the pilot symbols. For both the single branch and the dual branch reception case, the error floors occur for $l = 8$, and are not that obvious for $l = 1$. This can explained by the dominance of the decorrelation as an error causing mechanism with increasing SNR. As the SNR increases, the errors caused by AWGN are insignificant, and thus, the decorrelation plays the main role. So the further the information symbol from the pilot, the worse the performance, as expected. Fig. 6.7 tells us that ρ (for a fixed $\gamma_b =$ 10 dB, 12 dB, 14 dB, 15 dB), achieves its smallest value at $l = 1$ and $l = 14$, is symmetrical for $1 \leq l \leq 14$ about $l = 7$ and $l = 8$ and achieves its largest value at $l = 7$ and $l = 8$, which is in the middle of a frame. The difference between the BER's at $l = 1$ and $l = 8$ when $\gamma_b < 34$ dB is slight, it is hardly observable in Fig. 6.9. But it can be seen from the numerical results shown in Table. 6.1. Comparing the BER's of 16-QAM for $l = 1$ and $l = 8$ listed in Table. 6.1, we find the BER's at $l = 8$ are smaller than those at $l = 1$ when $\gamma_b \leq 26$ dB. For example, at $\gamma_b = 10$ dB, $P_b = 7.038E-02$ for 16-QAM at $l = 1$ and $P_b = 6.923E-02$ for 16-QAM at $l = 8$, while ρ achieves the largest value at $l = 8$. Thus, Fig. 6.7, Fig. 6.8, Fig. 6.9 and Table 6.1 show us the inverse relationship between the BER performance of 16-QAM and the behavior of ρ as well as the BER performance relative to different symbol locations, which are consistent with our previous conclusions. The preceding discussion and conclusions are also true for the cases of BPSK and QPSK, as demonstrated by the relevant plots and data in Fig. 6.13, Fig. 6.14, Fig. 6.18, Fig. 6.19,

Fig. 6.10, Fig. 6.15 and Table 6.1.

Another important conclusion drawn from Fig. 6.10, Fig.6.15 and Fig.6.9 is that for practical values of SNR per bit ($0 - 34$ dB), there is only a slight performance difference between different symbol locations, so the position dependence is negligible. We can also say that with the PSAM parameter settings in our system model, the decorrelation caused by Doppler shift is trackable within practical SNR ranges and the channel estimation error caused by AWGN dominates that caused by decorrelation. Therefore, the error floor as well as the performance dependence on the symbol location does not occur until large SNR. This may be less true when other parameter settings or other interpolator filters are used in the PSAM system. Furthermore, in real systems, there will be other sources that cause estimation error, such as the phase errors in carrier synchronization and errors in timing recovery, etc. These factors may result in the earlier occurrence of an error floor or result in a stranger dependence of the BER on symbol location appearing at smaller values of SNR. In the next section, we will discuss the performance with different windows applied to the sinc interpolator, from which we can observe the influence of different windows on the estimation error, the BER performance and their dependences on the symbol location.

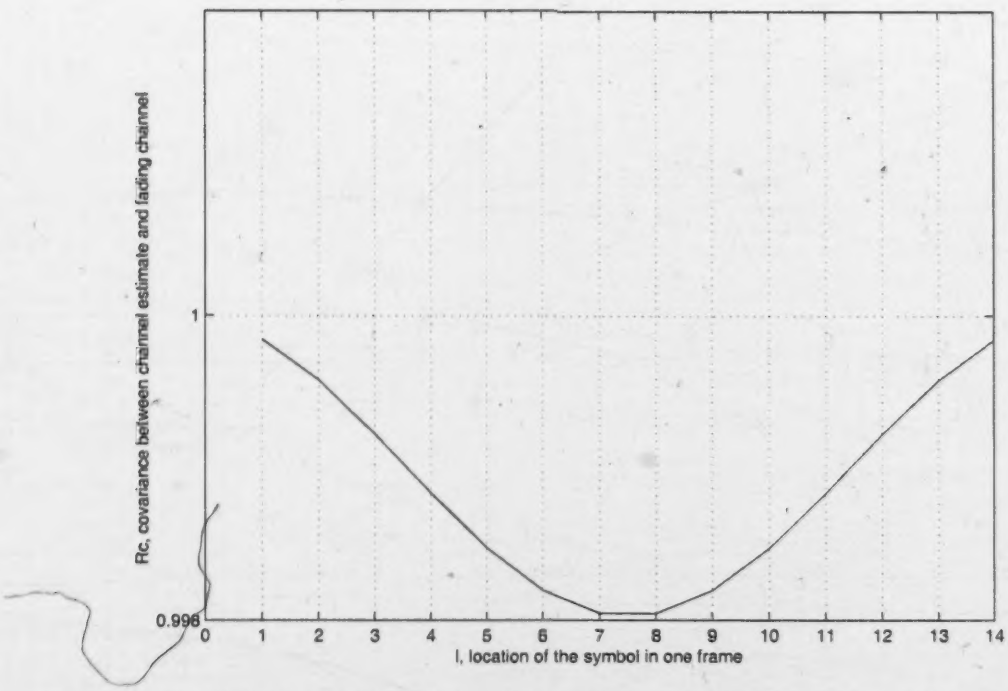

Fig. 6.4. Relationship between the covariance, *Rc*, and symbol location, *l*, for a Hamming window applied to the sinc interpolator.

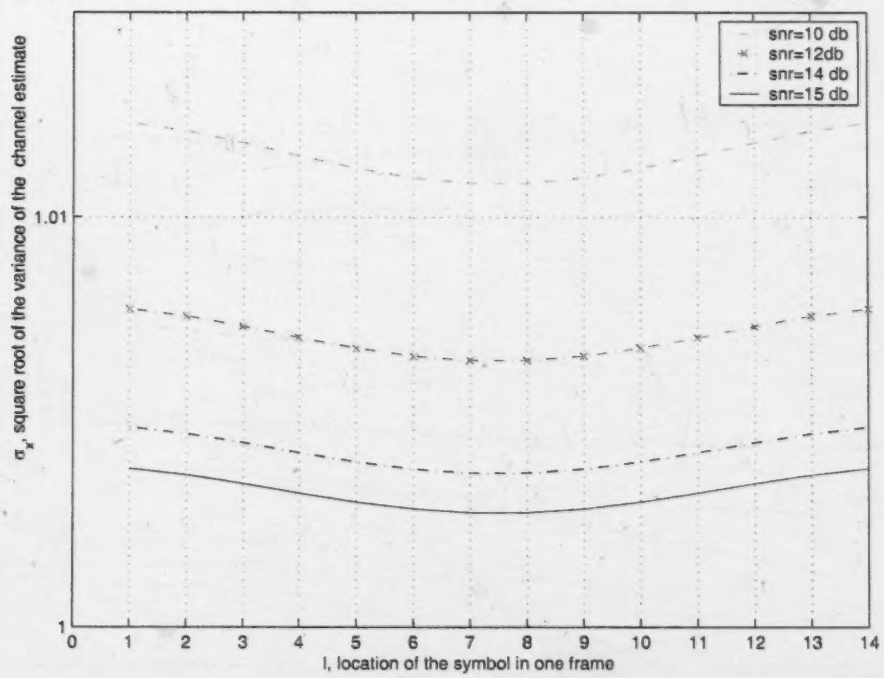

Fig. 6.5. Relationship between the square root of the variance of the channel estimate of 16-QAM, $\sigma_{\hat{x}}$, and symbol location, l, for a Hamming window applied to the sinc interpolator for fixed values of SNR per bit of 10 dB, 12 dB, 14 dB and 15 dB.

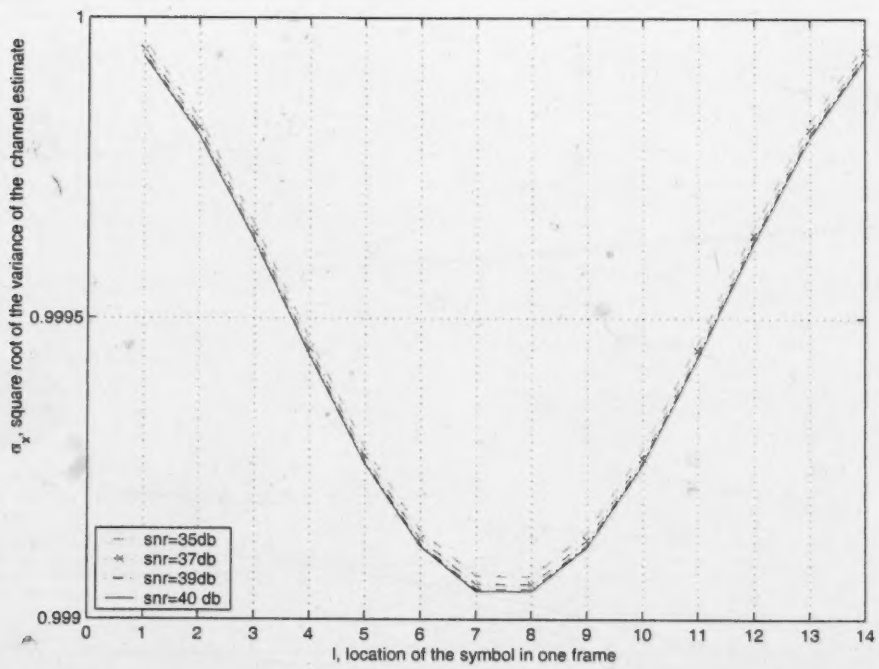

Fig. 6.6. Relationship between the square root of the variance of the channel estimate of 16-QAM, $\sigma_{\hat{x}}$, and symbol location, l, for a Hamming window applied to the sinc interpolator for fixed values of SNR per bit of 35 dB, 37 dB, 39 dB and 40 dB.

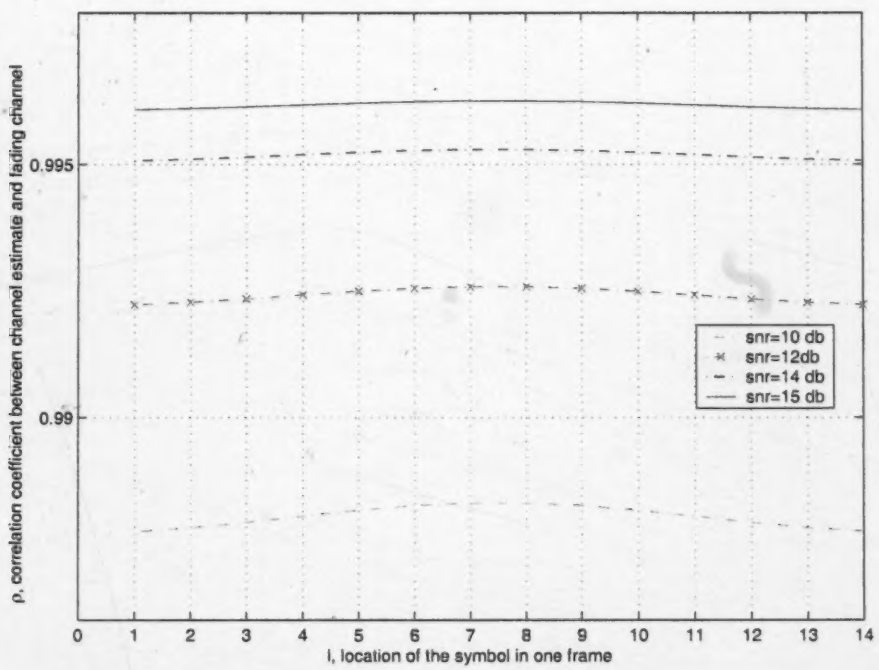

Fig. 6.7. Relationship between the correlation coefficient between the channel and the channel estimate of 16-QAM, ρ, and symbol location, l, for a Hamming window applied to the sinc interpolator for fixed values of SNR per bit of 10 dB, 12 dB, 14 dB and 15 dB.

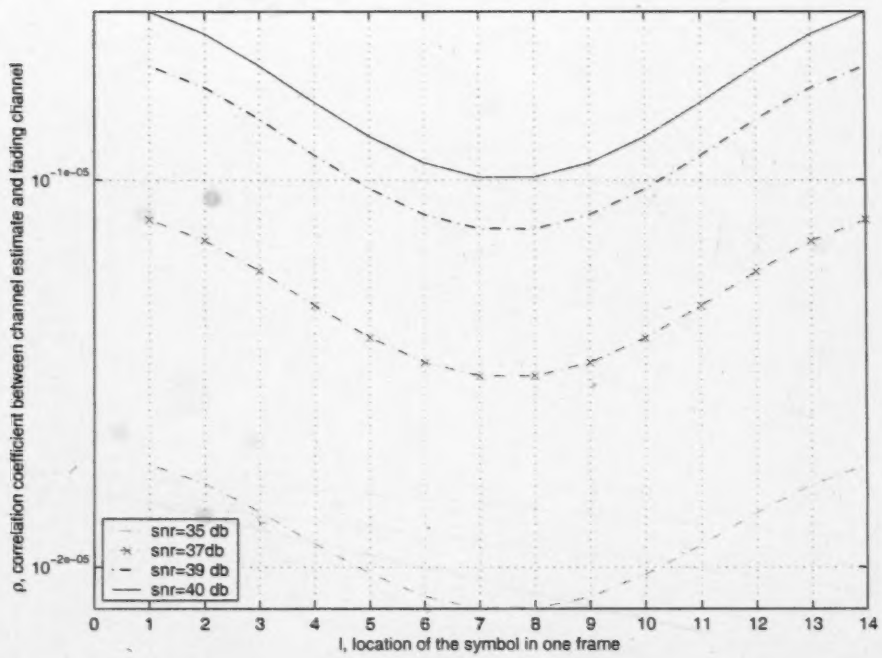
ρ, correlation coefficient between channel estimate and fading channel
10^-1e-05
10^-2e-05
snr=35 db
snr=37db
snr=39 db
snr=40 db
0 1 2 3 4 5 6 7 8 9 10 11 12 13 14
l, location of the symbol in one frame

Fig. 6.8. Relationship between the correlation coefficient between the channel and the channel estimate of 16-QAM, ρ, and symbol location, l, for a Hamming window applied to the sinc interpolator for fixed values of SNR per bit of 35 dB, 37 dB, 39 dB and 40 dB.

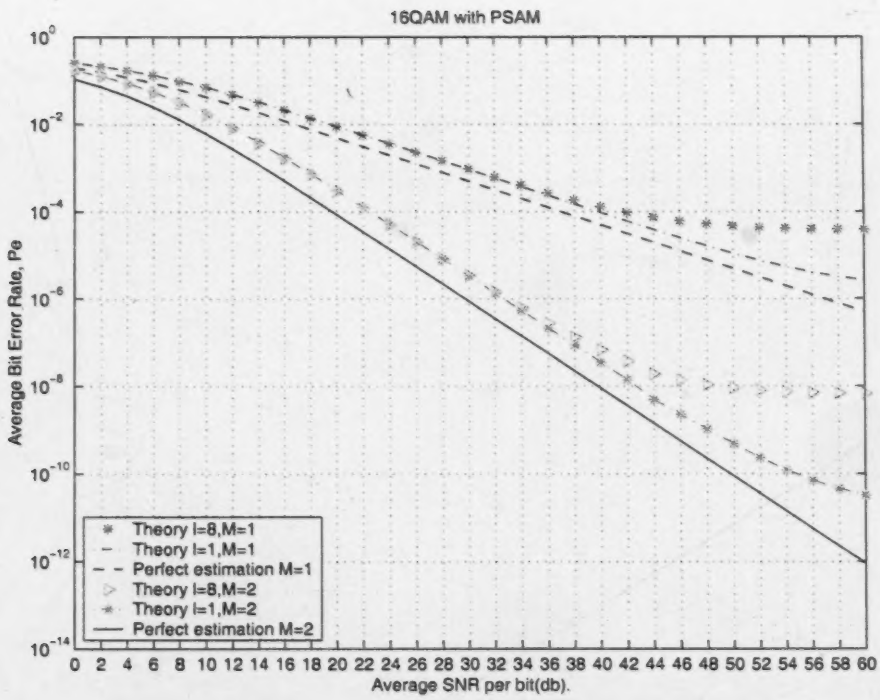

Fig. 6.9. The BER performance of 16-QAM for $l = 1$ and $l = 8$ with a Hamming windowing applied to the sinc interpolator for $L = 15$, $K = 30$, and $f_D T_s = 0.03$; M is the number of diversity branches and l is the symbol location in one frame.

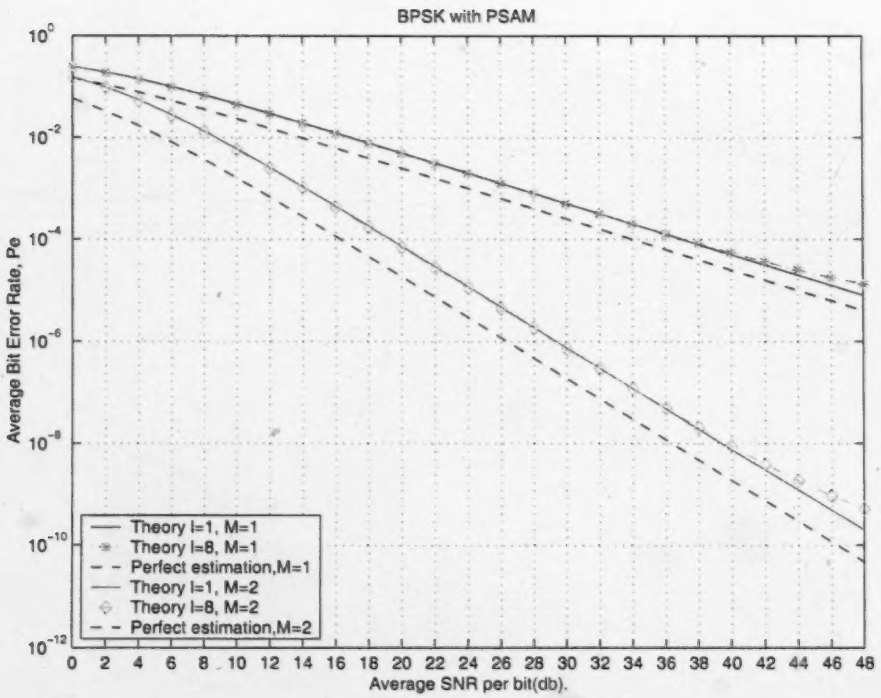

Fig. 6.10. The BER performance of BPSK for $l = 1$ and $l = 8$ with a Hamming window applied to the sinc interpolator for $L = 15$, $K = 30$, and $f_D T_s = 0.03$; the parameter, l, is the symbol location in one frame.

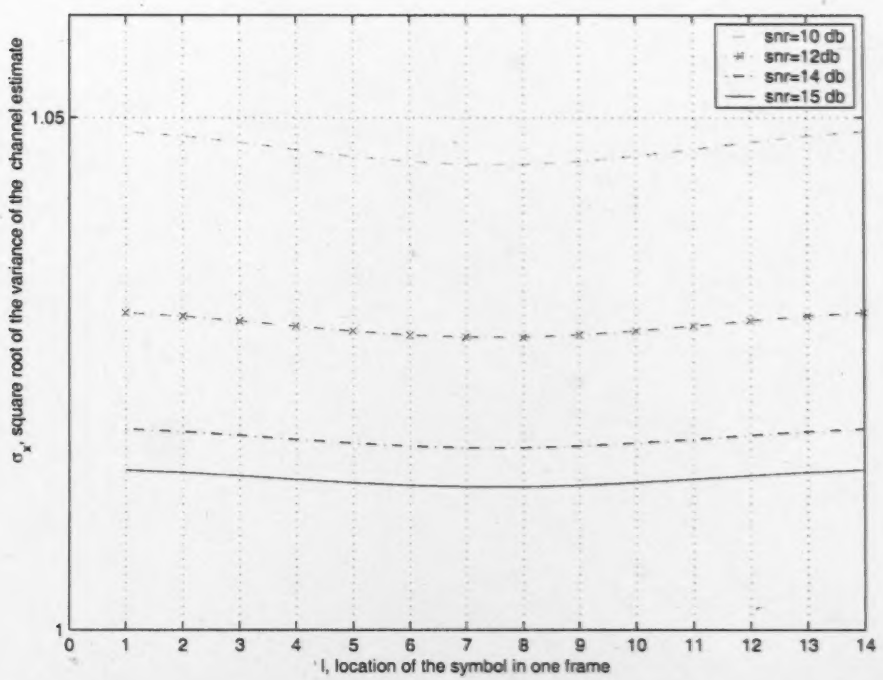

Fig. 6.11. Relationship between the square root of the variance of the channel estimate of BPSK, $\sigma_{\hat{x}}$, and symbol location, l, for a Hamming window applied to the sinc interpolator for fixed values of SNR per bit of 10 dB, 12 dB, 14 dB and 15 dB.

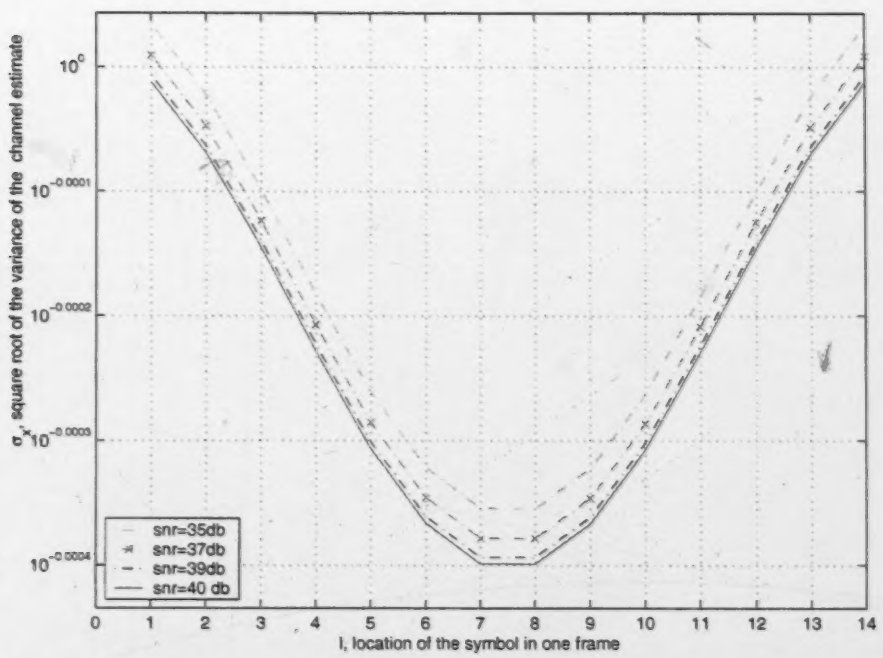

Fig. 6.12. Relationship between the square root of the variance of the channel estimate of BPSK, $\sigma_{\hat{x}}$, and symbol location, l, for a Hamming window applied to the sinc interpolator for fixed values of SNR per bit of 35 dB, 37 dB, 39 dB and 40 dB.

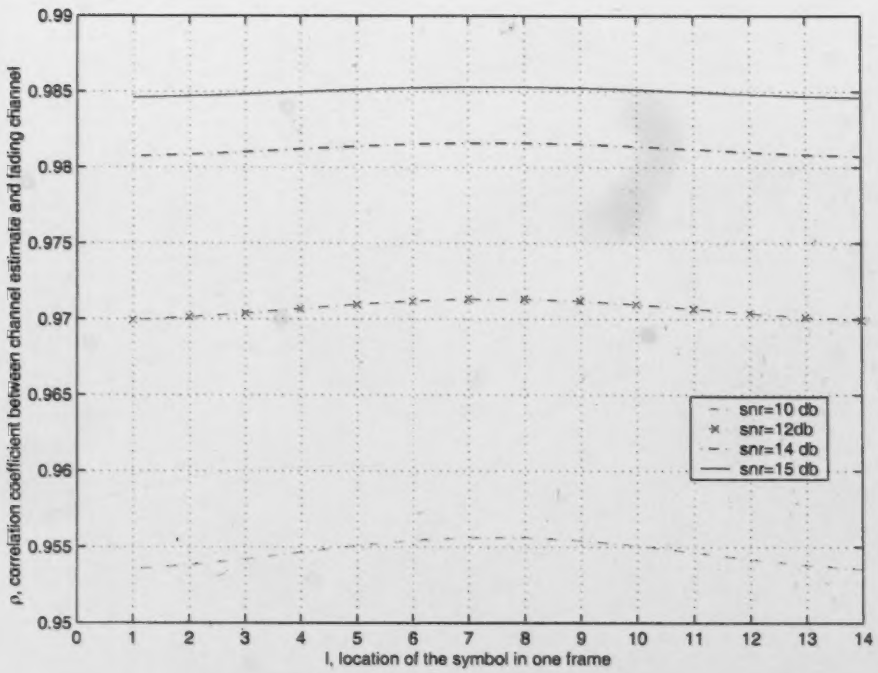

Fig. 6.13. Relationship between the correlation coefficient between the channel and the channel estimate of BPSK, ρ, and symbol location, l, for a Hamming window applied to the sinc interpolator for fixed values of SNR per bit of 10 dB, 12 dB, 14 dB and 15 dB.

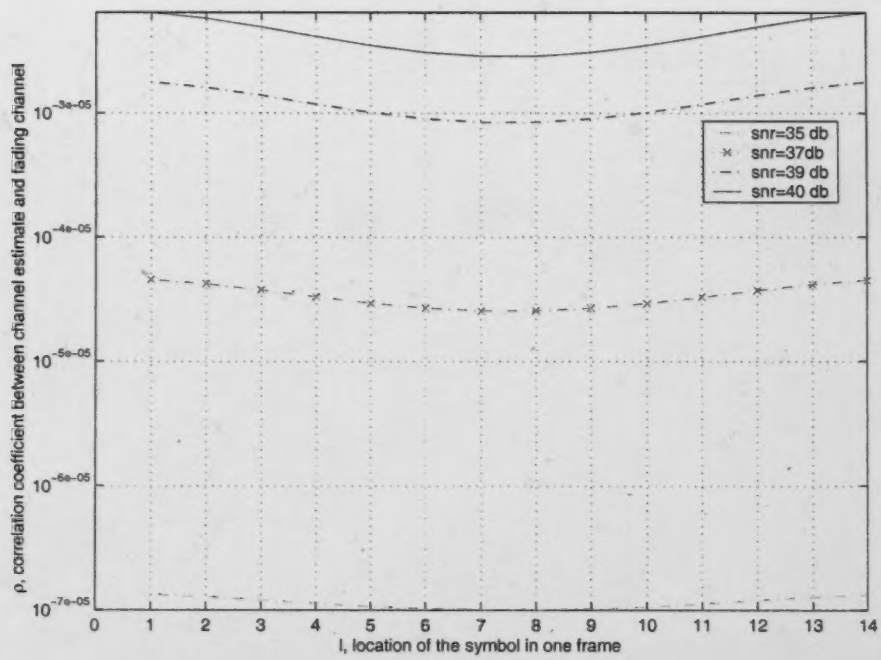

Fig. 6.14. Relationship between the correlation coefficient between the channel and the channel estimate of BPSK, ρ, and symbol location, l, for a Hamming window applied to the sinc interpolator for fixed values of SNR per bit of 35 dB, 37 dB, 39 dB and 40 dB.

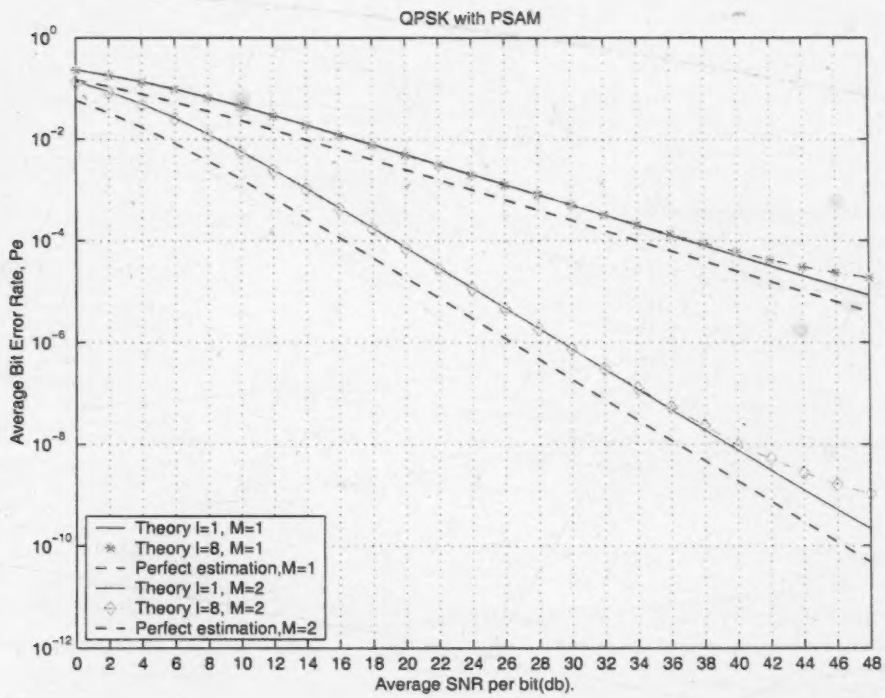

Fig. 6.15. The BER performance of QPSK for $l = 1$ and $l = 8$ with a Hamming window applied to the sinc interpolator for $L = 15$, $K = 30$, and $f_D T_s = 0.03$; the parameter, l, is the symbol location in one frame.

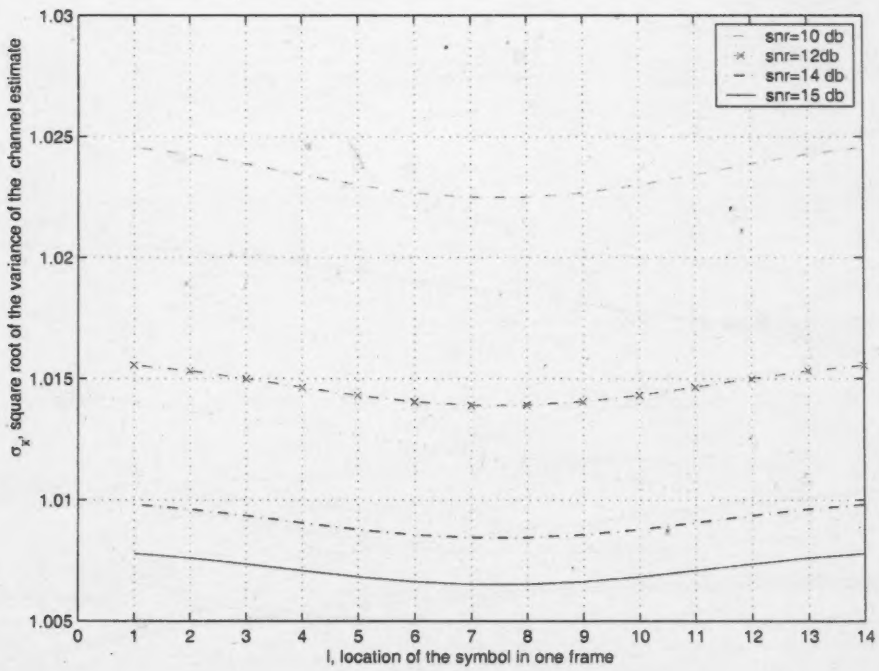

Fig. 6.16. Relationship between the square root of the variance of the channel estimate of QPSK, $\sigma_{\hat{x}}$, and symbol location, l, for a Hamming window applied to the sinc interpolator for fixed values of SNR per bit of 10 dB, 12 dB, 14 dB and 15 dB.

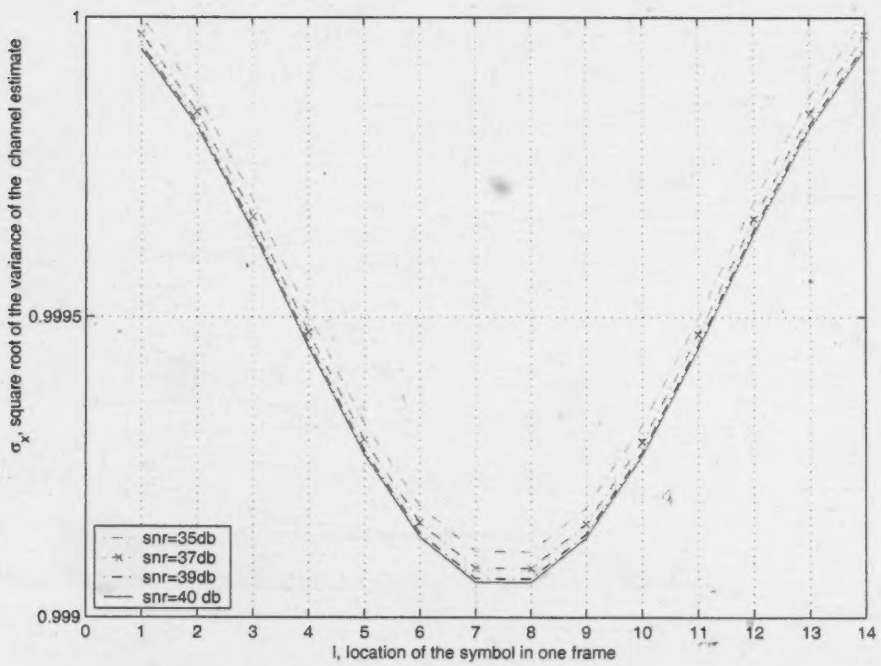

Fig. 6.17. Relationship between the square root of the variance of the channel estimate of QPSK, $\sigma_{\hat{x}}$, and symbol location, l, for a Hamming window applied to the sinc interpolator for fixed values of SNR per bit of 35 dB, 37 dB, 39 dB and 40 dB.

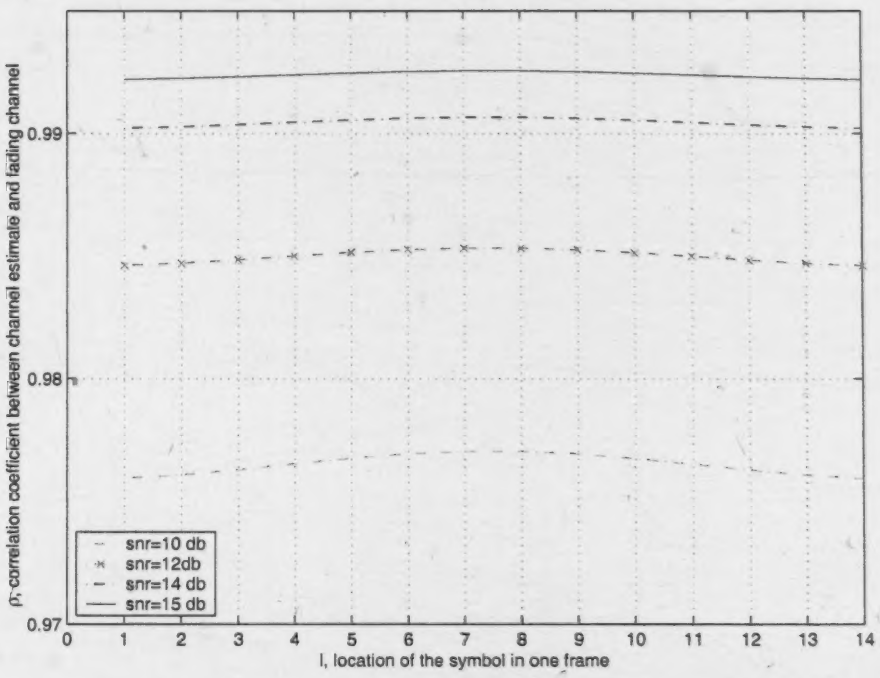

Fig. 6.18. Relationship between the correlation coefficient between the channel and the channel estimate of QPSK, ρ, and symbol location, l, for a Hamming window applied to the sinc interpolator for fixed values of SNR per bit of 10 dB, 12 dB, 14 dB and 15 dB.

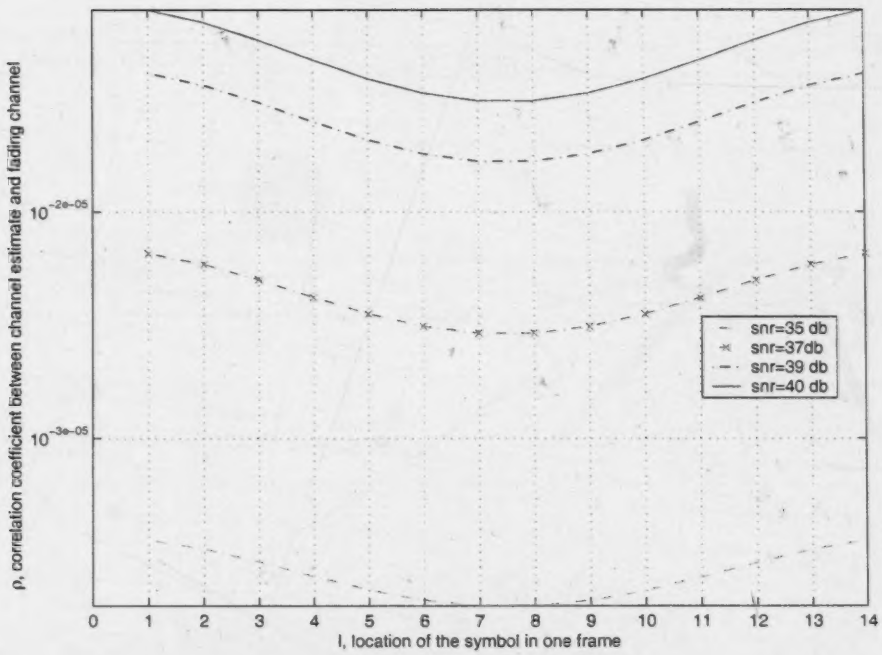

Fig. 6.19. Relationship between the correlation coefficient between the channel and the channel estimate of QPSK, ρ, and symbol location, l, for a Hamming window applied to the sinc interpolator for fixed values of SNR per bit of 35 dB, 37 dB, 39 dB and 40 dB.

6.3 Selection of Window Functions for Channel Estimation/Interpolation

The sinc interpolator with the Hamming window structure applied in our system model is taken from [16]. According to [16], the Hamming window is applied to eliminate the frequency dispersion caused by abrupt truncation in the time domain when a rectangular window is used. This raises an interesting question about the influences on the system performance achieved with different selections of window functions for the channel estimation. We first show the severe degradation of the BER performance for 16-QAM caused by using a rectangular window applied to the sinc interpolator. Then we compare the system performance with a rectangular window, a Blackman window, a Hanning window, a Hamming window and a Kaiser window applied.

Fig. 6.23 and Fig. 6.24 show the BER's of 16-QAM for single branch and dual branch reception with a rectangular window and a Hamming window applied to the sinc interpolator, respectively, as a function of the average SNR per bit. Both theoretical and simulation results for $l = 1$ and $l = 8$ as well as the BER for perfect channel estimation are presented. Note first that our theoretical results and simulation results are in excellent agreement within $\gamma_b = 0 - 40$ dB. One sees from Fig. 6.24 and Fig. 6.23 , that the BER's at $l = 8$ exhibit error rate floors that are in evidence for values of SNR greater than 30 dB and 46 dB for the rectangular window and the Hamming window, respectively. The error floors are caused by decorrelation which originates in the channel variations and in the channel estimation filtering. The abrupt truncation of the rectangular window relative to the Hamming window severely degrades the estimation accuracy, and the BER performance, by causing decorrelation. It is also shown in Table 6.2 that starting from small SNR (around 6 dB), the BER performances are better for the information symbols closer to the pilot for both the diversity and non-diversity cases. This is due to the dominance of decorrelation as a component in the channel estimation error when a rectangular window is applied.

Fig. 6.25 shows the BER performance of single branch reception 16-QAM for $l = 8$ with different windows applied to the sinc interpolator. In the practical range of SNR per

bit, $0-35$ dB, with a rectangular window applied, the system gives the worst performance. Meanwhile, the BER performances with a Hanning, a Hamming and a Kaiser window applied are very close and outperform the performances with a rectangular and a Blackman window applied. It is evident for values of SNR per bit greater than 35 dB, that the system performs best with a Kaiser window applied, then a Hamming window, followed by a Hanning window. At $P_b = 2 * 10^{-4}$, the interpolator with a Kaiser window outperforms that with a Hanning window by approximately 1.5 dB and that with a Hamming window by approximately 0.7 dB. Fig. 6.26 illustrates the BER performance of MRC 16-QAM for $l = 8$ with different windows applied to the sinc interpolator with $M = 1, 2, 4$. It demonstrates that the diversity system performs best with a Kaiser window applied to the sinc interpolator. And the value of the SNR at which we can observe that the system with the Kaiser window performs better become smaller as the diversity order increases. So overall, the system gives the best performance with a Kaiser window applied, where the shape parameter, $\beta = 4.86$ [38].

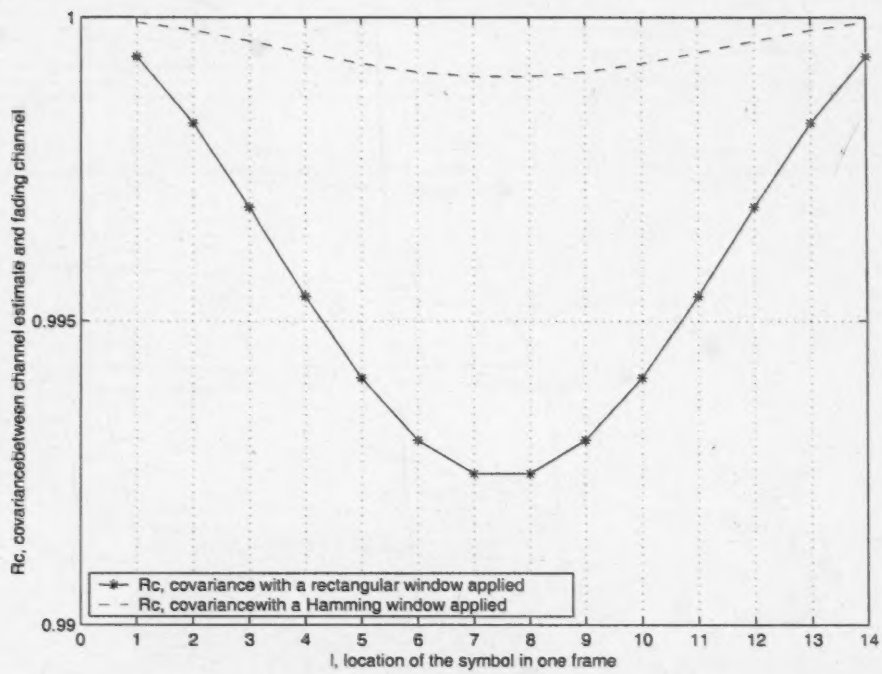

Fig. 6.20. Relationship between the covariance, *Rc*, and symbol location, *l*, for a rectangular window applied to the sinc interpolator for fixed values of SNR per bit of 15 dB, 20 dB, 30 dB and 40 dB.

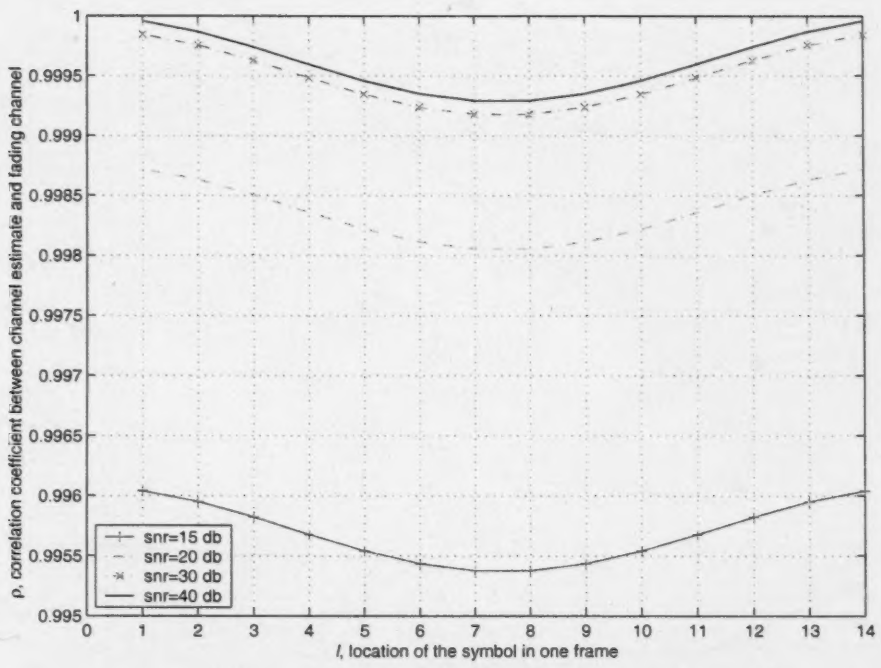

Fig. 6.21. Relationship between the correlation coefficient, ρ, and symbol location, l, for a rectangular window applied to the sinc interpolator for fixed values of SNR per bit of 15 dB, 20 dB, 30 dB and 40 dB.

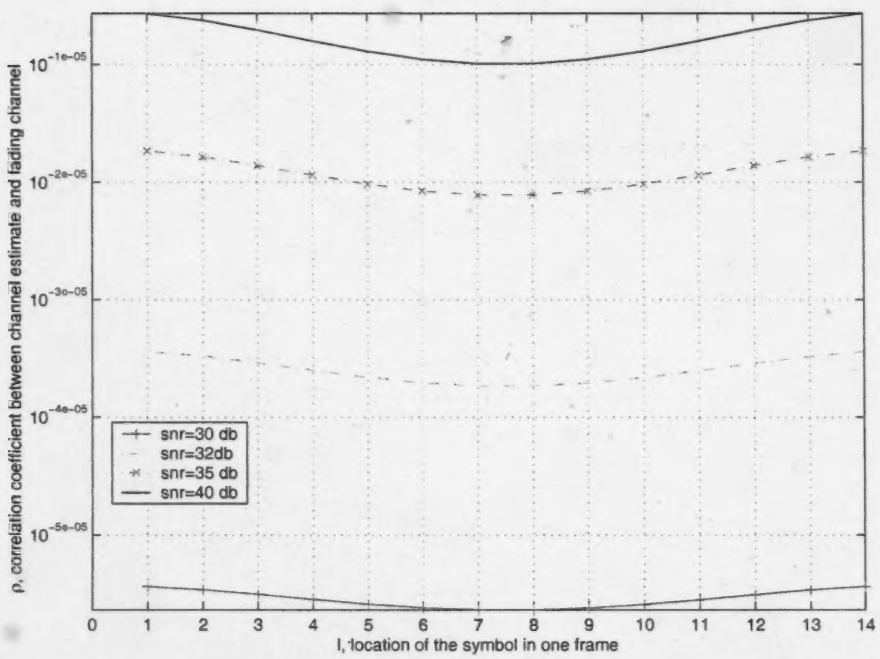
ρ, correlation coefficient between channel estimate and fading channel
l, location of the symbol in one frame
snr=30 db
snr=32db
snr=35 db
snr=40 db

Fig. 6.22. Relationship between the correlation coefficient, ρ, and symbol location, l, for a Hamming window applied to the sinc interpolator for fixed values of SNR per bit of 30 dB, 32 dB, 35 dB and 40 dB.

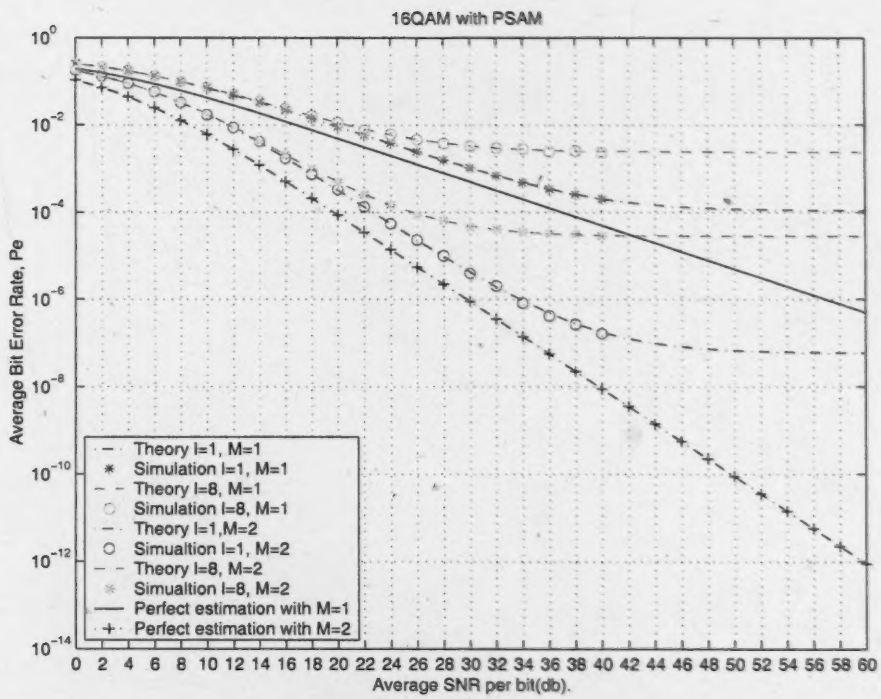

Fig. 6.23. The BER performance of 16-QAM with dual-branch diversity and a rectangular window applied to the sinc interpolator for $L = 15$, $K = 30$, and $f_D T_s = 0.03$; M is the number of diversity branches and l is the symbol location in one frame.

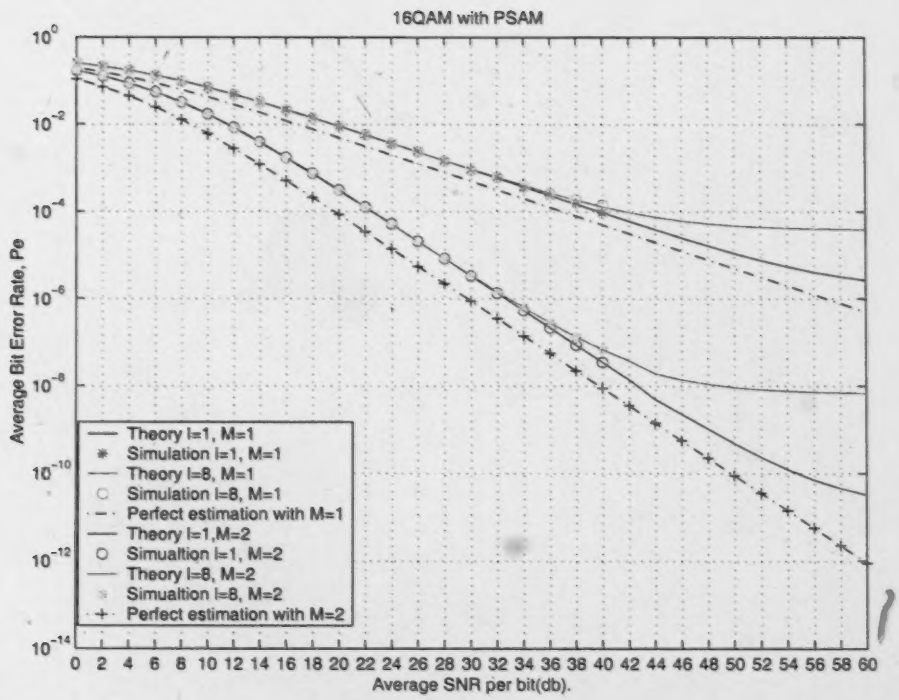

Fig. 6.24. The BER performance of 16-QAM with dual-branch diversity and a Hamming window applied to the sinc interpolator for $L = 15$, $K = 30$, and $f_D T_s = 0.03$; M is the number of diversity branches and l is the symbol location in one frame.

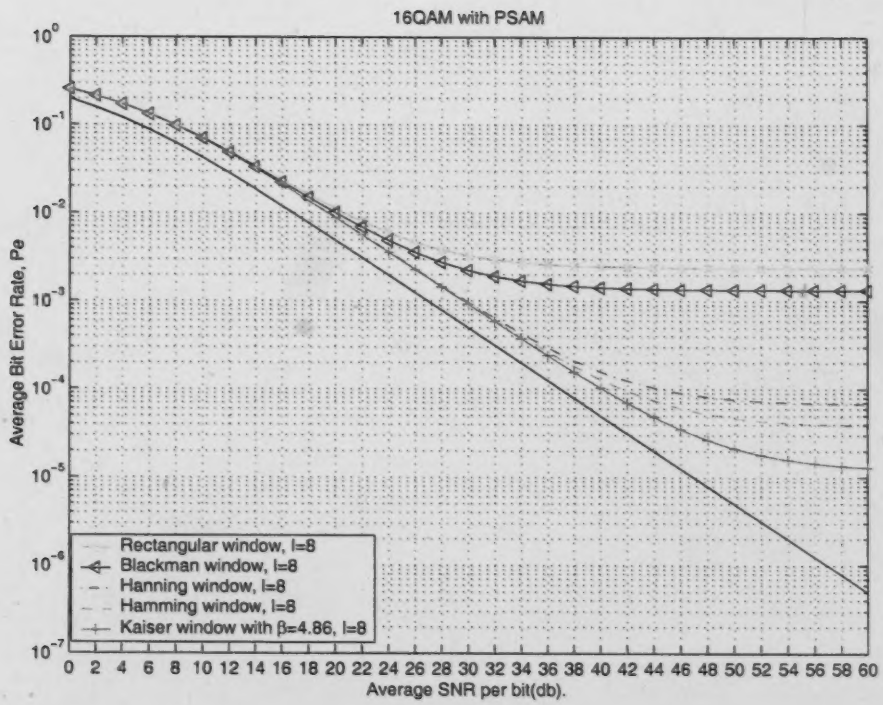

Fig. 6.25. The BER performance of single branch 16-QAM for $l = 8$ with different windows applied to the sinc interpolator for $L = 15$, $K = 30$, and $f_D T_s = 0.03$; the parameter, l, is the symbol location in one frame.

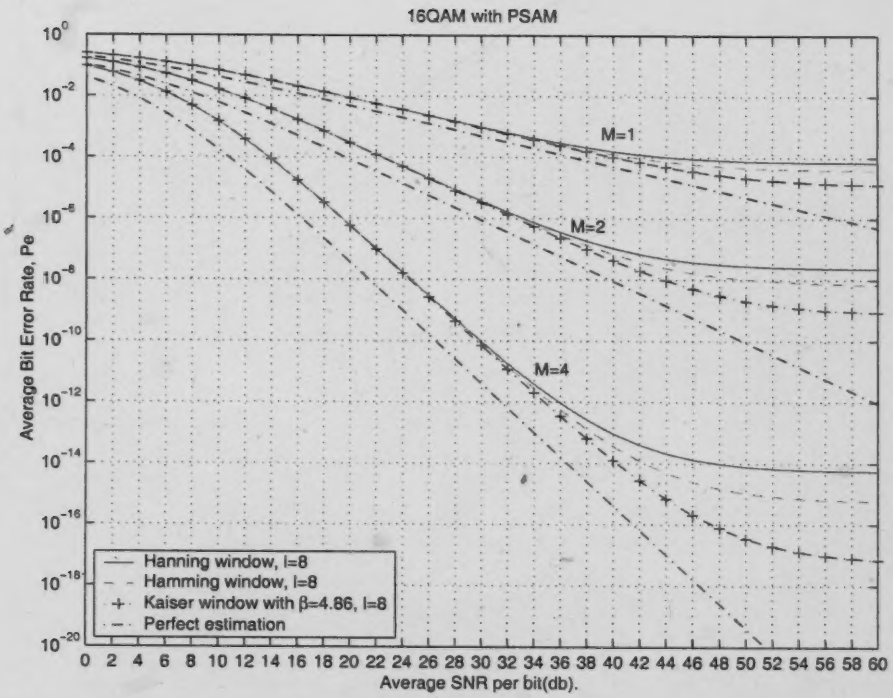

Fig. 6.26. The BER performance of MRC 16-QAM for $l = 8$ with different windows applied to the sinc interpolator for $L = 15$, $K = 30$, and $f_D T_s = 0.03$; the parameter, l, is the symbol location in one frame.

TABLE 6.1

BER of BPSK, QPSK and 16-QAM with single branch reception

Modulation	*BPSK*	*BPSK*	*QPSK*	*QPSK*	$16-QAM$	$16-QAM$
$\gamma_b(dB)$	$l=1$	$l=8$	$l=1$	$l=8$	$l=1$	$l=8$
0	2.498E-01	2.468E-01	2.326E-01	2.299E-01	2.557E-01	2.539E-01
2	1.933E-01	1.905E-01	1.812E-01	1.786E-01	2.137E-01	2.118E-01
4	1.422E-01	1.398E-01	1.348E-01	1.326E-01	1.719E-01	1.701E-01
6	1.003E-01	9.838E-02	9.621E-02	9.444E-02	1.329E-01	1.312E-01
8	6.831E-02	6.694E-02	6.631E-02	6.499E-02	9.857E-02	9.713E-02
10	4.539E-02	4.443E-02	4.447E-02	4.354E-02	7.038E-02	6.923E-02
12	2.963E-02	2.899E-02	2.923E-02	2.860E-02	4.860E-02	4.774E-02
14	1.912E-02	1.869E-02	1.895E-02	1.853E-02	3.267E-02	3.207E-02
16	1.223E-02	1.196E-02	1.217E-02	1.190E-02	2.152E-02	2.112E-02
18	7.789E-03	7.616E-03	7.763E-03	7.593E-03	1.397E-02	1.371E-02
20	4.943E-03	4.834E-03	4.933E-03	4.828E-03	8.984E-03	8.826E-03
22	3.130E-03	3.063E-03	3.127E-03	3.064E-03	5.738E-03	5.648E-03
24	1.980E-03	1.939E-03	1.979E-03	1.943E-03	3.649E-03	3.605E-03
26	1.251E-03	1.227E-03	1.251E-03	1.232E-03	2.314E-03	2.299E-03
28	7.900E-04	7.771E-04	7.905E-04	7.823E-04	1.465E-03	1.469E-03
30	4.987E-04	4.926E-04	4.993E-04	4.980E-04	9.271E-04	9.426E-04
32	3.148E-04	3.130E-04	3.154E-04	3.184E-04	5.863E-04	6.094E-04
34	1.987E-04	1.995E-04	1.992E-04	2.050E-04	3.709E-04	3.988E-04
36	1.254E-04	1.279E-04	1.259E-04	1.334E-04	2.348E-04	2.657E-04
38	7.911E-05	8.276E-05	7.964E-05	8.824E-05	1.488E-04	1.817E-04

TABLE 6.2

BER of 16-QAM with a rectangular window applied to the sinc interpolator

$\gamma_b(dB)$	$l=1, M=1$	$l=8, M=1$	$l=1, M=2$	$l=8, M=2$
0	2.556E-01	2.563E-01	1.755E-01	1.756E-01
2	2.145E-01	2.144E-01	1.305E-01	1.307E-01
4	1.729E-01	1.728E-01	8.991E-02	9.007E-02
6	1.337E-01	1.339E-01	5.685E-02	5.714E-02
8	9.914E-02	9.978E-02	3.289E-02	3.330E-02
10	7.076E-02	7.183E-02	1.747E-02	1.795E-02
12	4.885E-02	5.028E-02	8.603E-03	9.074E-03
14	3.285E-02	3.455E-02	3.985E-03	4.391E-03
16	2.166E-02	2.356E-02	1.763E-03	2.083E-03
18	1.410E-02	1.612E-02	7.556E-04	9.940E-04
20	9.097E-03	1.121E-02	3.174E-04	4.899E-04
22	5.847E-03	8.016E-03	1.319E-04	2.561E-04
24	3.756E-03	5.962E-03	5.474E-05	1.453E-04
26	2.421E-03	4.650E-03	2.285E-05	9.099E-05
28	1.572E-03	3.816E-03	9.689E-06	6.310E-05
30	1.033E-03	3.287E-03	4.220E-06	4.813E-05
32	6.925E-04	2.952E-03	1.916E-06	3.973E-05
34	4.770E-04	2.740E-03	9.232E-07	3.486E-05
36	3.408E-04	2.606E-03	4.812E-07	3.196E-05
38	2.549E-04	2.522E-03	2.761E-07	3.019E-05
40	2.006E-04	2.469E-03	1.761E-07	2.917E-05

Chapter 7

Conclusions

Every wireless system has to combat propagation impairments, one of the classical problems in wireless communication. Diversity has been proved to be an effective way to mitigate the effects of multipath fading caused by multipath propagation. When channel estimation is perfect, MRC diversity is the optimal linear diversity combining technique. However, inaccurate channel estimation will degrade the system performance of coherent demodulation and MRC diversity combining. Thus, a good channel estimation technique is desirable. An important estimation method, PSAM, provides quality estimation information with proper parameter settings. The estimation errors are originally caused by the AWGN in pilot symbols and the decorrelations between the pilot symbols and the data symbols. The type and size of the interpolation filter, adopted in a PSAM system, is also a critical factor for the quality of the channel estimate. In this thesis, we study the system performance for BPSK, QPSK and 16-QAM with PSAM as the estimation method and MRC as the diversity combining method in a Rayleigh fading channel. A complete discussion of the effects of channel estimation errors on the demodulation and MRC diversity have been given. The influence of the interpolation filter was also considered. Independent diversity branches were assumed. In summary:

1. The conceptual errors in [1] and [14] were clarified. The corrections and explanations were given in detail. The method proposed in [14] to calculate the BER for any

modulation schemes with MRC weighting errors is only an approximation. It is incorrect to evaluate the exact BER with estimation error by averaging SNR per bit over the conditional BER with coherent demodulation. The conditional BER with estimation error is a function of both the SNR and the phase error. Reference [1], provided an approximate BER expression for single branch reception and estimation error. It considered the channel amplitude and its estimate was independent of the the channel phase shift and its estimate. We derived a jpdf of the channel amplitude, its estimate and the phase error between the channel phase shift and its estimate in Rayleigh fading. Note that the channel and its estimate have different variances.

2. New, exact closed-form expressions for the BER of 16-QAM with perfect estimation and both the single branch reception and MRC diversity in a Rayleigh fading channel were obtained. The method described in [4] was used for the derivation. The results show the great improvement brought by diversity. In addition, the results provide a good method for the comparison between the BER performance with perfect estimation and that without perfect estimation. The method can be used to derive the BER for general M-QAM with MRC diversity.

3. New, exact, analytical expressions were derived for the BER of BPSK, QPSK and 16-QAM with PSAM, channel estimation error and both the single branch reception and MRC diversity in a Rayleigh fading channel. The effects of AWGN, decorrelation and the interference from the quadrature components on the BER performance are all considered. The sensitivity of the diversity systems to the channel estimation error was investigated and quantified. The results can be applied to general M-QAM with minor modification but more cumbersome definitions, notations and development. Moreover, the results can also be applied for the BER performance analysis for other systems using other estimation methods.

4. New and complete discussions of the relationships among the BER performance, the correlation coefficient, ρ, between the channel and its estimate and the different symbol location in one frame of a PSAM system were presented. A PSAM system

provides good quality estimates with proper parameters set, thus, the dependence of the BER performance on the information symbol locations is negligible for practical ranges of SNR values. Also, the behavior of ρ can be used as an indicator to show the tendency of the BER, that will help simplify the procedure for the system designers to evaluate/compare the system performance.

5. The influences of different interpolation filter windows on BER performance were examined. The results show that theoretically, Kaiser window gives the best performance.

Bibliography

[1] X. Tang, M.-S. Alouini, and A. J.Goldsmith, "Effect of channel estimation error on M-QAM BER performance in Rayleigh fading," *IEEE Trans. Commun.*, vol. 47, pp. 1856–1864, Dec. 1999.

[2] J. G. Proakis, *Digital Communications*, McGraw-Hill, New York, 4th edition, 2001.

[3] F. Xiong, *Digital Modulation Techniques*, Artech House, Boston, 2000.

[4] L. Hanzo, T. Webb, and T. Keller, *Single- and Multi-carrier Quadrature Amplitude Modulation: Principles and Applications for Personal Communications, WLANs and Broadcasting*, Wiley, Chinchester, UK, 2002.

[5] P. K. Vitthaladevuni and M.-S. Alouini, "A recursive algorithm for the exact BER computation of generalized hierarchical QAM constellations," *IEEE Trans. Inform. Theory*, vol. 49, no. 1, pp. 297–307, Jan. 2003.

[6] S. Chennakeshu and J. B. Anderson, "Error rates for Rayleigh fading multichannel reception of MPSK signals," *IEEE Trans. Commun.*, vol. 43, no. 2/3/4, pp. 338–346, Febuary/March/April 1995.

[7] C.-J. Kim, Y.-S. Kim, G.-Y. Jeong, J.-K. Mun, and H.-J. Lee, "SER analysis of QAM with space diversity in Rayleigh fading channels," *ETRI Journal*, vol. 17, no. 4, pp. 15–25, Jan. 1996.

[8] A.Annamalai, C.Tellambura, and V.K.Bhargava, "Exact evaluation of maximal-ratio and equal-gain diversity receivers for M-ary QAM on nakagami fading channels," *IEEE Trans. Commun.*, vol. 47, pp. 1335–1344, Sep. 1999.

[9] X. Dong, N. C. Beaulieu, and P.H.Wittke, "Signaling constellations for fading channels," *IEEE Trans. Commun.*, vol. 47, pp. 703–714, May 1999.

[10] M. K. Simon and M.-S. Alouini, "A unified approach to the performance analysis of digital communication over generalized fading channels," *Proc. IEEE*, vol. 86, pp. 1860–1877, Sep. 1998.

[11] M.G.Shayesteh and A.Aghamohammadi, "On the error probability of linearly modulated signals on frequency-flat Ricean, Rayleigh, and AWGN channels," *IEEE Trans. Commun.*, vol. 43, pp. 1454–1466, Feb. 1995.

[12] A. J. Goldsmith and S.-G. Chua, "Variable-rate variable-power MQAM for fading channels," *IEEE Trans. Commun.*, vol. 45, no. 10, pp. 1218–1230, Oct. 1997.

[13] J. G. Proakis, "Probabilities of error for adaptive reception of M-Phase signals," *IEEE Trans. Commun.*, vol. 16, no. 1, pp. 71–80, Feb. 1968.

[14] B. R. Tomiuk, N. C. Beaulieu, and A. A. Abu-Dayya, "General forms for maximal ratio diversity with weighting errors," *IEEE Trans. Commun.*, vol. 47, no. 4, pp. 488–492, Apr. 1999.

[15] J. K. Cavers, "An analysis of pilot symbol assisted modulation for Rayleigh fading channels," *IEEE Trans. Veh. Technol.*, vol. 40, no. 4, pp. 1389–1399, Nov. 1991.

[16] Y.-S. Kim, C.-J. Kim, G.-Y. Jeong, Y.-J. Bang, H.-K. Park, and S. S. Choi, "New Rayleigh fading channel estimator based on PSAM channel sounding technique," in *Proc. IEEE Int. Conf. Commun.(ICC)*, Montreal, Canada, June 1997, pp. 1518–1520.

[17] K. Yu, J. Evans, and I. Collings, "Performance analysis of pilot symbol aided QAM for Rayleigh fading channels," in *Proc. IEEE Int. Conf. Commun.(ICC)*, 2002, vol. 3, pp. 1731–1735.

[18] T. S. Rappaport, *Wireless Communications Principles and Practice*, Prentice Hall PTR, New Jersey, 2nd edition, 2002.

[19] D.G.Brennan, "Linear diversity combining techniques," *Proc. IRE*, vol. 47, pp. 1075–1102, June 1959.

[20] M. K. Simon and M.-S. Alouini, *Digital Communication over Fading Channels: A Unified Approach to Performance Analysis*, Wiley, New York, 2000.

[21] B. Sklar, *Digital Communications: Fundamentals and Applications*, Prentice Hall, Upper Saddle River, NJ, 2nd edition, 2001.

[22] J. K. Cavers, "On the validity of the slow and moderate fading models for matched filter detection of Rayleigh fading signals," *Canadian J. Elect.& Comp. Eng*, vol. 17, no. 4, pp. 183–189, Oct 1992.

[23] W. Davenport and W. Root, *Introduction to the Theory of Random Signals and Noise*, IEEE Press, reprint 1987, New York, 1958.

[24] G. L. Stuber, *Principles of Mobile Communication*, Kluwer Academic Publishers, Norwell, MA, 2nd edition, 2001.

[25] W. C. Jakes, *Microwave Mobile Communications*, IEEE press, reprint, New York, 1974.

[26] R.H.Clark, "A statistical theory of mobile-radio reception," *Bell Syst. Tech. J.*, pp. 957–1000, July-Aug. 1968.

[27] M. Abramowitz and I. A. Stegun, Eds., *Handbook of Mathematical Functions with Formulas, Graphs, and Mathematical Tables*, Dover, New York, 1974.

[28] M. Schwartz, W. R. Bennett, and S. Stein, *Communication Systems and Techniques*, IEEE Press, reprint 1995, New York, 1966.

[29] M. J. Gans, "The effect of gaussian error in maximal ratio combiners," *IEEE Trans. Commun. Tech.*, vol. 19, no. 4, pp. 492–500, Aug. 1971.

[30] X. Dong, *Coherent signaling and receiver diversity for fading channels*, Ph.D. thesis, Queen's Univ., Kingston, Canada, Dec. 2000.

[31] A. Annamalai, C. Tellambura, and V. K. Bhargava, "Analysis of hybrid selection/maximal-ratio diversity combiners with gaussian errors," *IEEE Trans. Wireless Commun.*, vol. 1, no. 3, pp. 498–512, July 2002.

[32] B.R.Tomiuk, "Effects of weighting errors in maximal ratio combiners on the bit error rates of digital diversity systems," M.S. thesis, Queen's Univ., Kingston, Canada, 1995.

[33] I. S. Gradshteyn and I. M. Ryzhik, *Table of Integrals, Series, and Products*, Academic Press, San Diego, CA, 6th edition, 2000.

[34] E. W. Ng and M. Geller, "A table of integrals of the error functions," *Journal of Research of the National Bureau of Standards-B. Mathematical Sciences*, vol. 738, no. 1, Jan.-Mar. 1969.

[35] A. Papoulis and S. U. Pillai, *Probability, Random Variables and Stochastic Processes*, McGraw Hill, Boston, 4th edition, 2002.

[36] D. J. Young and N. C. Beaulieu, "The generation of correlated Rayleigh random variates by inverse discrete Fourier transform," *IEEE Trans. Commun.*, vol. 48, pp. 1114–1127, July 2000.

[37] D. J. Young and N. C. Beaulieu, "Power margin quality measures for correlated random variates derived from the normal distribution," *IEEE Trans. Inform. Theory*, vol. 49, pp. 241–252, Jan. 2003.

[38] A. V. Oppenheim, R. W. Schafer, and J. R. Buck, *Discrete-Time Signal Processing*, Prentice Hall, New Jersey, 2nd edition, 1999.

Vita

Lingzhi Cao

Education

- 09/2001–Present University of Alberta, Canada

  Master of Science: Electrical and Computer Engineering.

- 05/1995-06/1999 Shanghai Jiaotong University, China (SJTU)

  Bachelor of Engineering: Communication Engineering

  Advanced Placement Class (Honor Class).

Working Experience

- 09/2001–Present University of Alberta, Canada

  Research Assistant and Teaching Assistant

- 06/1999-08/2001 Shanghai Bell Alcatel Mobile Communication System Company

  Network optimization engineer (SBAMC)

  02/1999-08/2001 Business Area Two Technical Central Support Dept.

  07/1999-02/2000 Chief Engineer Office of GSM radio network.

Awards

- 2000 Excellent New Staff, SBAMC

- 97 Honor of Outstanding Student, SJTU
- 95,96,97,98 People's Scholarship, SJTU
- 95,96,97,98 Shuping College Student Special Scholarship, SJTU

Publication

- L.Cao and N.C.Beaulieu, "Exact Error Rate Analysis of Diversity 16-QAM with Channel Estimation Error", submitted to *IEEE* Transactions on Communications.

Interests

- Traveling, ballroom dancing, skating, Hawaiian guitar